University of Cape Town

Faculty of Engineering and the Built Environment

School of Architecture, Planning and Geomatics

SPATIO-TEMPORAL ANALYSIS OF COASTAL SEDIMENT EROSION IN CAPE TOWN THROUGH REMOTE SENSING AND GEOINFORMATION SCIENCE

A thesis submitted in partial fulfilment of the requirements for the degree of

Master of Science in Engineering (Geomatics) at the University of Cape Town

Author: Lynn Fanikiso

Supervisor: Associate Professor Dr Julian Smit

Co-Supervisor: Dr. Moreblessings Shoko

2022

DECLARATION

I understand what plagiarism is and that it is wrong. I hereby certify that the work presented here is my own based on my own personal research, experimentation as well as the contribution of my supervisors. I have acknowledged all various sources by both citation and referencing using the Harvard style. This thesis has been submitted to the Turnitin module and I confirm that my supervisor has seen my report and any concerns revealed by such have been resolved with my supervisor. I have no intention to allow anyone else to copy or pass this work off as their own.

Signed by candidate

SIGNATURE

29/12/2022

DATE

ACKNOWLEDGEMENTS

First and foremost, I would like to thank God for strength, persistence, guidance and provision throughout this master's journey. I extend my deepest gratitude to my parents Nyaladzo and Musa Fanikiso, who have continuously supported my aspirations financially and been a source of both comfort and inspiration throughout this journey. Many thanks to the University of Cape Town's Postgraduate funding office without whose support or advice, this master's journey would not have been possible.

I acknowledge and appreciate the South African National Hydrographer, SA Navy for sharing their tidal data with me and to Ms Ruth Farre who took the time to further explain their data management processes. I am grateful to Gregg Oelofse and his team at the City of Cape Town's Coastal Management Branch for facilitating my fieldwork and sharing pertinent resources with me. I extend my eternal gratitude to Alex Sequeira who came to my rescue when my hardware failed me. I am thankful to Mr. Dirk Mathee, Mr. Kelly Shongwe and Mr. Brent Kotzee who braved the frustrations associated with my fieldwork with me whilst sharing crucial land surveying knowledge. Mignon Wells, Thomas Slingsby and Nicholas Lindenberg have my eternal respect for all the technical GIS advice they have patiently imparted whilst being a sound board during the pivotal moments of data analysis.

I am indebted to my supervisors, Associate Professor Dr Julian Smit and Dr. Moreblessings Shoko for giving me creative control of my thesis, exercising the utmost patience, imparting both technical and research wisdom as well as their unwavering support when advocating on my behalf. I am filled with the deepest gratitude to my support structure both in Botswana and South Africa; to my siblings, roommates,lab mates and friends who made the pandemic isolation bearable.

LIST OF FIGURES

LIST OF TABLES

LIST OF EQUATIONS

TABLE OF CONTENT

LIST OF ABBREVIATIONS & ACRONYMS

ALS	Airborne Laser Scanning
BLI	Bare Land Index
BSI	Bare Soil Index
CMU	Coastal Management Unit
DEA	Department of Environmental Affairs
DEM	Digital Elevation Model
DFFE	Department of Forestry, Fisheries and the Environment
DGPS	Differential Global Positioning System
DInSAR	Differential Interferometric Synthetic Aperture Radar
DoDs	Difference of DEM's
DSAS	Digital Shoreline Analysis System
DSM	Digital Surface Model
DTM	Digital Terrain Model
EEZ	Exclusive Economic Zone
EPR	End Point Rate
ESA	European Space Agency
GIS	Geographic Information System
GRD	Ground Range Detected
HAT	Highest Astronomical Tide
HWL	High Waterline
ICMA	Integrated Coastal Management Act
LAT	Lowest Astronomical Tide
LiDAR	Light Detection and Ranging
LRR	Linear Regression Rate
LST	Land Surface Temperature
MHHW	Mean Higher High Water
MHW	Mean High Water
MIR	Middle Infrared

ML	Mean Sea Level
MNDWI	Modified Normalized Difference Water Index
NDMI	Normalized Difference Moisture Index
NDWI	Normalized Difference Water Index
NIR	Near-infrared
NNC	Neural Network Convolution
NSM	Net Shoreline Movement
PBDM	Planning and Building Development Management Department
PPK	Post-Processing Kinematic
RTK	Real-time kinematic positioning
SANHO	South African Navy Hydrographic Office
SCE	Shoreline Change Envelope
SDGs	Sustainable Development Goals
SLC	Single Look Complex
SVM	Support Vector Machine
SWIR	Short-wave Infrared
TIFF	Tag Image File Format
TIR	Thermal Infrared
TLS	Terrestrial Laser Scanning
UAV	Unmanned Aerial Vehicle
USGS	United States Geological Survey
UTM	Universal Transverse Mercator
VH	Vertical Horizontal
VV	Vertical Vertical
WLR	Weighted Linear Regression Rate
XML	Extensible Markup Language

ABSTRACT

Coastal erosion can be described as the landward or seaward propagation of coastlines. Coastal processes occur over various space and time scales, limiting in-situ approaches of monitoring change. As such it is imperative to take advantage of multisensory, multi-scale and multi-temporal modern spatial technologies for multi-dimensional coastline change monitoring. The research presented here intends to showcase the synergy amongst remote sensing techniques by showcasing the use of coastal indicators towards shoreline assessment over the Kommetjie and Milnerton areas along the Cape Town coastline. There has been little progress in coastal studies in the Western Cape that encompass the diverse and dynamic aspects of coastal environments and in particular, sediment movement. Cape Town, in particular; is socioeconomically diverse and spatially segregated, with heavy dependence on its 240km of coastline. It faces sea level rise intensified by real-estate development close to the high-water mark and on reclaimed land. Spectral indices and classification techniques are explored to accommodate the complex bio-optical properties of coastal zones. This allows for the segmentation of land and ocean components to extract shorelines from multispectral Landsat imagery for a long term (1991-2021) shoreline assessment. The DSAS tool used these extracted shorelines to quantify shoreline change and was able to determine an overall averaged erosional rate of 2.56m/yr. for Kommetjie and 2.35m/yr. for Milnerton. Beach elevation modelling was also included to evaluate short term (2016-2021) sediment volumetric changes by applying Differential Interferometry to Sentinel-1 SLC data and the Waterline method through a combination of Sentinel -1 GRD and tide gauge data. The accuracy, validation and correction of these elevation models was conducted at the pixel level by comparison to an in-field RTK GPS survey used to capture the current state of the beaches. The results depict a sediment deficit in Kommetjie whilst accretion is prevalent along the Milnerton coastline. Shoreline propagation and coastal erosion quantification leads to a better understanding of geomorphology, hydrodynamic and land use influences on coastlines. This further informs climate adaptation strategies, urban planning and can support further development of interactive coastal information systems.

Key Words: Coastal Erosion; DSAS; Shoreline change; Interferometry; Waterline method

1 INTRODUCTION

The coastal zone is considered an important, highly sensitive ecosystem that accounts for 18% of the Earth's surface area and governed by complex physical and bio-chemical processes (Loubersac, 2003). It is essential for life on earth due to oceanic de-nitrification, organic matter burial, or sedimentary mineralization (Ståhlberg et al., 2006). They are linked to the decomposition of organic matter particularly where carbon and nitrogen cycling are concerned (Burdige, 2005). Both of which, contribute to global primary production as they influence the amount of available nutrients in ecosystems. (Eliot, 2016; Rust, 1991). It then follows that because of the complexity of such aforementioned foundational processes, the resultant environments such as beaches, estuaries, salt marshes, or mangroves face exploitation for socioeconomic gain.

Coastal developments interrupt the natural response of these ecosystems to climate change. Rising atmospheric Carbon dioxide (CO_2) concentrations lead to more acidic oceans disrupting habitats and biodiversity (Environmental Protection Agency, 2017). Increased global temperatures result in warmer oceans and thus an accelerated rate of sea level rise, as well as an increment in the recurrence and strength of storms (Department of Environmental Affairs: Climate Change, 2018). Sea level rise is a geohazard and there is a need to invest in research that focuses on coastal monitoring especially with active coastal processes such as shoreline erosion and marine inundation (Deronde et al., 2008).

Not enough research and effort is put into sandy coastal areas even though they are highly dynamic and face a multitude of stress stimuli with very little to poor management. Because of the aesthetic pleasure of sandy shores, as well as their ecological value, they attract the development of infrastructure leading to socio-political pressure on these ecosystems. In the case of South Africa, this was intensified early on by very limited coastal legislature supporting the conservation of the coastal zone stemming from the Sea-shore Act 21 of 1935. It was amended until 1997 and made obsolete by the National Environmental Management: Integrated Coastal Management Act 24 of 2008 (ICMA), which allowed for a more cohesive approach to coastal management.

Moreover, due to their spatial influences, execution of coastal management plans without comprehension of the coastal dynamics only further propagates the problems of a mobile

coastal boundary and its associated geohazards complicated further by human intervention (Eliot, 2016; Harris et al., 2011). For these reasons, which will be further expanded upon; this study has applied remote sensing and GIS applications towards the monitoring and quantification of coastal erosion through shoreline assessments and beach profiling.

1.1 BACKGROUND

South Africa has a well conserved linear coastline spanning roughly 3000 km, 23% of which is under protection and approximately 27% is rocky shore, 42% sandy beach, and 31% mixed shore (Claassens et al., 2022; Harris et al., 2011). Narrowing down to the Western Cape Province, 240 km of coastline is governed under the Cape Town municipality and is world renowned for its beaches, however being a coastal city means there are constant efforts in ensuring coastal protection (Colenbrander et al., 2014). The presence of beaches greatly increases Cape Town's tourism potential, however sea level rise threatens accessibility along coastal roads and railways, as well as attractions such as tidal pools (Dube et al., 2021). Although socioeconomically uneven and spatially segregated, multiple communities are dependent on the Cape Town coastline. The need for the advancement of expertise, assets, legal frameworks, and attitude has become more apparent with the threat of enhanced climate change, as well as fast and widespread coastal development (Cartwright, 2011).

Dating back to as early as 1995, Searson and Brundrit (1995) analyzed tide gauges in Simon's Bay and suggested a sea level rise of 2cm per decade. Later, Mather (2008) took it a step further by using a wider set of gauges to determine that that sea levels along South Africa's southwestern and southern Cape coast were rising at 1.57mm per annum (Mather, 2008; Searson &Brundrit, 1995). The sea-level rise risk has been further intensified by the fact that real estate development doubled between 1980 and 2007 near the high-water mark and on reclaimed land (Colenbrander et al., 2014).

Cape Town, therefore presents as the ideal case study for rushed coastal management implementation because it was thought that sea level rise would remain constant and engineering solutions would be sufficient measures for a variable coastline (Colenbrander et al., 2014). This is affirmed and evident with the reclamation of land at Cape Town's foreshore and at Sea Point, which legitimized sand dune mining and the in-filling of coastal wetlands, which had previously served as coastal buffers (Colenbrander et al., 2014). As

early as 2004, Tol warned that South Africa could lose close to 11% of wetlands due to coastal engineering solutions to mitigate sea level rise (Wigley, 2011).

Sandy shore research is important because they are the first to be affected by coastal dynamics and sediment erosion, which have serious short- and long-term effects on coastal land use from built assets to landforms and their associated ecosystem services (Eliot, 2016). Currents, waves, weather systems and tides are responsible for the redistribution of coastal sediments. The erosion and accretion of sediment in turn affects water movement leading to the development of coastal landforms. The actual shoreline experiences the most change where accumulation of sediment leads to dynamic low relief coastal landforms such as coastal terraces or fore dunes (Boak &Turner, 2005). The variable nature of coastlines means their changes are not easily measured hence the need to formulate volumetric models to understand beach profiles and their influences.

Whilst strides have been made towards understanding South Africa's coastlines, coastal erosion remains a growing concern. Socio-economic gain has overshadowed the urgency of coastal monitoring and management. The combination of hydrodynamics, geology and anthropogenic changes make the coastal zone a complex phenomenon to assess. Coastal access and usage decisions also hinge on legislative guidance. Global prompts such as the Sustainable Development Goals (SDG's) can only be addressed specific to South Africa's localized context. It is clear that coastal area issues are layered and require the harmonious use of technical and legislative knowledge to effectively protect them.

1.2 PROBLEM STATEMENT

The global concern around climate change has grown significantly in recent years (Department of Environmental Affairs: Climate Change, 2018). The trickle-down effects of global warming such as extreme weather occurrences, biodiversity loss, food insecurity and sea level rise have become a harsher reality than before. Researchers have predicted global warming of 1.5-2^{o}C annually whilst South Africa is predicted to surpass this global rate, warming up by 4-6^{o}C in the next few decades (Pachauri &Meyer, 2014). South Africa continues to advance its climate response; however, underlying socio-economic issues hinder its sustainable development. Climate change has only exposed and further exasperated these vulnerabilities (Desportes &Colenbrander, 2016). The existing social inequalities from high

rates of poverty and unemployment that lead to the growth of informal settlements also means the impacts of global warming are severe in the context of South Africa.

The United Nations global call to achieve the 17 Sustainable development goals (SDGs) by 2030 has encouraged more climate focused research (Colglazier, 2015). The research presented here hinges on the following SDGs: sustainable cities and communities, climate action, life below water and life on land (Colglazier, 2015). They highlight the need to combat the effects of climate change whilst finding ways to conserve marine resources as well as the reduction of land degradation (Department of Environmental Affairs: Climate Change, 2018). The Department of Environmental Affairs (DEA) of South Africa now known as the Department of Forestry, Fisheries and the Environment (DFFE), lists the coastal zone as an area of climate change concern (Department of Environmental Affairs: Climate Change, 2018).

South Africa has a predominantly sandy shoreline and therein lies the basis of this research (Fourie et al., 2015). Coastal geo hazards such as sea level rise and storm surge flooding pose an imminent threat by causing ecological and socio-economic disruption particularly with the influence of enhanced global warming (Griffiths et al., 2010). There is increased adverse human influence in coastal zones with an exponentially growing population meaning economic pressure is placed on these ecosystems through real estate development, fisheries, recreation and tourism, offshore oil and gas exploration; all of which ultimately lead to ecosystem resource depletion (Department of Environmental Affairs : Oceans and Coasts, 2015).

1.3 SCOPE AND JUSTIFICATION OF STUDY

Data collection, storage and dissemination is imperative for coastal management. This further affirms the need to explore various research avenues that contribute to and advance coastal monitoring and mitigation strategies. Coastal management can be approached from several disciplines such as policy analysis, numerical modeling or paleoscience (Eliot, 2016). This study, however, is a computational analysis showcasing the merits of the application of surveying, remote sensing, and Geographic Information Systems (GIS) in monitoring coastal sediment movement. The ability to rapidly collect data about earth surface phenomena

without being in contact with it and being able to integrate this data in interactive information systems makes GIS an indispensable choice and tool in coastal studies.

Although there are various facets to the application of GIS in coastal management, the overall expectation of this study is to use satellite imagery for coastal erosion analysis. The soft shore beach areas of Milnerton and Kommetjie within Cape Town act as study sites to establish shoreline scenarios at various time frames, for comparison and predictive analysis. To demonstrate the methodology effectively, factors such as beach morphology and hydrodynamics will be considered by comparing different beach profiling techniques to link the long-term and short-term effects of erosion. Figure 1 on page 5 depicts the observable elements needed for a comprehensive coastal erosion-based decision support tool, centered on an ecosystem's response to external factors, as well as physical processes and energy inputs (Gens, 2010). To further streamline the perspective of this study, the detailed variables considered are highlighted in the aim and objectives subsection (Section 1.5 on page 6).

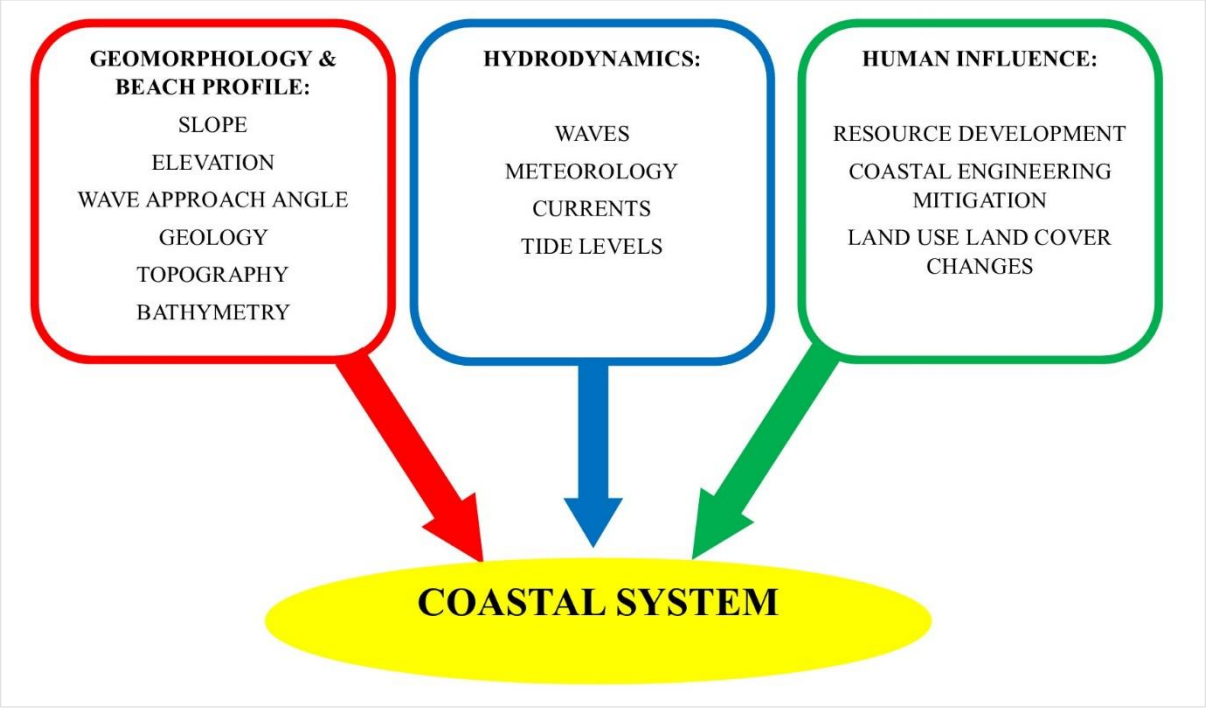

Figure 1 Coastal System Influence.

1.4 RESEARCH QUESTIONS

The following key questions assist have assisted in establishing a research framework:

1. Can optical and microwave based remote sensing techniques be applicable, optimal and accessible for both shoreline extraction and beach profiling approaches towards a well-rounded coastal erosion analysis?
2. What legal frameworks exist for coastal monitoring and how extensive has the implementation of this framework using GIS been applied in coastal sediment movement monitoring within Cape Town?
3. Which specific geo-processing techniques within optical and microwave remote sensing can be combined as suitable for both shoreline extraction and beach profiling approaches towards a well-rounded coastal erosion analysis?

1.5 AIM & OBJECTIVES

This is a geomorphology-based GIS study that aims to explore the synergy between optical and microwave based remote sensing techniques for coastal monitoring and mapping. The focus is on observing coastal sediment movement through the measurement of shoreline change, beach profiling and tide modelling. Based on the research questions and expected outputs, the objectives below have been formulated to guide this study:

Research Question 1: Can optical and microwave based remote sensing techniques be applicable, optimal and accessible for both shoreline extraction and beach profiling approaches towards a well-rounded coastal erosion analysis?

1. **Objective 1:** Combine coastal science and (optical and microwave) remote sensing principles for sediment change analysis by manipulating satellite imagery for volumetric change assessment of beaches.

2. **Objective 2:** Assess and classify the Kommetjie and Milnerton coastal areas through field work to validate satellite results.

Research Questions 2: What legal frameworks exist for coastal monitoring and how extensive has their implementation been towards applying GIS in coastal sediment movement monitoring within Cape Town?

1. **Objective 3:** Investigate the City of Cape Town's legal frameworks and how GIS has been adopted to mirror them for coastal area management.

Research Questions 3: Which specific geo-processing techniques within optical and microwave remote sensing can be combined as suitable for shoreline extraction and beach profiling respectively towards a well-rounded coastal erosion analysis?

1. **Objective 4:** By process of elimination, determine the most applicable and accessible satellite data processing methods for shoreline extraction.
2. **Objective 5:** Determine the effectiveness of satellite-based beach profiling.

1.6 RESEARCH SIGNIFICANCE AND PRACTICAL APPLICATIONS

Each section of coast is unique. Ultimately GIS-based research is meant to assist in making decisions that aid in resource development and management (Dunn et al., 2000). Studies such as this lay the foundation to further assist the City of Cape Town municipality in future targeted coastal management endeavors. There is much to be gained in first understanding these ecosystems because we can design tools specific to their environments. The more GIS technology is advanced in coastal monitoring the more we see its ripple effects and implementation in various sectors such as (Dunn et al., 2000):

1. Natural disaster assistant programs: In instances such as storm surges, coastal monitoring can help measure the amount of sediment loss along coastlines and determine the risk factor to coastal infrastructure or strategize around sand replenishment schemes. Consistent monitoring determines the distribution of resources or relief during coastal natural disasters.
2. Flood plain management and shore protection: Coastal flooding interventions and engineering solutions can be informed through modeling of sea level change and sediment budget assessments.
3. Land use regulation: Set back lines that determine the allocation of land to be developed on along coastal areas are informed through GIS using tools based on coastline proximity analyses (Desportes &Colenbrander, 2016).
4. Insurance planning: Insurance brokers use risk assessments to insure or finance property along coastlines. These are informed by GIS analysis of exposure to coastal damage.
5. Hydrography: Coastal areas are not easy to map due to the threat of boats running aground. Using remote sensing tools to measure the sea floor can help to circumvent this threat and contribute to coastal navigation maps.

6. Biodiversity and ecosystem services management: GIS can also be used to map flora or fauna species along coastal areas and determine their influences or how best to support their continued survival or adaptation to climate change (Griffiths et al., 2010).

1.7 SUMMARY

The City of Cape Town is heavily dependent on its coastline but there are limited efforts towards coastal monitoring. The combined effects of advanced climate change and coastal development put pressure on these coastal ecosystems. The socio-economic disparity within South Africa only exacerbates their degradation and soft shorelines are the first to be affected. This study intends to add to the groundwork towards coastal monitoring by proving the applicability of satellite data to quantify coastal sediment movement which is an overlooked aspect of the South African coastline.

Concepts of coastal geography, urban planning legislature and data analysis techniques are synergized to produce a comprehensive, well-balanced study that encapsulates both coastal and geospatial science by establishing a baseline theory in chapter 2 on page 9 which is extended by an objective review of the current state of literature in chapter 3 on page 43. All of which are streamlined into an appropriate methodology in chapter 4 on page 52. The results are presented and analyzed statistically as well as visually in chapter 5 on page 87. The drivers and indications of these results are discussed in chapter 6 on page 136 which have informed the conclusions and recommendations on page 142. The approved ethics clearance that supports all aspects of this study can be found in APPENDIX G ETHICS CLEARANCE on page 173.

2 THEORETICAL FRAMEWORK

This chapter synthesizes the underlying principles of coastal environments and remote sensing. As already stated, remote sensing is multi-faceted, however its applicability lies in first understanding the components of the phenomenon of interest. As such, this chapter is presented in two main sections. The first section addresses the major influences on coastal environments whilst the second emphasizes the compatibility of remote sensing as a tool to achieve the above stated objectives. The chapter then concludes by demonstrating how these theories are combined for a well-rounded shoreline analysis.

2.1 BEACH PROFILE MORPHODYNAMICS

Coastlines are affected by both exogenic and endogenic geological, biotic, tidal, and climatic forces over various time scales, which is why we are often don't notice their changes. These forces manage to strike a delicate but dynamic balance (Rust, 1991). These influences are unpredictable leading to the difficulty of relating their causes and effects. Therefore, they are characterized as coastal hazards. It is imperative to understand the underlying geological principles of coastlines especially because the distribution of shoreline types is determined by the nature of rock formations and these forces. With all these elements to consider, researchers have a consensus of the typical shape of a beach profile (Bernard O. Bauer &Davidson-Arnott, 2002; Gens, 2010). The features shown in Figure 2 are further addressed in this chapter. Coastal zones are divided into the following:

- Intertidal zone: Represents the tidal balance zone with a variety of bare soil exhibiting different geologies, grain-size, and moisture gradients.
- Subtidal zones: Occurs below the low tide mark and is permanently covered by seawater thus being highly influenced by water motion and is observable within the microwave band.

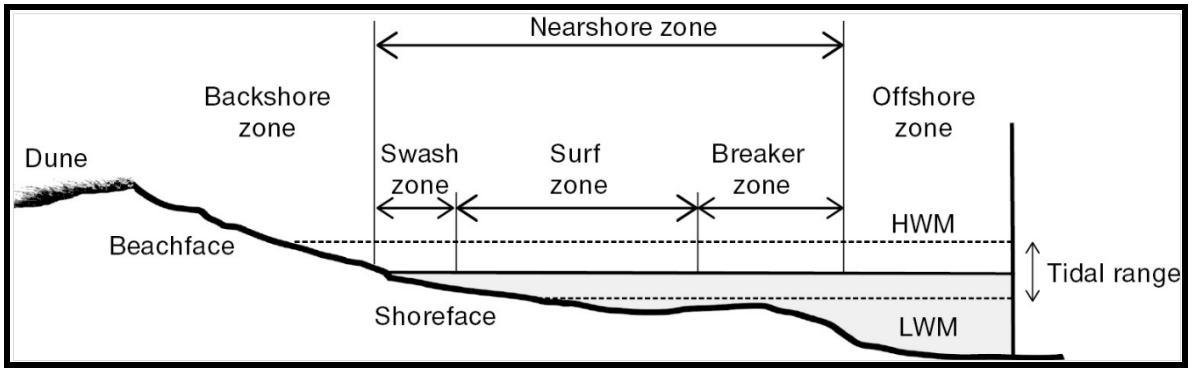

Figure 2 A cross-sectional profile of key features in a beach system

Source:(Hamylton, 2017)

A beach is defined simply as the buildup of loose sediment along a body of water and its movement is characterized by two processes (Bird &Coasts, 1984; Environmental Protection Agency, 2017).

1. Coastal erosion: The disintegration or removal of beach sediments by wave action, currents, or drainage.
2. Coastal accretion: The restoration of loose sediment to the visible portion of a beach thus raising the beach level and making it wider.

2.1.1 SEDIMENT TRANSPORT MECHANISMS

Coastal erosion is dependent on sediment supply and the beach profile. There are two main types of beach sediment (Merwe, 2017):

1. Biogenic: Consists of material broken down from organic, living organisms such as coral skeletons.
2. Abiogenic: Sand material is derived from the non-living components of an environment such as when erosion acts on rocks.

Sediment sources can be sand bars, rivers, and even as surrounding cliffs and rocks erode; sediment supply is affected. Erosion occurs if the supply of sediment is less than its export. The surf zone as depicted in Figure 2 on page 10 determines velocity, therefore, the strength of wave runup based on depth (slope) and the distance they must travel. Therefore, for example, a gentle slope is associated with a wide surf zone (Harris et al., 2011; Ingle, 2011). Trace movement studies through in-field or laboratory modelling are often the marine science

prescription to observe these factors but have proven to be tedious and dangerous (Ingle, 2011).

Generally, coastal sediment is eroded by longshore or cross shore movement. Longshore currents are associated with only wave energy and angle of approach (Bird &Coasts, 1984). Sediment is suspended in the sea water as waves approach the shoreline obliquely and refraction causes them to turn parallel instead. Thus, shoaling occurs and as the waves break the turbulence deposits the suspended sediment. Longshore currents move sand in a sawtooth like movement as depicted in Figure 3 (Almar et al., 2019). On the other hand, cross shore movement is more complex because it produces an overall perpendicular current based on incident short waves, mean waves that cause offshore transport, and long waves that lead to either offshore or onshore movement (Sallenger Jr et al., 2002). Longshore movement is usually focused on the shoreline whilst cross shore has a greater spatial extent and is responsible for temporal coastal erosion during high energy wave events and can lead to beach lowering (Bernard O. Bauer &Davidson-Arnott, 2002). Long term coastal erosion is the result of both these movement types.

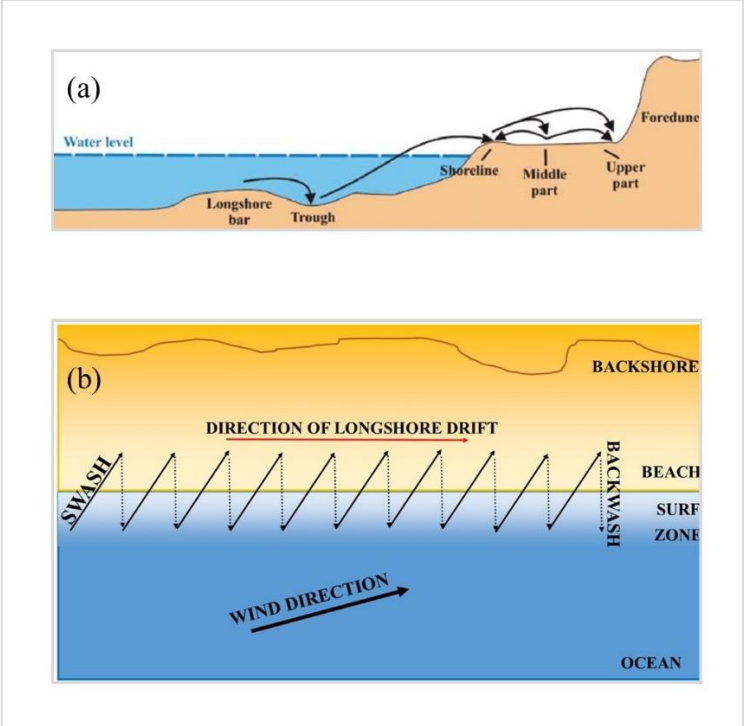

Figure 3 (a) Cross-shore sediment movement, Source:(Kovaleva et al., 2016) (b) Longshore sediment drift

The Bruun rule of erosion, shown in Equation 1 below, is best known for deducing shoreline recession based on sea level change (Bruun, 1962). It assumed a closed sediment supply system between beaches and the nearshore whilst taking the offshore sea floor into consideration as well (Eliot, 2016). It has been used worldwide in three dimensional applications, but its validity has been under constant scrutiny because it is essentially meant for two dimensional instances (Bruun, 1988). It ignores underlying concepts of longshore movement and wave theory whilst heavily placing its reasoning on the beach slope. The formula is a linear relationship that can be summed up by a 1 cm sea level rise means a 1 m retreat of the coastline.

Equation 1. Bruun Rule Equation Source:(Bruun, 1988)

$$R = \frac{SL}{h+B} = \frac{S}{tan\beta}$$

Where:

R=shoreline recession (m)
S= sea level rise (m)
L=length of sea floor affected by sea level rise (m)
h=is the depth of closure (m)
B=dune height above sea level (m)
β=average slope

This equation has been the basis of coastal sediment movement studies, however multi-tiered tools such as remote sensors are proving to be efficient enough to overcome its short comings and allowing for spatio-temporal observations (Bruun, 1988; Toure et al., 2019).

2.1.2 SHORELINE TYPES

The parameters in the Bruun equation show how integral the physical characteristics of a beach profile are in shoreline assessment. Whilst coastal evolution is a complex concept to observe, literature advises that the prevailing morphology is the best basis for beach mapping, as well shoreline classification (Harris et al., 2011). There are three main specifications in beach types, and they are governed by the following (Bird &Coasts, 1984; Musekiwa et al., 2015).

1. Exposure: The degree to which a coast is exposed to wave energy and ocean swell.
2. Beach width: The distance between the back beach and the high tide water line or ‘dry’ line. Beaches are essentially shock absorbers of wave action. A wider beach will dissipate wave energy better than a narrow one.
3. Beach slope: The average angle/gradient of the beach that defines if a beach is steep (more than 11°) or shallow (less than or equal to 0.5°).

These have been the main characteristics in classifying shoreline types as (Eliot, 2016):

1. Dissipative: Wave energy is dissipated as it approaches because of flat, wide surf zones with fine sand.
2. Reflective: The limited surf zone from narrow, steep beaches often mean that the full force of wave movement is felt, and these are often associated with coarser sand.
3. Intermediate: These are determined by the nature of rip currents and sand bars.

The infographic in Figure 5 shows how the factors discussed above are related and integral to coastal analysis. It simply reiterates the expectations associated with different shoreline types. It is clear that sediment distribution has a direct linkage to near shore seabed energy.

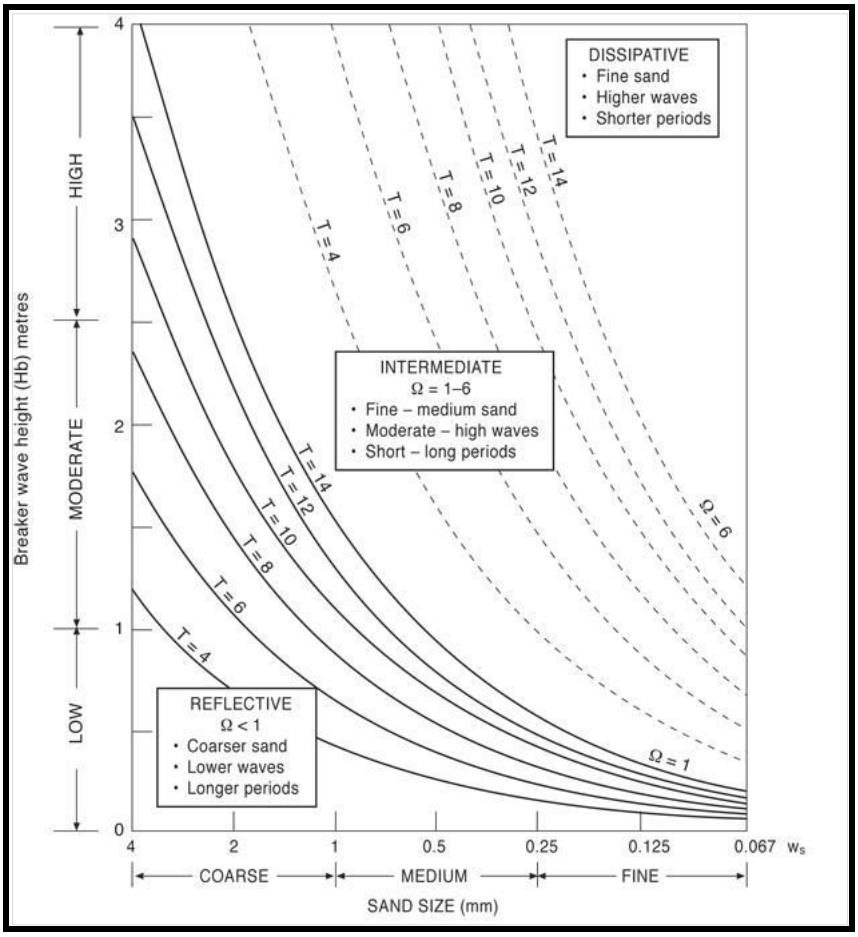

Figure 5 Beach type influences

Source:(Short, 2012)

The geomorphology and beach profile aspect of coastal systems has been examined here and the section that follows will address the hydrodynamic considerations towards coastal erosion because as previously mentioned water movement is a cause and effect in the creation of coastal landform (Eliot, 2016). As water levels rise and fall so does the spatial extent of their impact (Rongxing Li &F, 2001). There is a need to understand the factors that drive water movement and how best to include them in the analysis.

2.1.3 TIDES

Tides are the oscillatory response of oceans to the gravitational effects of the sun and moon as well as the rotational force of the Earth (Bird &Coasts, 1984; Searson &Brundrit, 1995). They are a major factor in this study because they directly affect coastal geomorphology by altering sea levels and thus the spatial exposure of beaches. These fluctuations are recorded by tide gauges, referenced to an astronomical datum and are reflective of solunar phases

(Bird &Coasts, 1984). For example, when the earth and sun are in alignment with a new or full moon leading to a higher, combined gravitational force, the tides are higher and described as spring tides (Bird &Coasts, 1984). When the sun and moon are at right angles to the Earth, however, and their gravitational forces are dispersed, tides are lower and called neap tides. In addition, tides are further classified based on the following height ranges (Geocaching, 2014):

1. Microtidal: < 2 m
2. Mesotidal: 2 m ≤ 4 m
3. Macrotidal: > 4 m

Meteorological factors such as wind, atmospheric pressure, storm surges, and oceanographic attributes such as temperature and salinity, river outflows, as well as infrastructural development in port areas are important coastal influencers. However, it is the intricate astronomical cycles that play an integral role in tide modelling and interpretation. This is because it takes roughly 28 days for the moon to return a similar position relative to Earth but 18.6 years to return to the exact same position (Bird &Coasts, 1984). Ultimately tide dynamics are linked to astronomy and wave theory (Searson &Brundrit, 1995). The consistent measurement and observation of tide data helps to extract astronomy based harmonic constants that help infer amplitude and phase of the tide movement (Ocean Rhythm, 2021). Although there are well over 100 harmonic constituents used for this, 37 have the greatest effect on tides and although the following are considered the main constituents, only the first 4 are considered for the South African tide system (Ocean Rhythm, 2021):

1. M2: Semidiurnal principal lunar tide
2. S2: Semidiurnal Principal solar tide
3. K1: Diurnal Principal solar tide
4. O1: Diurnal Principal lunar tide
5. N2: Larger Elliptical Lunar
6. K2: Luni-Solar Declinational
7. P1: Principal Solar

The combination of these constituents helps to classify tides for a specific area. For instance, If M2, S2, and N2 have a larger amplitude, than K1 and O1, then tides can be considered as semi-diurnal. This means it will have 2 tide cycles in a day. If the opposite is true, then the tide will be classified as diurnal with a single high and low tide cycle (Virginia Institute of Marine Science, 2022).

Different coastal system components have been discussed here; however, we need to identify how best to incorporate them for a collective analysis. The following section discusses how remote sensing and GIS can be effective for this purpose. The foundational principles are used to elaborate on how measured data within coastal areas can be manipulated for visualization and statistical analysis.

2.2 APPLICATION OF REMOTE SENSING AND GIS IN COASTAL STUDIES

The evolution of remote sensing from just government-sponsored military research to civilian access has led to much needed technological advancements in shoreline mapping (Brock &Purkis, 2009). The objective with remote sensing is always to provide optimum continuity of observation and extend the range of measurable parameters to meet the need for increasing knowledge of environmental factors (Ferretti et al., 2007). Nowadays with online platforms to easily download data, using satellite imagery is the most convenient and inclusive approach to coastal erosion assessment (Amaro et al., 2014).

The ultimate task for coastal zone remote sensing is executing high precision analysis on well corrected images for various time frames. Multiple researchers have highlighted that identifying water lines or wetting limits is integral for shoreline delineation when using images (Amaro et al., 2014; Boak &Turner, 2005; Deronde et al., 2008; Foody et al., 2007; Toure et al., 2019). To incorporate the influence of geological forces and climatic conditions, seasonal changes, waves, tides, and storms indicates these, and several other studies, have attempted both long- and short-term analysis proving how effective of a tool remote sensing is.

2.2.1 THE THEORY OF REMOTE SENSING

Coastal processes occur over various space and time scales as such it is imperative to use technologies that allow for well-rounded parameter measurement and model-based analyses(Davidson-Arnott et al., 2003). Remote sensing in the context of coastal monitoring is best described as using sensors to collect data about the Earth surface without being in contact with it (Ashraf et al., 2011; Ccrs, 2004). For coastal studies it is ideal to use multisensory, multiscale and multitemporal imagery to account for the various measures of change (Amaro et al., 2014). This has caused varied attempts at combining time-series aerial imagery along with Digital Elevation Models (DEM's) obtained through terrestrial surveys and Interferometric Synthetic Aperture Radar (InSAR) remote sensing techniques (Gens, 2010; Toure et al., 2019; Wigley, 2011).

Remote sensing is based on the theory that every surface of the earth has a specific spectral signature, which is related to its unique interaction with electromagnetic energy (Ccrs, 2004). Certain wavelengths can be absorbed, reflected, or transmitted based on the nature of the surface (Deronde et al., 2008). Reflectance is defined as the ratio of the radiance of reflected energy to the radiance of the incoming energy at a certain wavelength (Gibson &Power, 2000). The part of the spectrum not absorbed or transmitted is reflected and detected by sensors thus determining the visual appearance of the material. In this way, each material has its own spectral signature by which it can be identified, therefore each pixel in an image contains a unique reflectance value that can be used for the identification of specific Earth surface materials (Ashraf et al., 2011; Deronde et al., 2008; Loubersac, 2003).

Visible light or optical aerial photography is the earliest form of remote sensing, nonetheless the acquisition of data within other wavelengths and thus developments in multispectral or hyperspectral data collection ensued (Lee et al., 2011; Stockdon et al., 2002; Toure et al., 2019). Based on this knowledge and the absorption characteristics of Earth surface materials, for the sake of environmental monitoring; we can design sensors that detect and record radiation for specific types of energy from the Earth's surface (Gibson &Power, 2000).

2.2.1.1 SPECTRAL PROPERTIES OF LITTORAL SYSTEMS

The diversity of coastal areas is evident through their spatial and temporal variation; for this and the many other mentioned reasons, there is a need to invest in enhancing knowledge in this sphere of study. Identification of the appropriate remote sensor is dependent on the bio-optical parameters of littoral system surfaces (Loubersac, 2003). Coastal areas are characterized as being optically complex zones due to biological, physical, and chemical productive processes (Boak &Turner, 2005). The spectral response of sea water and thus the littoral zone depends on (Eliot, 2016):

1. Waves
2. Winds
3. Pollutants
4. Turbidity
5. Temperature
6. Water blooms
7. Plankton
8. Nature of Sea floor
9. Sediment content

These factors form the basis of classifying sea water into two groups (Loubersac, 2003):

a) ***Case 1***: Optical properties are influenced by phytoplankton and their related resultant products.
b) ***Case 2***: Suspended sediments and dissolved organic matter are the major influence here.

The introduction of coastal bands in satellite sensors has addressed the research gap regarding the detection of the bio-chemical components of coastal waters, however, there is still significant work to be done regarding coastal sediment detection. Case 1 algorithms are not applicable in Case 2 scenarios due to the difference in sea water constituents and because of optical similarities of these environments, spectral confusion often occurs (Loubersac, 2003). It can lead to misinterpretation of image elements hence the reason the consensus is to use multiple data sources (Barbosa et al., 2014; Horritt et al., 2001).

Clear water has a low reflectance, and the maximum is achieved in the blue section of the spectrum; thus, its reflection decreases as wavelength increases. Turbid water on the other hand has a higher reflectance within the red portion (Loubersac, 2003). The reflectance of sand is constant between near-infrared and blue-violet bands and depends on its composition (Ashraf et al., 2011). When it's water content increases, the reflectance decreases without affecting its spectral curve shape (Deronde et al., 2008; Loubersac, 2003). The deposition of organic matter such as microflora, phytoplankton may alter spectral response because of the introduction of chlorophyll (Rust, 1991). With all these considerations regarding remote sensing of coastal environments, Figure 4 below further showcases how the reflectance of these components varies with wavelength as relates to the presence of Colored dissolved organic matter (CDOM), sediment and chlorophyll.

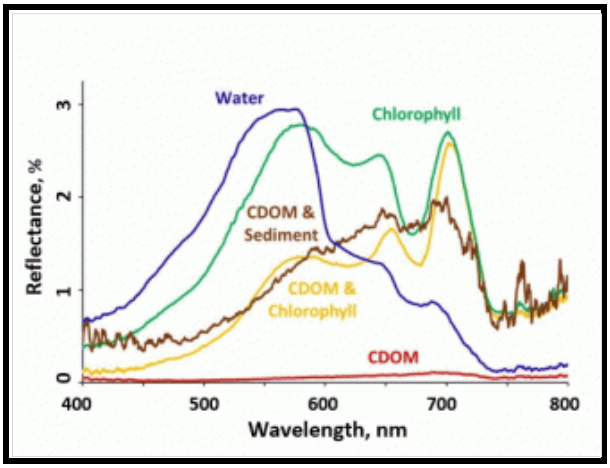

Figure 4 Influence of bio-optical factors on water body spectral signature.

Source:(University of Minnesota)

Band arrangements have changed with sensor design and some authors have been adamant that different bands must be used for different tide levels because it accounts for spectral confusion and relates to the amount of beach exposure captured during image acquisition (Acharya et al., 2016). For example, waterlines are best extracted using the near Infrared (NIR), short wave infrared (SWIR) and thermal infrared (TIR) during high tides, however these are less impactful during low tides whilst ratioing NIR with the visible band such as in the Normalized Difference Water Index (NDWI) helps to reduce the effect of turbid water (Foody et al., 2007). This is because in clear water, NIR is transparent.

It is evident that the slightest change in environmental conditions can alter the bio-optical response of water bodies including the timing of image acquisition when remote sensing is used. This is considered in satellite sensor designs by incorporating the appropriate wavelength bands. The following section (2.2.1.2) addresses how these bands can be combined and manipulated to extract usable land cover data.

2.2.1.2 COASTAL DETECTION AND EXTRACTION TECHNIQUES

Toure et al. (2019) cautions that any remote sensing techniques applied towards coastal inundation must find a balance between noise reduction and edge detection because shorelines are naturally occurring edges. There are several, adequate pre-processing filters, and correction tools to achieve image enhancement, however shoreline detection methods can be categorized into 4 groups as outlined below:

1. **Edge Detection**

   The goal here is morphological segmentation by interpreting object geometry within a particular landscape (Zollini et al., 2020). Through similarity criterion, region growing with germ algorithm (SGR) and watershed transformation (WS) have been the two major mathematical algorithms in this area of research. Whilst WS focusses on image gradients, SGR uses spatial relation and has proven to be the most favorable (Toure et al., 2019).

2. **Band thresholding**

   This is the easiest of the methods whereby a specific value is selected to segment an image usually by means of histogram stretching. Studies have drawn inspiration from the foundational work that led to Otsu thresholding and developed it further for panchromatic images, however it has proved inadequate for the complexity of multispectral imagery (Boak &Turner, 2005).

3. **Classification**

   The boundary between separated land and sea image components is taken to represent the shoreline (Hamylton, 2017). In this instance multispectral images are simplified

into homogenous classes based on their land cover reflectance patterns (Tingzon et al., 2020). These can either be pixel or object-based classifications.

a) Pixel classifications only take the images pixel values into consideration. In the past K-means has been the most popular of the supervised techniques for shoreline delineation studies. This clustering method has been further improved by the formulation of the ISODATA classification. Growing interest in machine learning has caused a shift into using neural networks and Support Vector Machines (SVM) (Bahari et al., 2014). Although there are several types such as probalistic neural networks (PNN) and generalized regression neural networks (GRNN), convolutional neural networks (CNN) have become popular in remote sensing for their vectorization capabilities on images (Gomez et al., 2014).

   SVM has offered more accuracy with less sampling variance as opposed to algorithms like Maximum likelihood. Although originally a binary classifier, SVM uses a hyperplane identification technique that separates classes based on specified training samples or support vectors. It creates well defined boundaries because it focusses on the pixels at the edge of these boundaries (Bahari et al., 2014). CNN'S on the other hand seeks out relations between defined data sets thus a class can occupy multiple dimensions within the feature space to create clusters (Atkinson &Tatnall, 1997). The greatest advantages of CNN and SVM are that they require less training data and do not assume an underlying distribution, however neural networks have been associated with overfitting. Where unsupervised techniques have been used, Principal Component Analysis (PCA) is often used to better the classification by creating a high variance amongst the poorly correlated pixels.

b) Object-oriented classification on the other hand incorporates a pixel's spectral and spatial resolution as well as other defining components such as texture. There has been significant growth in its application with the formulation of tools like the Object Merging Index (OMI). It also has the advantage of being combined with other techniques such as region growing

4. Spectral Indices

These are also a form of clustering classification that uses image band ratios. Asmadin et al. (2018) conducted a comparative study on 7 water index algorithms by applying Spectral Angle Mapper (SAM) classification towards land-sea segmentation (Asmadin et al., 2018). Keeping in mind that the main land cover types we are likely to encounter in coastal areas are soil, vegetation and water based helps to narrow down the spectral indices we can use to enhance our images enough to delineate shorelines to the following:

a) Normalized Difference Water Index (NDWI): There are three variations of this index to date, however the original is derived from the Near Infrared (NIR) and green band channels (Mcfeeters, 1996). It leads to a clear distinction by water surfaces having positive values whilst all non-water surfaces have a negative value, however it has not proven to be competent enough to fully suppress ground signals from soil or urban areas. Xu (2006) proved that water and urban areas had the same reflectance in both the green and NIR bands and so to overcome this, he suggested the use of the MIR band instead and Asmadin et al., (2018) statistically proved that water had greater absorption values within the MIR band (Asmadin et al., 2018; Xu, 2006). MNDWI simply allows for a crisper contrast. The third version uses both NIR and MIR bands, is often called the Normalized Differential Moisture Index (NDMI) and is associated with soil moisture studies (Gao, 1996).

b) Normalized Difference Vegetation Index (NDVI): This has been one of the most widely used indices for vegetation monitoring that incorporates the NIR and Red bands (Tingzon et al., 2020). Vegetation health applications are a major research area in remote sensing. The high reflectance of vegetation in NIR and absorption in the Red make it ideal in using vegetation limits as a delineating factor for coastal monitoring because vegetation reflects as a positive value. The greater the vegetation density, the higher the value.

c) Bare Soil Index (BSI): This would be ideal for coastal areas because calcareous soils have a high reflection in the visible spectrum whilst varying depending on moisture or humidity in the NIR and MIR bands. It is best accompanied by soil moisture collection fieldwork. On the other hand, bare

soil has a similar spectral response to urbanized areas, and this often creates spectral confusion similar to NDWI (Nguyen et al., 2021).

d) Bare Land Index (BLI): Distinguishing between developed and undeveloped land cover is also an appropriate strategy for coastal areas, however the inclusion of a thermal band in the calculation is a limiting factor because not all satellite sensors have a readily available thermal band (Nguyen et al., 2021).

Spectral indices are well researched and documented with a wide and highly accommodating range (Gomez et al., 2014). There are several indices that can be compared but the few mentioned here are simply to showcase the thought process that goes into determining an appropriate methodology. Having identified the possible beach system proxy indicators and their associated extraction techniques, we need to identify the available remote sensors to support the study objectives as well as how other researchers have applied all these principles to achieve shoreline delineation.

2.2.2 SENSOR DESIGN

The ability to distinguish between land covers is based on sensor specifications. It is the surface reflectance they record that allows us to identify the spectral signatures of different land surfaces (Gibson &Power, 2000). The first remote sensors were dependent on the sun as an illumination energy source as is the case with optical sensors. Nowadays, the advent of active sensors such as those that operate in the microwave range, produce their own radiation by projecting a signal and measuring the amount reflected. Their greatest advantage is that they are not dependent on variable illumination conditions (Ccrs, 2004).

Sensors can be mounted on any ground, air or space borne platform. Satellites allow for the continual repetitive coverage of the Earth's surface (Gibson &Power, 2000). Aerial platforms used to be solely based on aircrafts and collected very detailed and specific images based on the observers' necessities however the introduction of programmable UAV's has made data acquisition all the easier and more attainable (Edwards, 2001). The proximity of ground-based sensors and their ability to record more refined data means they are ideal to better

characterize imaged targets and validate other sensor platforms, they usually act as a means of ground truthing (Ashraf et al., 2011).

The different height standards for these platforms means that the swath of Earth surface observed varies. Particularly for satellites, the paths or orbits followed by sensors vary and may be geostationary (viewing the same portion of the earth), sun synchronous (maintaining constant time of observation) or Near-polar (north south trajectory) (Ccrs, 2004). Satellite platform motion is also characterized as ascending or descending passes because the satellites travel up one side of the Earth and down the other (Ashraf et al., 2011). Although the imaged area is called a swath, the smallest area of ground that is sampled is referred to as the instantaneous field of view (IFOV) or the pixel size of the sensor and this in turn relates to the concept of image resolution. Spatial, spectral, and temporal resolutions are the main consideration in identifying appropriate datasets.

2.2.3 SENSOR PLATFORM SELECTION

A multitude of remote sensors have been designed with functions in mind within their resolution competences. The potential of GIS is evident in how we use predesigned instruments and software packages to adapt to study objectives. GIS is flexible and superimposable in any field of study, which only speaks to its interdisciplinary nature. This subsection intends to identify and compare different sensors as well their technological advancements thus formulating the justification for the sensor platforms this study intends to use.

2.2.3.1 OPTICAL SENSORS

As stated, optical remote sensing is dependent on the visible portion of the electromagnetic spectrum, approximately within the 0.4-0.7µm wavelength range (Gibson &Power, 2000). Images are the result of the combination of the three primary colors red, green, and blue; each resultant color has its own specific wavelength (Ccrs, 2004).

2.2.3.1.1 AERIAL PHOTOGRAPHY

The ability to capture the near-instantaneous state of an environment is the biggest advantage of aerial imagery. They are ideal in scenarios where the spatial resolution takes precedence

over spectral resolution (Ccrs, 2004). What is referred to as IFOV for satellites is called the angular field of view in UAV's. The orientation of the camera is also of great importance; it can be oblique (side looking) which is ideal for mapping large areas to deduce terrain relief, or vertical which are built for rapid capture whilst controlling geometric distortion (Jeong et al., 2018). Navigation systems are often a part of UAV systems for accurate coordinate capture as well as inbuilt mechanisms that compensate for platform motion. As the UAV moves along the flight line, overlapping images are captured in rapid succession to ensure continuity of the scene for stereoscopic viewing because the overlap of two images means 2 different viewing perspectives, which is ideal in formulating a 3D based stereo model and the ability to infer these geometric measurements is called photogrammetry (Ccrs, 2004).

The biggest benefit of aerial photography is the ability to control the frequency of data collection along with spatial resolution, as well as the easy maintenance and calibration the sensor for optimum spectral resolution (Edwards, 2001). Quality and accuracy are always a concern however, the use of cost-effective digital color and infrared photography has grown particularly in marine based surveys. Digital technologies are more trustworthy for change detection, the use of light sensitive computer chips has done away with the need for digital film and the tedious, costly process of developing them. Images are now easily uploaded to be rectified and analyzed computationally. There is still the need to correct for the conversion of radiance to reflectance for the image mosaicking process as well as geometric correction and verifying ground control points (Malthus &Mumby, 2010).

2.2.3.1.2 OPTICAL SATELLITES

Space borne remote sensing platforms have contributed significantly to advancements in geospatial science. The launch of the Landsat satellite in 1972 made medium-resolution satellite imagery easily available and accessible (Gibson &Power, 2000). Since then, various commercial, high-resolution optical satellites have been launched such as IKONOS and Quick Bird; furthermore, satellites have been launched for the sole purpose of marine observations such as the Coastal Zone Color Scanner in 1978 (Di et al., 2003). Optical based imagery is often used for the extraction of the shoreline in coastal studies (Malthus &Mumby, 2010).

2.2.3.2 LIDAR (Light Detection and Ranging)

LIDAR based sensors operate by transmitting a pulsed laser beam towards a target and its reflectance is recorded (Stockdon et al., 2002). The pulse return time determines the distance between the sensor and the target objects, and this data is captured in the form of a dense point cloud (Ashraf et al., 2011). LIDAR is dependent on factors such as the altitude, attitude, and the scan angle of the sensor to determine the 3D position of each laser beam onto the earth surface (Pe'eri &Long, 2011). The components of a LIDAR system differ slightly depending on whether it is airborne, or ground based. In cases where funding is available, airborne bathymetric LIDAR systems are often the preference for their water penetrating capabilities (Wozencraft &Lillycrop, 2003).
The integral elements of an airborne LIDAR system that make it effective are:

1. **Differential-GPS (d-GPS**): Calculates the position of the sensor which, also incorporates the scan angle to determine the 3D position of every laser beam on the actual surface
2. **Inertial Navigation System**: Calculates the attitude of the sensor

LIDAR data has proven to be pivotal in topographic mapping of coastal areas specially to showcase erosion and accretion, which is achieved by subtracting Digital Terrain Models (DTM) (Thiebes et al., 2013). This technology can attain accuracies of up to 5-10cm and several studies have showcased the applicability of LIDAR data in shoreline surveillance (Brock &Purkis, 2009; Deronde et al., 2008; Klemas, 2011; Wozencraft &Lillycrop, 2003). The greatest advantages of LIDAR data in shoreline mapping are:

1. The ability to adequately map detailed information about the topography, near shore bathymetry and vegetation for a well-rounded perspective on the entirety of coastal environments.
2. The already incorporated statistically formulated tidal datum that allows an output that is truly referenced, and issues associated with using the waterline as proxy are overcome.

LiDAR is the most suitable for shoreline modelling because with a wavelength of 520nm (blue-green laser) it is operational for bathymetric measurements whilst a 1064nm (NIR laser) wavelength is effective for terrestrial topography. LiDAR can thus give a better

depiction of the coastal zone that includes the seabed (Klemas, 2011). This is because electromagnetic energy is greatly reduced with increased wavelength in water.

2.2.3.3 MICROWAVE SENSORS

The 1mm-1m wavelength range of the electromagnetic spectrum affords us a better opportunity to avoid spectral confusion by utilizing radar signals characterized by amplitude and phase (Ccrs, 2004; Filipponi, 2019). The amplitude relates to the strength of the radar response and thus is responsible for reflectance which results in greyscale imagery. The Phase is a single SAR wavelength or a translation of the distance between the sensor and target (Cracknell, 2010). These two factors reconstruct the imaged scene based on signal backscatter or brightness which is determined by the biophysical attributes of the target (Filipponi, 2019). For example, the rougher the surface, the greater the backscatter and the brighter the feature under observation whereas a flat surface would appear dark. The echoed signal can be complex, a multi layered surface would lead to a higher signal proportion (Ferretti et al., 2007).

Whilst this may be visually evident, pixel intensity or digital numbers must be normalised into a computationally detectable format by means of radiometric calibration. Three variations of calibration exist (European Space Agency, 2021; Miranda et al., 2015; Schmidt et al., 2020):

1. Beta (β^0) calibration: Reflectivity expressed within slant range (Surface Brightness)
2. Gamma (γ^0) calibration: Reflectivity associated with the perpendicular plane to the slant range (flattened)
3. Sigma (σ^0) calibration: Reflectivity expressed within ground range (Surface Backscatter)

Factors such as local incidence angle, dielectric current and polarisation of ground targets also relate to surface reflectivity and conductivity (Kaplan et al., 2021). Dry natural materials have a dielectric constant of 3 to 8 however water has a constant of up to 80. As such moisture in soil or vegetation results in significant reflectivity. The theory of polarisation is based on the rotation of electromagnetic energy as it passes through dynamic materials. This energy is transmitted or received as either horizontal (H) or vertical (V) and helps to measure reflectivity.

Differential Interferometry Synthetic Aperture Radar (DInSAR) is now the preferred approach with radar data in coastal erosion studies. The phase difference between two images taken from two different points of view as a satellite traverses the same orbit, is used to obtain an interference pattern to extract terrain change, deformation patterns and elevation (Ferretti et al., 2007; Mason et al., 1999). The difference between these two views is the baseline. If the baseline is too short, signal phase difference can be undetectable whilst too long of a baseline may introduce additional noise in an image (Prats-Iraola et al., 2015). DInSAR has been used to map coastal zones as well as generate DEM's and has the advantages of being able to penetrate shallow waters to capture bathymetric features, as well as being operational in all weather and day or night conditions (Horritt et al., 2001). The temporal lag between the two acquisitions with different angles is still an issue (i.e., low coherence due to long baseline, decorrelation caused by incidence angles impacting the backscattering, and changes in surface roughness from a tidal cycle to another). This limits the use of this method to single-pass interferometry systems for which there is no temporal decorrelation.

Remote sensing is clearly an appropriate tool for coastal monitoring. The variety in technology and data accessibility determines study limitations. The theory associated with beach systems and remotely sensed data is combined below to determine appropriate measurable coastal indicators.

2.2.4 COASTAL OBSERVATION INDICATORS

The coastal factors presented in section 2.1 on page 9 show how dynamic beach systems can be. The most appropriate methods must be applied for the detection of coastal landform indicators that act as proxies for erosion. Based on the prescription of Boak and Turner's (2005) work, indicators have been categorized as visibly discernible features, tidal datum based and on extraction techniques (Boak &Turner, 2005). The choice in indicators is usually decided looking at the temporal resolution within the context of the study. Table 1 below summarizes these indicators (Boak &Turner, 2005; Gens, 2010; Toure et al., 2019).

Table 1. Coastal indicators

Indicator Category	VISIBLE	TIDAL-DATUM	EXTRACTION
Definition	Physical morphological features that can be seen in imagery.	Combination of beach profile with a specific vertical elevation through tidal parameters.	Extracting shoreline features using image processing techniques.
Examples	High tide wet/dry boundary, vegetation, dune line	Mean Sea Level (ML), Mean Lower Low Water (MLLW)	Elevation modelling
Potential data sources	Aerial photographs, Coastal maps and charts, Historical photographs, Multispectral satellite remote sensing, Microwave sensors	Tide data, Coastal maps, and charts	LIDAR, GPS shorelines, stereo-optical images, SAR, Beach surveys, Microwave sensors
Advantages	Relatively easy, more indicators to work with	Objective and numerically definite.	Good and easily adjustable resolution during field surveys Data collection easily adjustable to tide levels for optimum coverage
Disadvantages	The manual approach means visual interpretation is very subjective. Affected by wind, tide, meteorological factors	Datum shifts and conversions are an intricate concept to execute. Inconsistent tide data collection.	Field surveys can be tedious

2.2.4.1.1 THE WATERLINE METHOD

Whilst Interferometry is the first choice for elevation modelling in satellite remote sensing, Mason et al. (1995), introduced a more precise technique that combined proxy and datum-based coastal indicators called the waterline method, which incorporated the use of both images and hydrodynamic models (Mason et al., 1995). Image processing techniques were used to determine the position of the water's edge and thereafter a hydrodynamic tide-surge model coinciding with the acquisition time of the images was used to predict water elevations that were then superimposed along the waterline. The use of multiple images depicting various tidal conditions meant a cluster of waterlines could be generated and used to build a gridded DEM with both spatial and temporal dimensions and thus occurrences such as erosion could be measured (Mason et al., 1995). The hydrodynamic models introduce a more well-rounded approach because the tide momentum and wind stress are also influencers of coastal erosion. Only the incorporation of bathymetric data would strengthen this technique.

Beach profiles may have the same general structure, but the slight differences caused by sedimentary evolution and water movement means that there is a need to identify more definite indicators to properly define individual study sites (Toure et al., 2019). The detection of these indicators allows for the understanding of the profile's environmental modifications. The assortment of these indicators is usually the reason an array of sensors and geoprocessing tools is recommended to account for the dynamic spatial, temporal, and reflective properties of littoral surfaces (Gens, 2010; Toure et al., 2019). Although the waterline is the most accessible and widely used indicator, its subjectivity is why datum-based indicators are introduced by means of sea level data which is not a visually detectable indicator and as such image extraction techniques must be applied to the data for digital model generation (Amaro et al., 2014; Gens, 2010)

2.2.4.1.2 RELATING SOUTH AFRICA'S LAND AND HYDROGRAPHIC DATUMS FOR COASTAL MAPPING

South Africa uses a 2D+1D coordinate system. This is to say horizontal and vertical coordinates occur on different datums (Department of Rural Development and Land Reform, 2013). The Surveyor General has specified the national land leveling datum as measured

from the Hartebeesthoek94 Datum, referenced from the WGS84 Ellipsoid. The South African Navy Hydrographic Office (SANHO) also has its own chart datum reference for its tide measurements being the Lowest Astronomical Tide (LAT) which is the lowest predictable tide over a period of 19years (Ocean Rhythm, 2021). As shown in Table 2 on page 32, SANHO determined the offset between the land and tide datums to be -0.98m in 2018 which is to say SANHO's soundings are measured 0.98m below the WGS84 ellipsoid. This is highlighted in red in Table 2 and Figure 5 on page 31, which shows how these datums relate based on a typical beach profile. Because the mean sea level (ML) fluctuates, a general tidal range is established between the Mean High Water (MHW) and Mean Low Water (MLW). The influence of neap and spring tides is also depicted in Figure 5 along with their specific chart datum levels in Table 2.

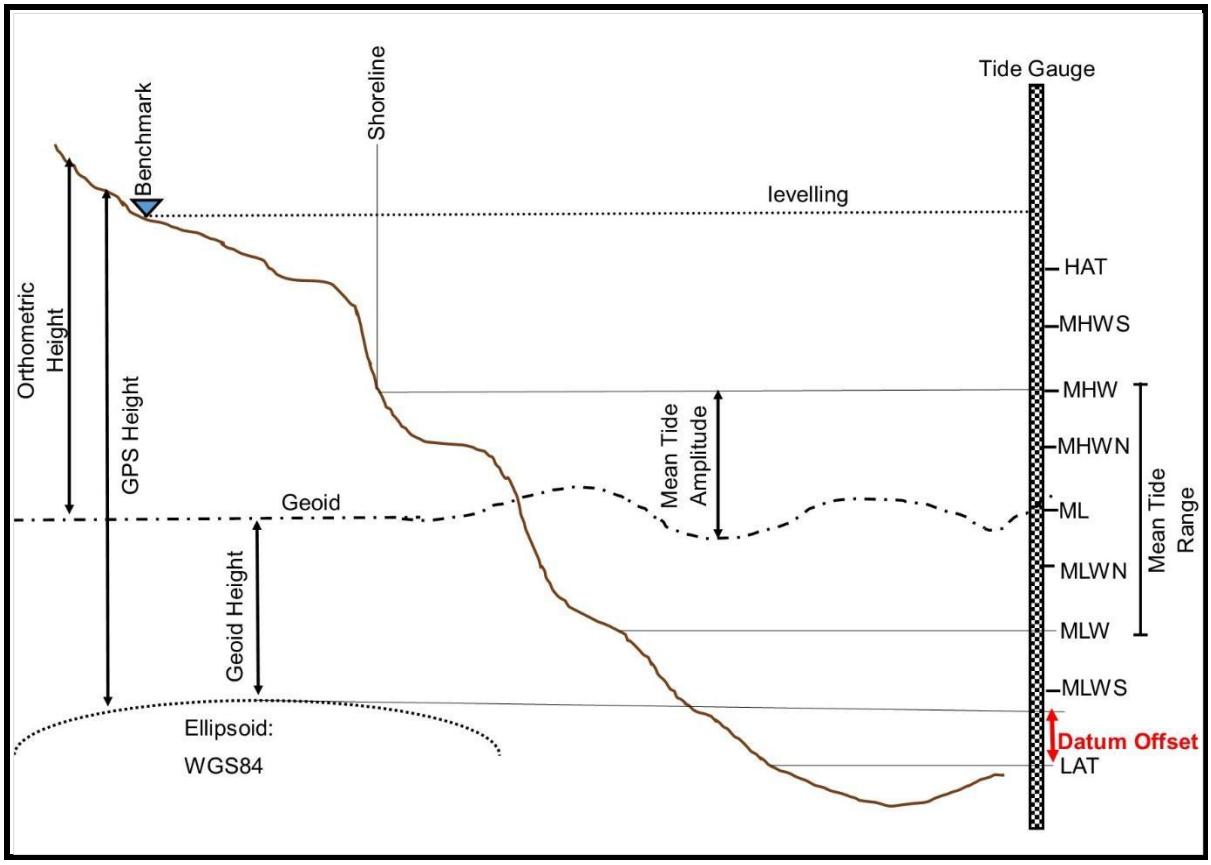

Figure 5 Comparison of land and hydrographic datums.

Table 2. Cape Town tidal levels (Source: SANHO-2,2018)

DESCRIPTION		LEVEL IN m	
		RELATIVE TO MEAN LEVEL	RELATIVE TO CHART DATUM
Highest Astronomical Tide	HAT	+1.04	+2.02
Mean High Water of Spring Tide	MHWS	+0.76	+1.74
Mean High Water of Neap Tide	MHWN	+0.28	+1.26
Mean Level	ML	0	+0.98
Mean Low Water of Neap Tide	MLWN	-0.28	+0.70
Mean Low Water of Spring Tide	MLWS	-0.73	+0.25
Lowest Astronomical Tide	LAT	-0.98	0.00
Chart Datum	CD	-0.98	0.00

2.3 CURRENT LITERATURE ON COASTAL REMOTE SENSING

The literature highlighted in this section draws from the fundamentals of the theoretical framework of sections 2.1 (page 9) and 2.2 (page 16); and illustrates how remote sensing researchers have embraced and challenged these concepts to address questions in their areas of interest. The general trend is in efforts shifting from just monitoring to predictive modelling with an inclination towards tide-coordinated shoreline generation (Li et al., 2003).

2.3.1 APPLICATION OF OPTICAL SENSORS IN COASTAL EROSION MONITORING

Satellites are the most widely used remote sensors for shoreline extraction due to their data being easily accessible. As per the usual prescribed methodology, images are pre-processed by undergoing geometric, radiometric, and atmospheric correction to normalize the reflectance values between the images. The ease of access to satellite data is evident in the numerous studies that have been conducted to varying degrees of resolution, region, time scales and software (Toure et al., 2019; Zollini et al., 2020).

In Batu Pahat, Malaysia SPOT 5 imagery was used to monitor shoreline changes between 1984 and 2013 by creating a spatial model in ArcGIS that was able to further predict sea level rise and potential future flood risk areas (Maulud &Rafar, 2015). A similar process was

applied by Guimarães et al. (2014) along the Amazon coastal zone using multiple Landsat sensors instead. After pre-processing and sorting, NDWI was used to implement the decision tree technique producing two different types of products that allowed for the identification of water bodies whilst dealing with cloud correction (Guimarães et al., 2014; Sousa et al., 2018). A simple image subtraction was enough for change analysis whilst in the Bay of Bengal edge detection was used to segment and threshold images based on NIR bands, and the change rates were determined through linear regression (Maiti &Bhattacharya, 2009).

Landsat 5 Thematic Mapper (TM) images have proven to be adequate in overcoming tidal factors for shoreline mapping at a spatial resolution of 30m (Guariglia et al., 2006). A study achieved coastal change decadal analysis from 1985 to 2015 through the Landsat Ecosystem Disturbance Adaptive Processing System software to extract shoreline information however ultimately shoreline extraction was achieved through visual interpretation (Guo et al., 2016). A prognostic coastal erosion model was produced by Shiyong et al. (2016) using high resolution data (0.5m) through the Digital Shoreline Analysis System (DSAS) extension within a GIS based environment. The rate of change was determined using images from 2011 to 2014 by extracting the shoreline through visual interpretation. DSAS was used to formulate the model based on the past historical positions of the shoreline and used to predict the shoreline for 2015. It was validated with the addition of field data acquired through a centimeter accurate Global Position System (GPS) in 2015 (Amaro et al., 2014; Toure et al., 2019). In some instances, researchers have preferred to use high resolution images such as from IKONOS or Worldview as validation for medium resolution images through super resolution mapping soft classification (Foody et al., 2007).

Some studies have shown a preference for data fusion through a combination of both sensors and extraction techniques. For example, Suwanprasit combined variations of spectral indices, image enhancement techniques and classification on images from Landsat 7, Spot 5, ASTER and THEOS satellites (Suwanprasit, 2015). The author was able to determine land cover changes that showed an increase of built-up areas whilst beach areas continued to spatially decline further highlighting the pressures of urban sprawl on coastlines. The best accuracy with a 0.99 Kappa Coefficient was deduced from combining SVM and NDVI on the Landsat image (Suwanprasit, 2015).

Sousa et al. (2018) pursued the application of geostatistical methods and digital image processing algorithms to formulate a computational solution in estimating the evolution trend of erosive processes (Sousa et al., 2018). The goal was to improve existing methodology to the point of formulating an automated process for shoreline extraction and time interval predictive models based on linear regression. Images were acquired from Landsat 5-TM and Landsat 8-Operational Land Imager (OLI) for the Icapuí municipality in Brazil. They applied the MNDWI algorithm along with a regression method based on the work of Sousa et al. (2012), which adjusted the linear regression equation to accommodate the extrapolation of time series imagery through a sequence of images from previous years (Sousa et al., 2018).

After extrapolation, Gaussian filters and thresholding were used for classification and noise removal through the application of Python programming processing libraries. Instead of the usual subjective visual interpretation approach, an edge detection algorithm was applied to extract the shoreline (Sousa et al., 2018). Mean Absolute Error was determined to be between 93% and 97%. Based on this methodology, they were able to identify the largest coastline variation, which they determined was mainly due to the lateral addition of sandy spits occurring in an east-west direction and that this approach is applicable in scenarios of rectilinear coast lines or complex situations where frontal and lateral accretion are involved. Although the authors managed to prove the capability of a computerized approach, they still suggested a field survey for validation as an alternative approach (Sousa et al., 2018).

2.3.2 APPLICATION OF LIDAR TECHNOLOGY IN COASTAL MONTORING

As discussed in the theory (Chapter 2 on page 9), shoreline position can be estimated through various techniques. LiDAR technology allows for rapid, low-cost, high-resolution, and high-accuracy morphological mapping. Victor Klemas (2011) used case studies to review the efficiency of LiDAR for shoreline observations citing a vertical accuracy of up to 10cm inclusive of both topographic and bathymetric modelling (Klemas, 2011). Scanners are ideal for shoreline delineation because their interaction with sea water results in a noisy output. Cross-shore profiling is popular with LiDAR data and a tidal datum is often used to improve the accuracy (White &Wang, 2003). Linear regression is applied to the cluster of collected points to determine the shoreline position based on the elevation datum (Klemas, 2011). Regarding accurate bathymetry modelling, LiDAR and acoustic sounding have proven to be

most accurate because multispectral imaging proves inadequate when addressing water column turbidity (Klemas, 2011; Pe'eri &Long, 2011).

Whilst a terrestrial LiDAR survey may prove tedious, Stockdon et al. (2002) and Morton et al. (2005) implemented the cross-shore profile method. Reflectors were fitted along a foreshore profile and the resultant regression line intersected with water level to extract shoreline points which were then extrapolated to form a shoreline (Morton et al., 2005; Stockdon et al., 2002). On the other hand, Robertson et al. (2004) used the contouring method to extract a tide referenced shoreline by applying a zero value to the water line and the chosen tidal datum was simply subtracted from the DEM (Robertson et al., 2004). This, however, proved to be less accurate because manual editing and re-digitization are required for correction. An automated segmentation-based approach that intersects a LiDAR DEM with a tidal datum surface has also been suggested (Gens, 2010).

Researchers have challenged this labor-intensive approach by opting to use a rapid survey method for morphological mapping. Utilizing only one reflector and instantaneously georeferencing cloud points within a Texas wetland, Xiong et al. (2019) compared their results to kinematic GPS measurements and found an optimum correlation enough to verify a vertical accuracy of 3-5cm and 2-3cm for their elevation models (Xiong et al., 2019). The authors agreed that the combination of TLS and GPS measurements as a highly dependable technique for erosion studies. Whilst they also concluded that ALS was the new frontier for applying LiDAR in coastal environments, there is still fieldwork associated it with the need for ground control points (Xiong et al., 2019).

This technique was implemented along the sandy East Sea coastline in Korea by integrating topographic data from both ALS and UAV data (Lee et al., 2019). Their quantification of shoreline change was calculated using Linear regression within the Digital Shoreline Analysis System (DSAS) tool whilst morphological changes were deduced by subtracting digital surface models. They compared the long-(2008-2018) and short-(2016-2019) term results to find a majority long term seaward movement of 1.64-9.22m whilst the short term showed a landward movement of 0.7-1.10m. Interestingly their surface models were able to detect volumetric changes with a $0.08m^3$ erosional deficit and $0.42m^3$ of accretion (Lee et al., 2019). They credited these changes to the infrastructural developments within the area. The

conflicting results between sub-sections of their study area proved how consecutive stretches of coastlines react differently under different environmental conditions.

The laser altimetry approach was instrumental in achieving both a visual and quantitative assessment of the spatial variability associated with barrier island morphologic changes in North Carolina (White &Wang, 2003). Researchers were able to determine over wash as the driving force behind landward migration. Volumetric changes were extracted from DEM's with 1.5m horizontal- and 0.15m vertical resolution and statistically linked back to coastal management styles and bad weather (White &Wang, 2003). This technique was only possible because of consistent annual data collection and proves the applicability of LiDAR data in a different coastal setting.

The United States Army Corps of Engineers (USACE) has showcased the potential of LiDAR data in large-scale coastal monitoring projects and have made it their primary source of data for the National Coastal Mapping Program (NCMP), which makes use of the Compact Hydrographic Airborne Rapid Survey (CHARTS) (Klemas, 2011). It implements an integrated sensor with a bathymetric- and topographic laser, along with a digital multispectral camera. It has led to the seamless formulation of bathy/topo grids, infrastructural footprints, shorelines, seabed imaging, and land cover classifications. Since 2004 this program has helped to create a regional coastal morphological change tool that encompasses both temporal and spatial dimensions. Coastal managers have consistently shown a preference for LiDAR because it is effective for flood zone demarcation, advising on beach-nourishment, and mapping real time storm effects. As popular as it is, it is expensive to maintain (Klemas, 2011).

2.3.3 APPLICATION OF RADAR SATELLITES IN COASTAL MONITORING

Whilst optical and LiDAR technologies were the cornerstone of coastal monitoring, it has evolved to incorporate Radar data. There is now a vested interest in this area of remote sensing research. 1978 saw the launch of the SeaSat satellite and thus the introduction of SAR imagery as a means for shoreline extraction (Loubersac, 2003). Several studies through the years have utilized edge-tracing, wavelet theory and speckle reduction tools (Horritt et al., 2001). To address the inability to prove shoreline positional accuracy, there have been attempts to combine contour models with speckle sensitive edge detectors.

With the progress within this field of study, it has become evident that the SAR echo detection depends on the state of the sea due to factors such as wind and waves causing echo fluctuations. It is evident that a shorter wavelength is far more accurate in determining a shoreline regarding Bragg scattering, which is the result of radar waves being reflected by turbulent sea spray (Zhang et al., 2021). In 2004, Baghdadi et al. (2004) concluded that due to the high incidence angles, Radarsat-1 images produced a well-defined shoreline, however the launch of Sentinel 1 rendered it obsolete with far more superior resolution (Baghdadi et al., 2004; Gens, 2010). The science behind radar remote sensing is complex and some studies have gone further to determine the significance of radar frequency on shoreline mapping. Interesting erosional studies have also been attempted in atypical coastal environments such as Antarctica where the task of compiling a geocoded image mosaic was achieved from Radarsat-1 SAR imagery (Jezek &Liu, 2005).

Edge detection or waterline extraction for radar images can be problematic due to the speckle noise (Niedermeier et al., 2005). Several approaches have been implemented to extract waterlines such as the multi-scale edge detection algorithm proposed by Mason and Davenport (1996). Other research avenues included active contouring, as well as wavelet-based edge detection methods adapted to SAR images, and k-means clustering (Barbosa et al., 2014). The Sentinel-1 SAR constellation (Sentinel-1A and Sentinel-1B) have a 12-day revisit time over the same area. Therefore, the acquisition period needed for sampling the whole tidal range can be reduced.

Coherence mapping featured in the use of ERS 1 images in a flood mapping study. Horritt et al. (2001) applied an automatic segmentation algorithm on the images through a statistically active contour model to overcome the limitation of the multiplicative nature of speckle noise causing inaccuracies in edge detection (Horritt et al., 2001). The work Mason produced as part of a research team in 1999 formed the foundation for coastal erosion studies (Mason et al., 1999). Waterlines were extracted and DEM's generated. An area of approximately 350km was depicted through height maps of a 50m spatial resolution and 40cm height accuracy. Subsequent maps were subtracted to determine the change in sediment, as well as link the results to a decrease in mean sea level (Mason et al., 1999). More currently, Salameh et al. (2020) used the foundation of Mason et al. (1995,1999,2000) to lay out an improved, efficient methodology for semi-automatic detection of waterlines where the use of post-processing

algorithms and active contouring allow for the generation of DEM's using sentinel 1 and 2 data (Salameh et al., 2020). These studies only prove how the evolution and adaptability of remote sensing technologies as well as their combination has led to an innovative theory that has shaped an important branch of research.

2.3.4 MULTI-DIMENSIONAL DATA FUSION FOR SHORELINE MEASUREMENT

The preference for multisource data has grown due to the implications of tidal variations on spatial resolution and spectral confusion (Andréfouët et al., 2003). Consolidating data from multiple sources allows for the creation of a unified, centralized perspective of the datasets to assist in formulating well informed decisions. Data must be collected, stored, transformed, and disseminated in a way that preserves the integrity of any study. The repeatability and thus the success of any study lies in its data management plan. It is evident that although each of these remote sensing techniques has their own merits, there are still shortcomings to be addressed. The solution lies in identifying appropriate data fusion or compatibility mechanisms. Several integration software's, algorithms and processes are designed to accommodate data fusion.

Malthus and Mumby (2010) reaffirmed the necessity of a more synergistic approach to the incorporation of remote sensing tools. Integrating various datasets in coastal erosion studies is inevitable because there's a need to identify the limits and influence of coastal waters along with human activities (Malthus &Mumby, 2010). For example, LiDAR may supply positional data whilst optical data offers spectral information and radar data focuses on the structural geo-morphodynamical aspects of the coastline. Although studies in the past have focused on individual aspects of coastal environments, there has been a shift towards more all-encompassing studies due to the growing attraction of integrated studies (Boak &Turner, 2005; Toure et al., 2019). Ultimately, shoreline detection is dependent on spatial and spectral resolution. The higher the resolution, the better the accuracy. Being able to control flying heights, acquisition times and sensor positioning means there is more flexibility in scale when using ground and airborne based platforms as well as being able to synchronize data collection according to tides as opposed to satellites which are bound to pre-programmed orbits (Jeong et al., 2018).

Deronde et al., (2008) conducted a study that combined remote sensing and soil science principles in 3 distinct study sites on the Belgian coast for the period of 2000 to 2004 with hopes of insight into the longer-term changes of erosion by using LIDAR and hyperspectral imagery for analysis (Deronde et al., 2008). Morphological filtering and the reduction of point density allowed for the creation of erosion and accretion maps by subtracting subsequent DTM's from each other. Vertical accuracy was approximated to be 5cm ±7mm. The volume differences were calculated first by polygon and secondly by coastal zone to integrate larger beach areas between the low water mark and dune foot. The inclusion of hyperspectral imagery further validated the study by using a CASI scanner which operates within the 545nm spectral range (visual and near-infrared range) for the years 2000 to 2003 and an AISA-Eagle (400 and 900 nm range) was used for 2004. Nearest neighbor was used to resample data to 2m x 2m. After geometric and radiometric correction, they were able to classify the beach sediment into 7 sand type classes based on the reflectance values of the sediment top layer using the linear discriminant classifier and sequential floating forward search algorithm (Deronde et al., 2008).

This was confirmed by field work in the form of sampling, which served as a means of training and validation of classifications, ensuring to collect both wet and dry samples to reflect both the intertidal and the supratidal beach because the effect of wetness on the spectral signature needed to be taken into consideration. It was found that these sand classes had a direct correlation to the topography and geomorphology of the shoreline, for example fine sand on the lower shore face features a particular mineralogical, grain size and sorting composition (Bernard O. Bauer &Davidson-Arnott, 2002). If found elsewhere on the beach, then the spatial dynamics of the sand classes can be determined and thus the morphodynamics of the coastal environment. As such sand classification allowed for a tracer analysis to determine sediment movement.

The combination of laser scan and hyperspectral datasets allowed for a comprehensive qualitative analysis of sediment dynamics inclusive of volumetric changes, mean height differences and sediment transport direction further highlighting the necessity to combine multispectral data and the potential of data fusion (Brock &Purkis, 2009; Thomson et al., 2010). Not many studies make use of hyperspectral data due to logistical and financial constraints. The low resolution of the Compact High Resolution Imaging Spectrometer (CHRIS) instrument on the Project for On-Board Autonomy (PROBA) satellite and Hyperion

on the Earth Observing-1 (EO-1) did make the use of space borne hyperspectral data undesirable (Deronde et al., 2008). As such, with adequate financial support airborne platforms are usually preferred especially with concerns of meteorological and tidal constraints. However, the introduction of UAVs with active sensors has led to more targeted data acquisition opportunities in coastal surveying and observing smaller time scales will allow us a better understanding of sediment transport processes. Major limitations were mainly organizational for this study; for example, no data could be sourced for 2003 and the datasets were not always in sync time wise (Deronde et al., 2008).

Amaro et al.(2014) designed a labor-intensive methodology that incorporated both moderate and high-resolution satellite imagery, as well as a Post Processing Kinematic (PPK) GPS survey (Amaro et al., 2014). It allowed for both a short- and long-term analysis of sediment movement on the Ponta Negra beach in Brazil. Their optical imagery proved that tidal height was the most significant factor in image acquisition with an accuracy of 0.5 pixels as such images were acquired during neap tides. 3-Dimensional (3D) modelling was based on geodetic surveys (Amaro et al., 2014). A local positioning reference base was established through the installation of geodetic stations based on the Brazilian Institute of Geography and Statistics NBR 14166 relative to the Brazilian Network of Continuous Monitoring of GPS System (RBMC). 3 other stations were installed with an approximate distance of 3.5km between them. From these stations, coordinates, standard deviation, ellipsoidal elevation and orthometric height were determined (Amaro et al., 2014).

A GPS receiver mounted on a quad-motorcycle acted as a rover receiver linked to the GPS antenna at the main reference base. The shoreline position and the 3D condition of the beach morphology were modelled within a horizontal and vertical accuracy of 5mm. To further validate results, Electronic Distance Measurement (EDM) instruments were used to evaluate the accuracy of the generated DEM through cross-shore topographic profiles. The major advantage of applying this LIDAR technique is the ability to organize a survey with a wide range of points covering a large area and generating sequential DEM’s to estimate volume balance and sediment accretion or erosion rates (Brock &Purkis, 2009). From error analysis it became apparent that the DEM’s generated here were equivalent to those from traditional topographic profiles. The terrestrial survey confirmed the satellite-based shoreline

propagation data and distinguished erosion-accretion segments along the beach (Deronde et al., 2008).

Based on their findings they were able to identify sediment supply zones along the beach and relate their findings to anthropogenic influences such as runoff from drainage systems in the area. This case study illustrated the influence of urbanization on coastal areas, and this presents an avenue to assist with decisions regarding coastal demarcation, defining coastal erosion risk areas and strategic intervention for coastal protection and urban sprawl. Studies such as this showcase the potential of predicting future shoreline positions based on multisource data from various spatio-temporal contributions.

Although there have been attempts to create sensors solely for coastal monitoring, they are only designed to measure a few parameters. The necessity of sensors with specific spectral resolutions based on the spectral signatures of coastal areas has been of particular concern to researchers. For example, mapping sediment transport at the mineral level is next to impossible because sensors cannot distinguish between minerals due to the close variability of reflectance spectra. Future designs need to be based on scientific and practical objectives for an effective data acquisition strategy for efficiency, reliability, flexibility, coverage, frequency, and risk (Malthus &Mumby, 2010).

The studies reviewed here conclude that optimum results are achievable with the combined effort of multiple remote sensing techniques. This chapter showcases how multifaceted coastal erosion studies can be and allows for an appreciation of how varying perspectives can be inspired from underlying theories.

2.4 SUMMARY

The Foundational concepts presented here showcase the potential of remote sensing as a tool for coastal monitoring. It has drawn on the major influences on coastal areas and specifically on sediment movement which is the shoreline defining process. It has highlighted the typology associated with shorelines, along with the accuracy that tide observations lend to shoreline assessments. Whilst there is an assortment of remote sensing platforms, their applicability is also determined by the chosen coastal indicators.

There have been several endeavors to conduct a comparative breakdown of remote sensing techniques based on differing project objectives (Boak &Turner, 2005; Cracknell, 2010; Hamylton, 2017). With countless researchers emphasizing the threat of coastal geohazards through the widespread modification of sandy shore ecosystems as well as the many factors involved, GIS has provided a multifaceted avenue to incorporate various perspectives (Desportes &Colenbrander, 2016; Klemas, 2011; Suwanprasit, 2015; Toure et al., 2019). The next chapter is a review of related literature, and it demonstrates how researchers have been able to manipulate these components to deduce actual coastal erosion measurements.

3 LITERATURE REVIEW

Past studies, scientific reviews and case studies are presented in this chapter to justify the stance adopted by this study in addressing the research objectives and to showcase how the principles of remote sensing have been applied in coastal monitoring as well as its implementation in related world scenarios. A case study of the Cape Town coastline is presented and related it to the city's urban sprawl spatially and legally, which addresses objective 3; Objective 3: Investigate the City of Cape Town's legal frameworks and how GIS has been adopted to mirror them for coastal area management on page 6 about the sphere of influence of legislature in coastal management. There is a need to acknowledge and appreciate technological advancements in this area of expertise. Through an objective comparison of methodology, the best approach for this study was deduced.

3.1 CASE STUDY: THE CAPE TOWN COASTLINE

This subsection examines the evolution of Cape Town's shoreline along with its geomorphological influences and delve deeper into the legislature that governs its coastal areas. Studies have concluded that the South African coastline has an equal proportion of rocky, rugged cliffs, sandy and mixed beaches; these include well sheltered bays as well as exposed stretches of coast (Department of Environmental Affairs : Oceans and Coasts, 2015; Fourie et al., 2015; Harris et al., 2011). South Africa's sandy coastlines are generally considered high energy and thus more susceptible to erosion (Cartwright, 2011). Although the south-west coast exhibits all the morphodynamical types, its beaches are wave dominated and have rocky subsections interspersed with smaller reflective and intermediary beaches (Harris et al., 2011). Understanding these soft shore dynamics helps to identify tools that take tidal characteristics and sediment volumetrics into consideration for the observation of coastal landforms and their boundaries (Deronde et al., 2008).

Several models have been attempted to relate and encompass the complexities between global and local sea level (Wigley, 2011). The most significant coastal geohazards within the Western Cape are:

1. Erosion
2. Inundation

3. Wind and wave impacts

The expectation is for enhanced global warming to increase average wind velocities (Theron &Rossouw, 2008). A 10% increase in wind speed is expected to lead to a 26% increase in wind stress, wave heights and thus wave power and ultimately a 40-100% increase in longshore sediment transport (Theron &Rossouw, 2008). Midgely et al. (2005) identified similar vulnerable coastal areas to Theron and Rossouw that included Northern False Bay, Table Bay, The South Cape Coast, Mossel Bay to Nature's Valley, and Saldanha Bay based on predicted climate change data (Midgley et al., 2005). Colenbrander et al., (2014) updated this list and went on to further generate the following map that illustrates Cape Town's vulnerable coastal areas as of 2014 (Colenbrander et al., 2014).

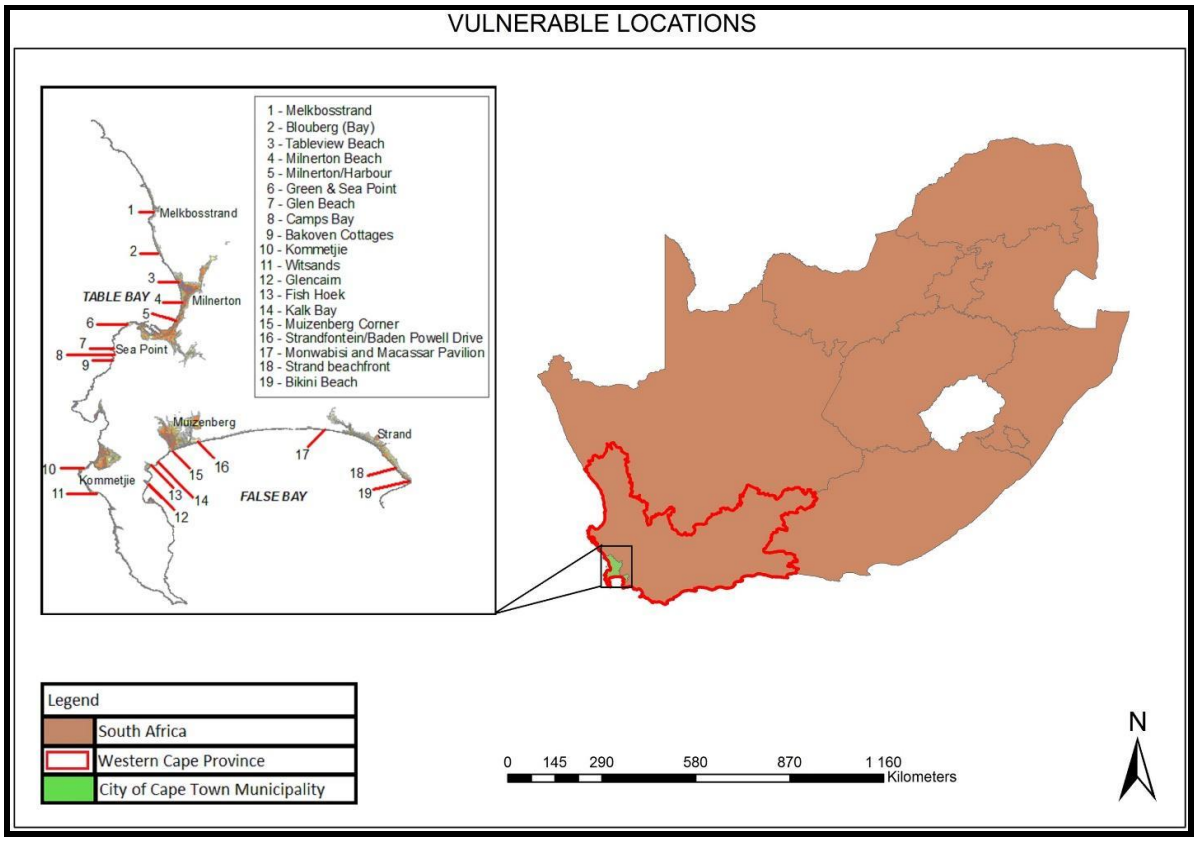

Figure 6 Vulnerable Cape Town coastline locations

Source:(Colenbrander et al., 2014)

To give a well-rounded perspective following factors were considered:

a) COASTAL TYPE AND HYDRODYNAMICS

Varying degrees of erosion, deposition, transportation, and accretion occur due to the combined effects of water and wind movement. Regular, semi-diurnal tides along the South African coastline are generally described as micro tidal, rarely going above a height of 2.2m (Searson &Brundrit, 1995). Near shore currents are influenced by wind direction along Table Bay. The combined effect of wind and waves has an overall effect of causing sediment transporting currents. North-easterly winds are prevalent in winter as opposed to south-westerly in summer (Hughes, 1992). Wave impacts have been altered by infrastructural developments whilst dune field rehabilitation and the presence of kelp beds acting as coastline defenders. Although they are effective in this regard, kelp is still harvested and cleaned off beaches when washed up even though they act as good dune fertilizers and binding agents to reinforce beach structure. Mechanized beach cleaning also causes destabilization of beaches (Mukheibir &Ziervogel, 2006).

b) GEOLOGY

The Cape Peninsula is characterized by 3 main types of foundation, the Malmesbury group (600 ma), the very resistant Table Mountain (520ma) group, which accounts for majority of the mountain ranges in the region, as well as the intruding Cape Granite (540ma) (Merwe, 2017). South Africa has few bays because of the prevalence of coast-parallel linear geological structures that prevent the formation of bays and in Cape Town, the headlands help to shield the sandy beaches from the direct contact with southwestern swells (Rust, 1991). They induce a refraction pattern that results in the logarithmic curve of the bays. Table Mountain's sandstone is the biggest contributor to the irregular Cape coastline. The alternation of resistant quartzite and less resistant Bokkeveld shale have created headland bays along the south Cape coast through the joints and faults from the Cape Fold belt (Hughes, 1992; Rust, 1991).

These weaknesses in the rock foundation have allowed wave action to shape the shoreline. The extent of weathering and erosion of the parent rock is also significant because as shown in Figure 5 on page 14, fine sand grains are typically associated with gentle sloping beaches (Colenbrander et al., 2014). A large portion of the Cape Flats and Peninsula is covered by Aeolian and marine sands. Fluctuations in sea level over millions of years have left behind shell fragments mixed in with beach sands as well as estuarine muds overlain by calcrete-cemented dune sand (Cartwright, 2011). With the prevailing soil type being sandy, coupled with high exposure; erosion is only intensified.

c) METEOROLOGICAL INFLUENCES

The South-western Cape bioregion has a very complex Mediterranean climate with inter-annual variability in weather patterns due to the influence of topography in the region (Hughes, 1992). Generally, with global warming, expected higher temperatures mean more atmospheric water vapor leading to increased orographic rainfall (Fourie et al., 2015). Low pressure systems have coincided with winter rain at temperatures ranging between 7^{o} and 15^{o} between April and August whereas high pressure systems in the spring from October to December lead to increased hot, dry berg winds with temperatures at 15^{o} and 26^{o} (Cartwright, 2011). The expectation is for coastland areas to experience the least increase in temperatures even with the influence of global warming (Hughes, 1992; Wigley, 2011). Increased temperatures could mean change in circulation patterns or sea surface temperatures causing an imbalance for the organisms' dependent on these ecosystems (Griffiths et al., 2010). Global warming is already increasing the occurrence and scale of sea-level rise, storms and thus erosion (Mukheibir &Ziervogel, 2006).

Cape Town has already experienced extreme weather events such as intense storm conditions in March 2003 and April 2005 as well as the more recent 2017/18 drought (Pascale et al., 2020). Extreme events are expected to increase along coastlines, and their combined effect will only increase erosion rates (Department of Environmental Affairs: Climate Change, 2018). Global warming will only increase the occurrence and scale of sea-level rise, storms and thus erosion (Mukheibir &Ziervogel, 2006).

d) COASTAL MODIFICATION AND DEVELOPMENT

Cape Town has experienced significant infrastructural development along its coastline and to accommodate this, several marine engineering solutions have been employed to mitigate the effects of the variable shoreline (Musekiwa et al., 2015). The most vulnerable areas occur on reclaimed land because of the effect of waves on the unstable deposited material as opposed to the original parent material. Sea walls have been the most common measure with varying degrees of success to prevent wave erosion by reducing incident energy and thus turbulence (Mukheibir &Ziervogel, 2006). The Sea Point sea wall has been operational for over 70 years, however high tides and storms result in the need for periodical repairs. Areas such as Strand, have poorly designed sea walls that lead to overtopped coastal roads and flooding of residential and commercial properties. Coastal realignment and dune cordons have been

suggested because current repair efforts and costs are unable to keep up with erosion rates (Colenbrander et al., 2014).

Coastal dunes act as a natural coastal defense around the City, however they are under threat because of sand mining or not getting replenished by aeolian sands from the Cape Flats or river systems due to development restrictions. Therefore, they require human intervention such as dune grass replanting or sand replenishment to continue to act as sea-level rise buffers (Colenbrander et al., 2014).

Less repair intensive structures such as the groynes along the False Bay coastline in Monwabisi placed perpendicular to the ocean and can be made of either wood, concrete, or rocks to specifically tackle long-shore drift and erosion. Their greatest disadvantage in this area has been the creation of dangerous currents that carry sand offshore (Colenbrander et al., 2014). Baden Powell Drive is a prime example for the effects of inundation, windblown sand and storm damage affecting structures that occur within the littoral zone that has led to repetitive sand clearing exercises (Cartwright, 2011).

Barrages and barriers are a suggested more costly alternative to protect areas around the Milnerton lagoon, Marina da Gama and the Victoria and Alfred Waterfront. Although these barriers make sense in being closed during periods of high-risk tides, they have the disadvantage of disrupting natural tides and adversely affecting the surrounding areas as well as blocking animal movement (Hughes, 1992). The building of barrages and alternatives like raising infrastructure such as the roads at Paardon Eiland would require in depth shoreline assessments. Seemingly several efforts have been implemented in this area of Table Bay including Dolosse to dissipate wave energy for the protection of reclaimed land, however these have a temporary life span (Colenbrander et al., 2014).

e) LEGAL FRAMEWORK

There are several definitions of the coastal zone, however, South Africa's 1982 Environmental Conservation Act spatially defines this zone as any land that is within 1000m of the high-water mark (Department of Environmental Affairs : Oceans and Coasts, 2015). In 1989 the Council for the Environment emphasized the inclusion of geomorphological coastal

features such as "*coastal lakes, lagoons, estuaries, dunes, beaches, rocky shores and, in some cases, offshore islands*" (Rust, 1991). Legally speaking, the coastal zone is defined as any area on, in and above coastal public property (Admiralty Reserve), the coastal protection zone, coastal access land and special management areas.

The significance of coastal goods and services in the past has never been fully understood. Estimates placed it at R168 billion annually in 1998 and roughly 35% of the country's GDP (Department of Environmental Affairs, 2021). South Africa's land use system had solely been land based and any considerations towards development had been up to the high-water mark and none seaward. This approach did not make sense especially because South Africa's continental Exclusive Economic Zone (EEZ) ranges a sizable 1 068 659 Km^2 (Department Of Environmental Affairs : Oceans And Coasts, 2015). Because of the layered complexities of coastal environments, the Integrated Coastal Management Act (ICMA) Act No. 24 of 2008) under the pretext of the Sustainable Coastal Development national policy was enacted to align with the global call for coastal conservation.

The ICMA provided a shift in mentality regarding coastal management (Department of Environmental Affairs, 2021). It was the first law that would ensure efficient usage of coastal resources for wealth creation and equity whilst making sure coastal ecosystems were protected as opposed to the Sea-shore Act of 1935 that was resource centered where the President owned the coastline on behalf of his constituents leading to fragmented and uncoordinated coastal management efforts (Department of Environmental Affairs, 2021). The ICMA was categorized as a Specific Environmental Management Act (SEMA) under the National Environmental Management Act. The underlying objectives of the ICM Act can be summarized as follows (Department of Environmental Affairs,2021):

"*Defining and determining the extent of the coastal zone;*
Provision for the coordinated and integrated management of the coastal zone;
Preserve, protect and enhance the status of the coastal environment as the heritage of all;
Ensure there is equitable access to coastal public property; and
To give effect to certain of South Africa's international law obligations"

This Act allowed for sectorial stakeholder involvement from the National Coastal Committee, Provincial Lead Agencies, Provincial Coastal Committees, and Municipal Coastal

Committees to the Voluntary Coastal Officers. Stakeholders were appraised on their roles and responsibilities for the successful implementation of the Act in a way that showed cooperation and inclusion (Department of Environmental Affairs,2021). The legislature makes a thorough description of the coastal zone both spatially and legally by distinguishing it into 3 categories namely coastal public property (Admiralty Reserve, seashore, coastal waters), the coastal protection zone (inland edge of coastal public property), and coastal access land (for use by the public to gain access to coastal public property). Subcategories were further used to define coastal waters, coastal protection areas, special management areas and coastal set back lines (Department Of Environmental Affairs : Oceans And Coasts, 2015). It must be noted that because of the variability along coastlines, these demarcations are adjustable and negotiable depending on coastal geohazard risk or coastal restoration plans (Griffiths et al., 2010). Above all, this Act created a mechanism to translate pertinent research into actionable management strategies and an enforceable legal system. The general environmental Act still ensures protection of coastal resources and coastal pollution control.

The fact that the ICMA regards South Africa's coastline as a 'limited and finite' resource only speaks volumes to the necessity of studies such as this one. It is now abundantly clear that the South African government acknowledges the importance and threats against coastal areas (Colenbrander et al., 2014). Ecosystem services that maintain the natural habitats, as well as face economic exploitation from human use are cause for concern that have led to the need for multi layered systematic conservation planning tools (Harris et al., 2011). The effectiveness of these tools depends on the availability of data. Due to the complexity of these environments and scarcity of data, researchers often use proxy data, which can skew the outcomes.

Sandy beaches have a very low priority in the scientific community and there is too often no data that speaks to their specific biodiversity (Mason et al., 2000). For example, in 2004, Lombard et al., 2004 labelled beaches simply as 'sand' for the South African National Biodiversity Assessment based on their widely accepted 5 proposed beach bioregions for South Africa (Harris et al., 2011). As such, proxy data must be incorporated to a resolution that does not impede the study. It is significantly easier to map beaches based on morpho-dynamics especially with the prevailing hypothesis that beaches are more physically changed than biologically and still the mapping of coastal zones is at a coarse resolution particularly because these physical characteristics are also variable (Harris et al., 2011). Although there

have been several attempts to characterize South Africa's coastline, there are several restrictions to contend with. There is, however, an increasing number of GIS-based ecological platforms that can suit the needs of coastline mapping.

f) COASTAL LAND USE PLANNING

The City of Cape Town's Coastal Management Unit (CMU) has undertaken risk assessment studies. For example, one of them quantified 3 risk scenarios over 25 years that considered sea-level rise, storm surges and their effect on tides (Colenbrander et al., 2014). GIS played a major role with the outcome being maps that visually communicated the different levels of inundation and relating them to coastal topography as well as public infrastructure (Hamylton, 2017). It helped to guide various stakeholders in future spatial planning endeavors. The perspective of "threatened value" helped to better communicate the effect and necessity of understanding coastal systems to politicians and business owners because the threat of economic cost led to the rapid succession of mitigation and adaptation responses (Colenbrander et al., 2014). It also exposed the impact of poor historical spatial planning decisions particularly in building close to the high-water mark and on reclaimed land (Hughes, 1992; Searson &Brundrit, 1995).

Coastal development criteria were reassessed in time for the then newly declared ICMA that spoke to municipality engagement in designing specific risk-averse strategies. The precautionary principle was enacted by proposing set-back lines as a nationalized law (Department of Environmental Affairs, 2021). This meant the inclusion of buffer zones where development would be prohibited and the delineation of a zoning scheme. This would allow coastal areas to be restored and protected whilst allowing for a multi-tiered management system that led to economic development as well as socio-institutional and adaptive strategies (Cartwright et al., 2008).

In this way the coast could remain a "*shared and common asset whilst preserving its aesthetic and heritage value*" as stipulated by the ICMA. Set-back lines were also more cost effective and flexible as compared to permanent coastal engineering solutions such as sea walls (Hughes, 1992). This strategy led to much controversy stemming from the frustration of the CMU with the constant cycle of private real estate owners being dependent on the municipality to take responsibility for repeatedly damaged coastal developments (Cartwright, 2011; Colenbrander et al., 2014). Further on, the CMU incorporated aspects of

hydrodynamics and the effects of urban developments to identify 19 specific areas within Cape Town at risk from sea level changes. A by-law was proposed by the CMU against illegal coastal land use. This instigated the argument that whilst coastal real estate is so sought after, the new restrictions would affect the socio-economic dynamics of Cape Town adversely (Cartwright, 2011).

This constraint was likened to South Africa's apartheid history where racial segregation prevailed. People of color were not allowed access to certain areas and even the prospect of owning coastal property was impossible. Some felt these new restrictions would only exasperate the existing economic divide and highlighted that although the proposed set back lines had merit regarding climate adaptation strategy, only the privileged few would benefit from this 'environmental protection' (Mukheibir &Ziervogel, 2006). Tension was also created within the municipality, with the Planning and Building Development Management Department (PBDM) indicating that the CMU had overstepped their boundary in the issuing of land rights. This proposed by-law did not complement existing land use guidelines such as subdivisions and rezoning. It was only accepted upon its amendment to only focus on coastal activities as opposed to land use (Cartwright et al., 2008). The CMU and PBDM finally agreed on the use of overlay zones whereby more site-specific conditions were added to both existing and proposed developments. Both CMU and PBDM would work hand in hand on a case-by-case basis to combine protective measures and building codes for more sustainable development (Cartwright et al., 2008).

This case study shows just how complex spatial planning can be within the context of coastal zone management and how informative applying GIS as well as intergovernmental collaboration can be. Based on quantitative GIS data, both CMU and PBDM were able to compromise and find practical ways to further mitigate against coastal geohazards. Cape Town's coastal urban edge was approved in May 2012. It has since guided in land use planning tactics and sustainable development (Colenbrander et al., 2014). This new approach has been well received and used as the blueprint for the rest of the province. There is a need for GIS applications in governance and it must be accompanied by adequate technology, resources, and expertise but above all a flexible mindset. The following methodology chapter seeks to streamline and give a detailed breakdown of how this study intends to exemplify aspects of the literature discussed along the Cape Town coastline.

4 METHODOLOGY

The literature review answers the Can optical and microwave based remote sensing techniques be applicable, optimal and accessible for both shoreline extraction and beach profiling approaches towards a well-rounded coastal erosion analysis? on page 6 and postures that optical satellite imagey is adequate for shoreline extraction whilst microwave-based data is ideal for satellite beach profiling. To actualize objective 1; Objective 1: Combine coastal science and (optical and microwave) remote sensing principles for sediment change analysis by manipulating satellite imagery for volumetric change assessment of beaches. on page 6, coastal indicators are observed to determine shoreline changes. The literature review has also communicated the previous research other scholars have conducted in identifying the appropriate remote sensing methods for coastal erosion observations.

The methodology formulated here draws from this previous research and is sectioned into two to fully encompass both shoreline extraction and beach profiling approaches towards a well-rounded coastal erosion analysis. This chapter intends to justify, detail, and highlight the relevance of the chosen tools to the specified aim and objectives. Principles of image processing are addressed, as well as factors such as study sites, data availability, manipulation, and procedural limitations to produce a semi tide coordinated assessment of coastal erosion. The chapter closes by highlighting the accuracy measures used to determine the effectiveness of the techniques presented here. The cohesive use of different data sources allows us to map coastal areas timely and ensure reasonably accurate positioning and orthometric height which are further ground-truthed through Global Positioning System (GPS) and LiDAR data (Deronde et al., 2008; Wigley, 2011).

4.1 STUDY SITES

Figure 7 on page 53 is a map that details the study site locale in the greater context of South Africa. The chosen study sites are Milnerton and Kommetjie, both of which are bound by the Atlantic seaboard in Cape Town.

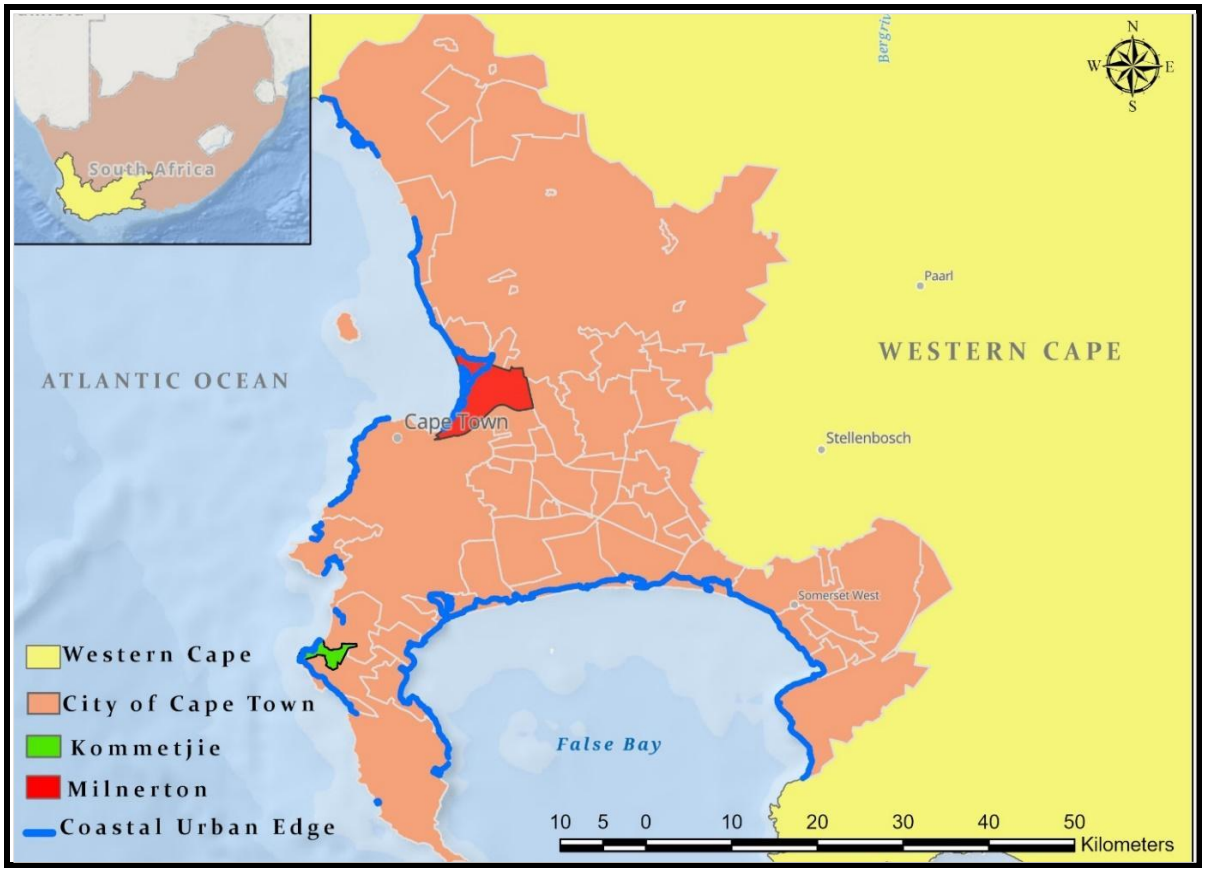

Figure 7 Map of study sites

Historical maps and reports show that Milnerton has a mobile erosive shoreline, however, it has experienced periods of both accretion and erosion (Hughes, 1992). Floods have consistently shaped the area with considerable influence from waves reflected by developments in the Cape Town Harbour. Kommetjie is just as exposed but with deeper waters closer to the shore. Milnerton is characterized by a combination of grey sandy textured soils (Hughes, 1992). There is also significant subsurface accumulation of organic matter, aluminum, and iron whilst there is clear clay accumulation along the Diep River with indications of plinthic and melanic soils (Hughes, 1992). Kommetjie also has a mixture of Greywacke and unconsolidated white sands. This is the result of the interchanging layers of dark grey fine-grained greywacke sandstone and shale from the Malmesbury formation (Colenbrander et al., 2014).

Some preventive measures against coastal erosion include dune field restoration at both sites however infrastructural developments have reduced their effectiveness and there is great

concern over the dune cordons at Milnerton thinning out. Kelp beds are common along the Kommetjie shoreline offering alleviation from storm surges by acting as wave energy dissipaters. Whilst little of the Kommetjie shoreline has been studied, Milnerton's shoreline erosion has caused extreme concern with the effect of high tides on storm drain outlets on the beach (Hughes, 1992). The complex lagoon environment of Woodbridge Island within this area is an ideal study site because its proximity to the shoreline means even a 5cm rise would damage the lagoon spit, the surrounding developed area as well as the city margins. A 1m rise would erode approximately half of the Island and floods would swamp the area roughly over a timeline of 50 years (Hughes, 1992). Being a built-up area means the damage is estimated to be within the hundreds of millions of Rands (Hughes, 1992). Identifying appropriate sites also depends on the availability of data that ensure optimum geographical cover and identifying appropriate shoreline proxy data.

4.2 VISUAL PROXY-BASED MEASUREMENT OF HISTORICAL SHORELINE MOVEMENT

The coastal indicators used in this aspect of the study are purely based on the visually discernible features of coastlines as shown in Table 1 on page 29. Image processing techniques are applied to extract shorelines, and they are further modelled to determine their propagation as well as their associated coastal erosion rates.

4.2.1 MATERIALS AND DATASETS

The expected deliverables were used as a guide in acquiring the appropriate data. Multisource data usage lies in proving the synergy between different remote sensing techniques by identifying their commonalities. In this case, position is the underlying commonality. The data is normalized by referring it to the same coordinate systems and datum, in this case being Hartebeesthoek94. Cost, accessibility, software, and equipment availability as well as compatibility are also influential. The main dataset type used for shoreline extraction in this instance was optical satellite data. To conduct both a long-term analysis of shoreline propagation, a combination of satellite sensors was used to account for varying launch and discontinuation dates. Table 3 below summarizes the most suitable and accessible satellite data used for analysis.

Table 3. Optical Satellite Specifications

SATELLITE TYPE	SATELLITE	TIME FRAME	RESOLUTION		
			Temporal (days)	Spatial (m)	Spectral Usage
OPTICAL	LANDSAT 4-5 TM	1991-2001	16	30	Green(B2) SWIR(B5)
	LANDSAT 7 ETM+	2001-2014	16	30	Green(B2) SWIR(B5)
	LANDSAT 8 OLI	2014-2021	16	30	Green(B3) SWIR(B6)
	SENTINEL 2	2016-2021	10	10	Green(B3) SWIR(B11)

The Landsat catalogue offers the most accessible long-term archive, and its consistent resolution creates uniformity within the study, however with every satellite launch the band positioning has changed as shown in the spectral usage column of Table 3. Sentinel 2 offers improved spatial resolution of up to 10m however its recent launch precludes it from contributing to a historical analysis of coastal erosion. It is used to investigate the effects of resolution on the positional accuracy of extracted shorelines in section 4.2.6 on page 66. The Landsat data was downloaded through the USGS data portal [1] whilst freely available Sentinel data was available through the online ESA Copernicus[2] platform. The Landsat data was used to extract shorelines for the period of 1991 to 2021 at 10-year intervals to assess shoreline change and the rate of geomorphological changes.

4.2.2 FUNCTIONAL COASTAL INDICATORS

As stated in the literature review (chapter 3 on page 43), coastal indicators are the measurable shoreline components that can be manipulated for analysis. The aim here was to conduct a historical shoreline analysis and since the longest archived data via the Landsat satellite constellation, is optical; the shorelines were extracted by visual interpretation and image processing. For this reason, wetting limits along the coastlines were used as coastal indicators meaning the wet/dry boundaries of the littoral zone were used to infer the high-water line. This also takes into consideration the effect of storm lines because storm surges are a big contributor to coastal erosion, therefore over wash penetration lines can be identified and recorded to highlight the limits of the active sand zone. As stated in the theory (Chapter 2, page 9) remote sensing technology discerns between land cover changes and through data

1 The United States Geological Survey, 2 European Space Agency

manipulation, we can separate land and ocean components as described in section 4.2.4 on page 59.

4.2.3 SOFTWARE AND TOOLS

A wide assortment of analysis tools was used in this study, however, ENVI was used to pre-process Landsat data. The extracted, vectorized and edited shorelines were imported into ArcMap to produce final images and statistical analysis of erosion using the DSAS AddIn, which is a United States Geological Survey (USGS) created tool for coastal monitoring. As shown in the literature review, it has been well received and used in studies all over the world. Below is a synopsis of the design and applicability of the tool.

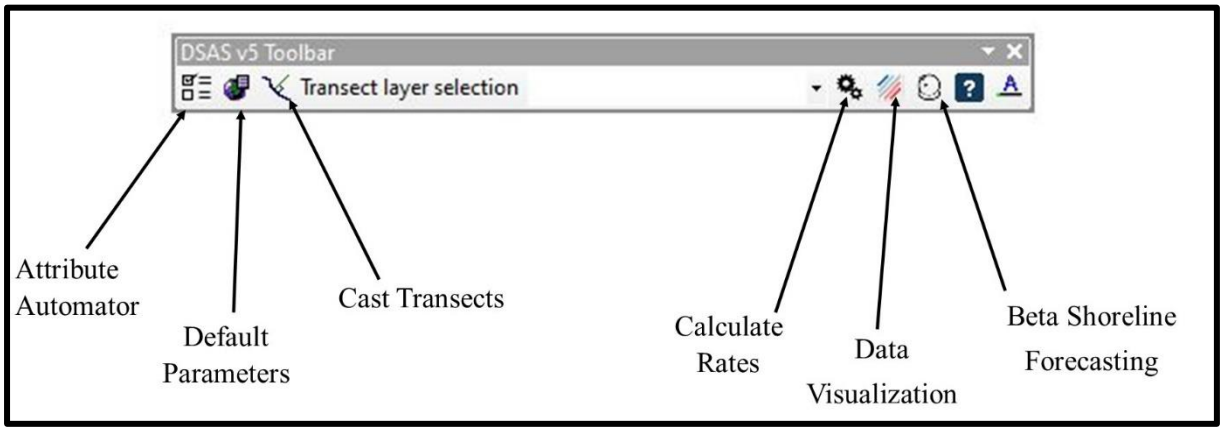

Figure 8 DSAS tool interface

Source:ESRI

DSAS has certain requirements for it to fully function. The most integral aspect of the tool is that it allows us to distinguish the baseline shoreline from those that need to be analyzed. As the name suggests, the Attribute Automator adds the necessary fields to usable shorelines. These are the date, uncertainty, and shoreline type for the shorelines whilst the baseline is defined by its ID, line segment grouping and the maximum distance that it can search for shorelines (Himmelstoss et al., 2018). These new added fields are then used to define the baseline and shoreline parameters whilst the search distance is used to cast transects between the baseline and shorelines. The following rates are calculated along these transects based on either linear or weighted regression (Gomez et al., 2014).

1. Shoreline Change Envelope (SCE): Total shoreline movement irrespective of date of acquisition.
2. Net Shoreline movement (NSM): The distance between the youngest and oldest shorelines

3. End Point Rate (EPR): This is the rate of change calculated by dividing the distance by the time elapsed.

DSAS is only as accurate as its input data, which is why attention to detail is so important during shoreline editing. It is suggested that satellite data pre-dating 2000 has an accuracy of ±10m and ±5m post 2000 (Oyedotun, 2014). The data must be stored in a personal database; great care must be taken to ensure all shoreline segments have the same directionality and the date must be edited to the American format. The results are visualized through an adjustable color bar and the forecasting tool is limited to only 10- or 20-year predictions (Himmelstoss et al., 2018). Section 5.4 on page 96 delves deeper into the DSAS calculations.

Taking all these factors into consideration, the following workflow was formulated to produce a concise methodology. It focuses on the summarized processes, outputs, and tools used in this analysis. It is color coded to highlight the expected report deliverables highlighted in grey and further reported on in chapter 5 on page 87. The subsections that follow the workflow delve deeper into these different components.

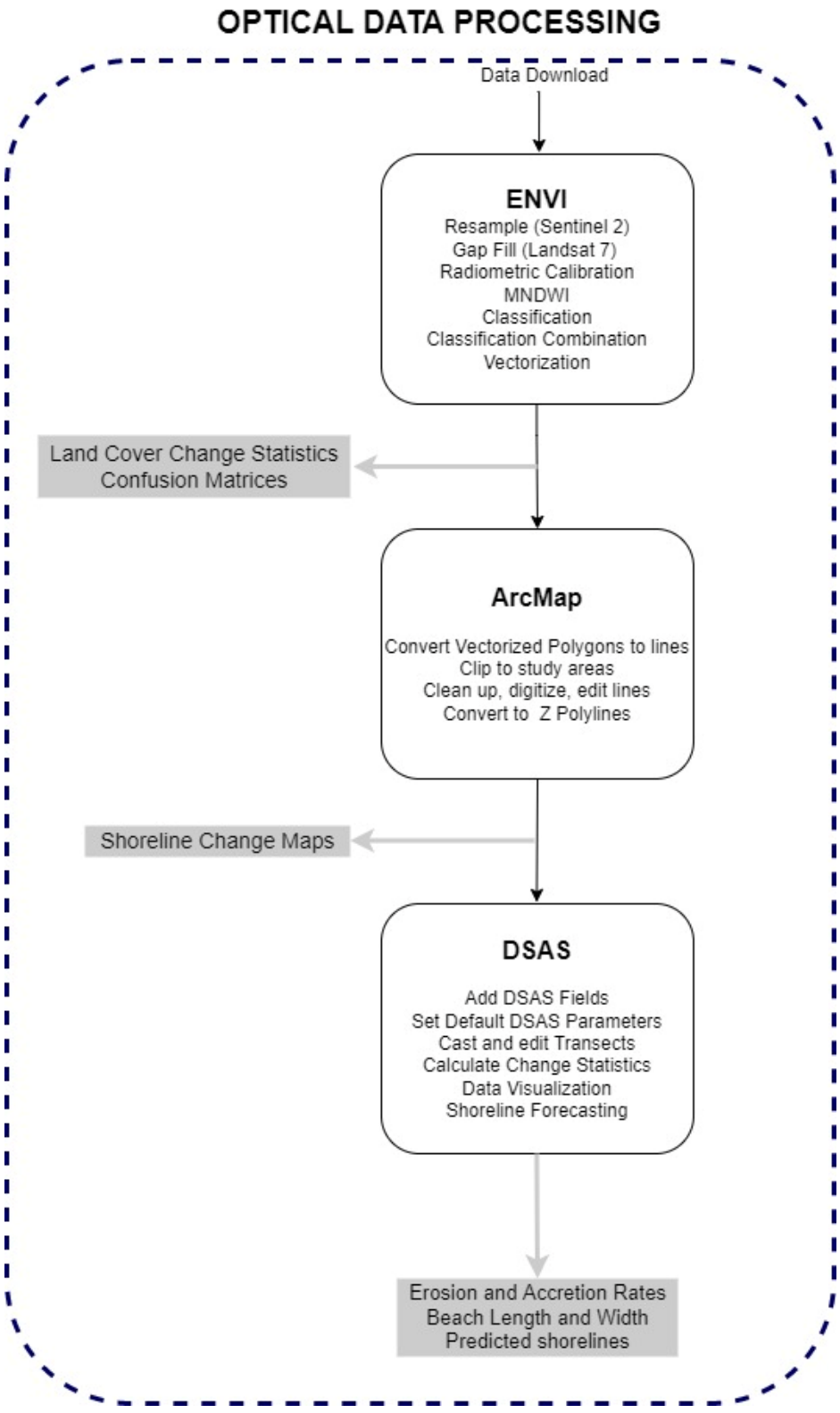

Figure 9 Optical data-based shoreline extraction and assessment process

4.2.4 LAND-SEA SEGMENTATION FROM OPTICAL SATELLITE DATA

The extraction process for the optical data is based on spectral reflection. Both pre-processing and information extraction have been described here whilst the analysis of each section is mirrored and discussed in chapter 5 on page 87. As previously stated, the optical data was used for a historical analysis and a combination of band ratioing and classification was used to separate the land and ocean components and infer the shoreline positions.

4.2.4.1 PRE-PROCESSING

Before any statistical analysis could be conducted, the data was pre-processed to ensure correct positioning and optimum spectral visualization. Visual enhancement was achieved through radiometric calibration and logarithmic contrast stretching to highlight darker areas (Chander et al., 2009; Gens, 2010). It must be noted that for instances where full Landsat-7 and -8 products were not supported by importing their XML files as is frequent practice in ENVI; their single band TIFF images were imported instead, and equation 2 below was applied for at sensor radiance correction via band math, the equation variables highlighted in *Table 4* below were sourced from within the coinciding band's metadata in the MTL.txt file (Chander et al., 2009):

Equation 2. Landsat radiometric calibration equation

$$\frac{Lmax_{\lambda} - Lmin_{\lambda}}{Q_{CalMax} - Q_{CalMin}} \times (B_n - Q_{CalMin}) + Lmin_{\lambda}$$

Table 4. Landsat-7&-8 Radiometric constants

VARIABLE	METADATA FORMAT
$Lmax_{\lambda}$	RADIANCE_MAXIMUM_BAND_#
$Lmin_{\lambda}$	RADIANCE_MINIMUM_BAND_#
Q_{CalMax}	QUANTIZE_CAL_MAX_BAND_#
Q_{CalMin}	QUANTIZE_CAL_MIN_BAND_#
B_n	Band

Geometric miscalculations were automatically corrected during radiometric calibration by employing coordinate reprojection for the data to occur within the UTM 34S zone, which is later reprojected to Hartebeesthoek 94 in ArcMap for the final analysis. Acquisition errors

such as the Landsat-7 data scan line data gaps that have occurred since 2003 were overcome with a gap filling AddIn within ENVI.

Atmospheric corrections such as cloud masking were attempted via the '*Calculate Cloud Mask Using Fmask Algorithm'* tool created by Zhe Zhu and Curtis E. Woodcock, which has now been embedded into the ENVI software (Zhe &C E Woodcock 2012). It is meant to separate clouds and cloud shadows from Earth components in imagery by combining physical cloud properties with Top of Atmosphere and Brightness Temperature measurements to detect and separate Potential Cloud Pixels (Zhe &C E Woodcock 2012). This algorithm manages to combine temperature, spectral variability, and image brightness to create a cloud mask. Several algorithms have been formulated with a specific focus of detecting clouds and snow particularly based on the reflection properties of the NIR and SWIR bands that are used to compute a whiteness index. Zhe Zhu and Curtis admitted that the algorithm performed best over vegetated areas, but not over bright land covers as was the case in this study (Zhu et al., 2015). It proved to only remove chunks of coastline and beaches, as well as waterbodies as shown in Figure 10 because the brightness of the beach areas caused them to be misclassified as clouds thus defeating the purpose of the study. For this reason, this study focused on using cloudless images, which further reduced the number of usable imageries.

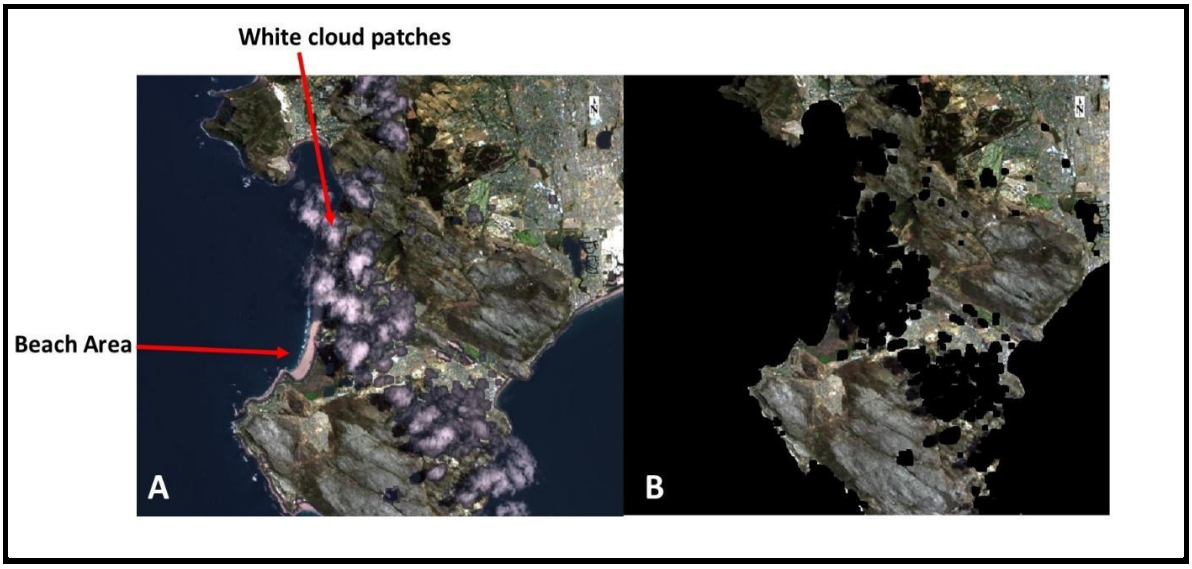

Figure 10 Cloud masking result

4.2.4.1.1 MNDWI CALCULATION FOR WATER BODY DETECTION

Further image enhancement was required post-image correction. This required significant consideration towards the suitable bands to use for the optimum detection of different land covers. The LITERATURE REVIEW on page 32 indicated that some authors have used different bands depending on the tide level at the time of image acquisition (Gens, 2010; Toure et al., 2019). however, regarding the spectral composition of the data used here, it is worth noting that the Landsat satellites have consistently passed over Cape Town at roughly the same time and as such the SWIR and Green bands can be consistently used for the optical data based on the MNDWI formula in Equation 3 below. As highlighted in the THEORETICAL FRAMEWORK chapter on page 9, MNDWI is a band ratio that improves the detection of water surfaces. It produces a 1 band grey scale image that depicts water surfaces as positive values whilst other land surfaces have negative values as shown in Figure 25 (b) on page 90. The rationale for choosing these bands is further explained in the SPECTRAL ANALYSIS section of the RESULTS and ANALYSIS on page 87.

Equation 3. MNDWI equation

$$MNDWI = \frac{Green - SWIR}{Green + SWIR}$$

Where Green = green wavelength band

SWIR= short wavelength infra-red band

4.2.4.1.2 APPLYING SVM CLASSIFICATION FOR COASTAL LAND COVER SEGMENTATION

Whilst the MNDWI improves the detection of water bodies, there is still a mechanism required to effectively segment the land covers found within coastal areas and determine the location of shorelines. Supervised classification was the chosen segmentation technique and operates by grouping similar pixels into one class. The boundary between land and ocean would thus represent a shoreline. Although several of the classifiers were tried and tested, the Support Vector Machine's (SVM) hyperplane identification technique and the back propagation of Neural Net (NNC) supervised classifiers proved to be the most robust based classification accuracy and Kappa coefficient statistics. To include all potential land cover influences in coastal areas, the following 8 training sites were digitized:

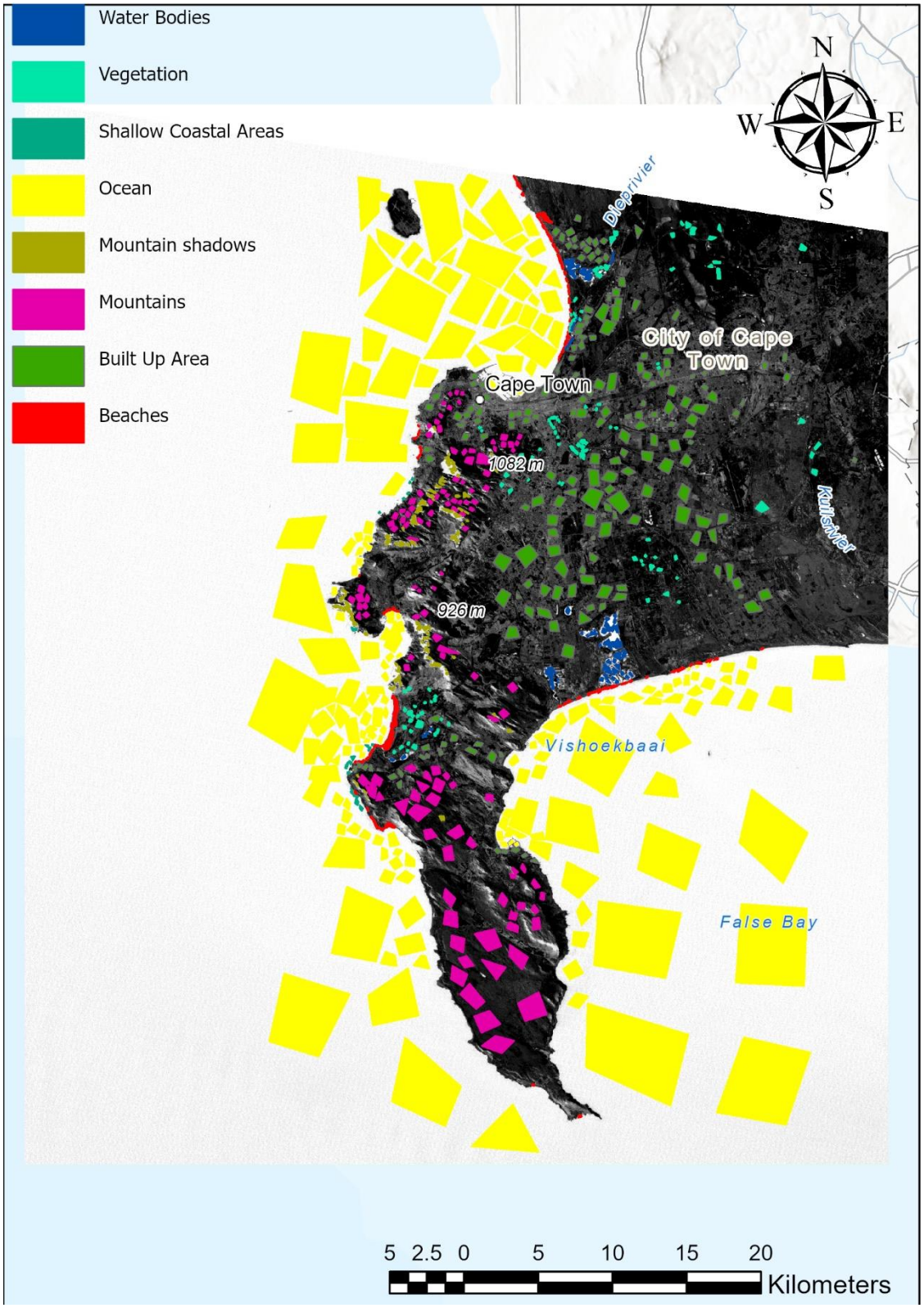

Figure 11 Classification Training Samples

The mountain shadow sites were added because with Cape Town being particularly hilly, there was spectral confusion between the shadows and inland water bodies whilst the shallow coastal sites were to account for the discrepancy caused by rocks and seaweed in the coastal areas. The beach areas had the least number of training samples because they are generally small, slivers of land. Figure 12(c) on page 63 shows how a classified image would look before the land-based classes were reclassified for a clear delineation between the ocean and land elements in Figure 12 (d). The actual shoreline was extracted by vectorizing the re-classification as in Figure 12 (e). Only images with a classification overall accuracy of more than 90% were used for further analysis. Land cover change statistics were also noted and addressed further in section 5.2 of the results.

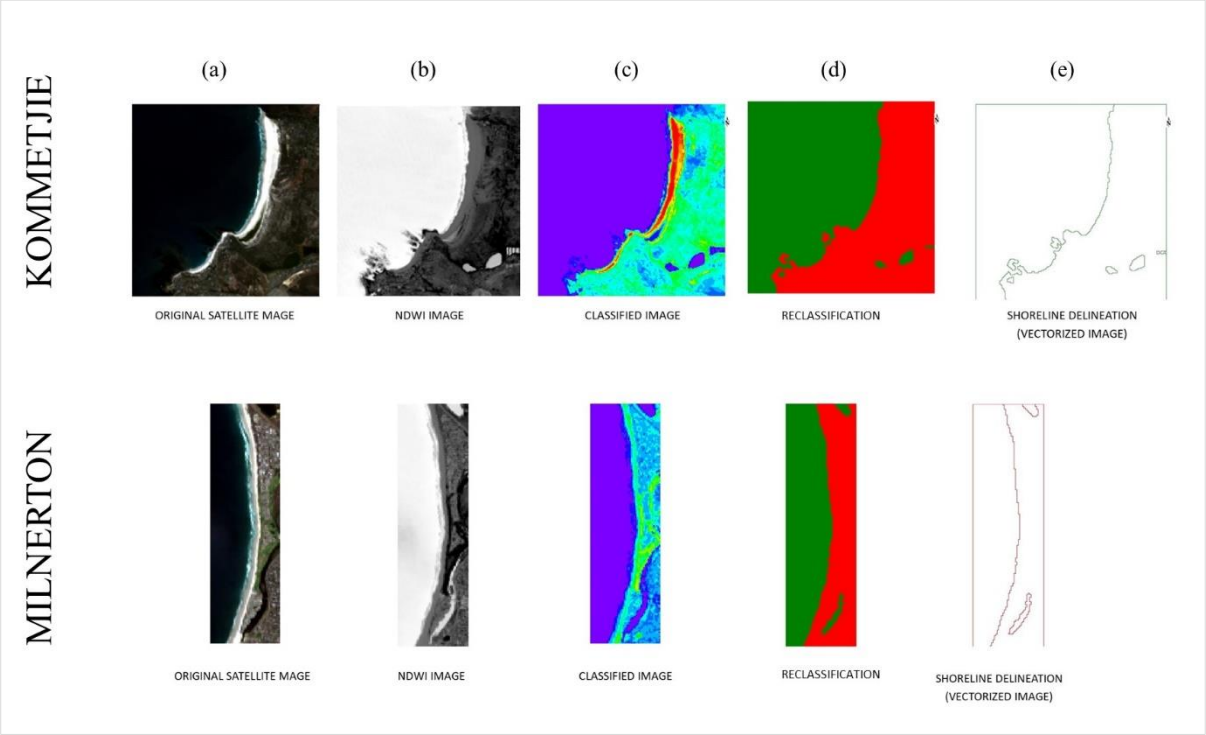

Figure 12 Optical data processing outputs

4.2.5 MULTITEMPORAL POST-CLASSIFICATION SHORELINE MOVEMENT MODELLING

The classification vectors still needed to be manually edited to a DSAS compatible format. Through digitization, they were further cleaned up, smoothed, and converted to polylines with elevation (Z) values. All the extracted shorelines were imported into a personal

geodatabase and making sure they were all projected to the Hartebeeshoek94 coordinate system. As explained in subsection 4.2.3 on page 56, new fields were added through the DSAS tool that help to establish the baseline, in this case the 1991 extracted shoreline (Himmelstoss et al., 2018). The rest of the extracted shorelines (2001, 2011, and 2021) were merged and differentiated by their varying dates of acquisition. Due to the fluctuation in distance between the shorelines, the tool was set to a maximum search distance of 500 m from the baseline. The area covered by the shorelines was measured digitally and found to be well within the 500m threshold. The baseline was set from a mid-shore position meaning it can detect shorelines on either of its sides.

The Land-water orientation was set to right as shown in Figure 13 below and is clearly reflected in Figure 11 on page 63 above. The data uncertainty was ±30m similar to the resolution of the satellite images whilst a seaward intersection was specified in the instance of non-linear shorelines. This is to say that all intersections between transects, and shorelines would occur seaward. It must be noted that the DSAS tool will not work if its metadata section is not fully completed.

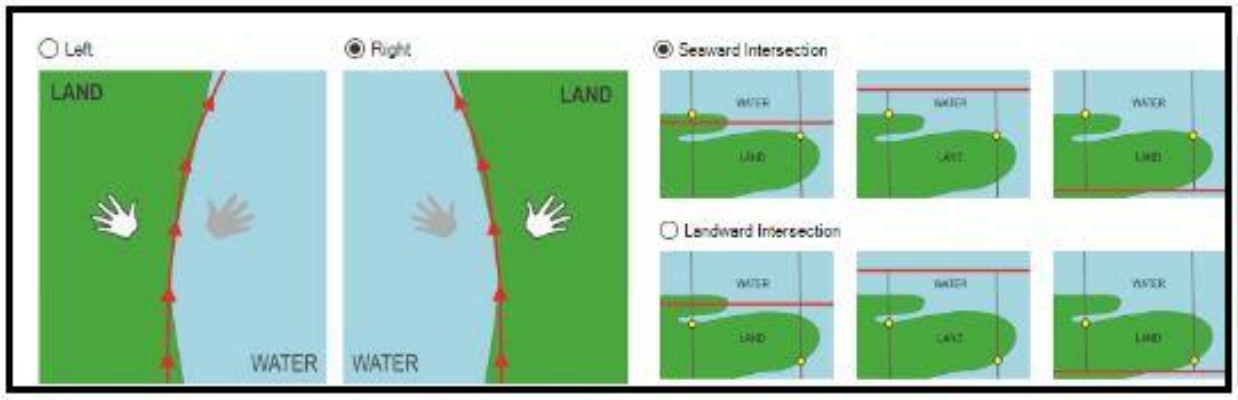

Figure 13 DSAS land-sea orientation

Transects were then cast based on the specified search distance and at a spacing of 5m. The directionality of the transects is dependent on the smoothing distance as depicted in Figure 14. The shorelines under assessment were more linear than curved, thus a smoothing distance of 500 was used.

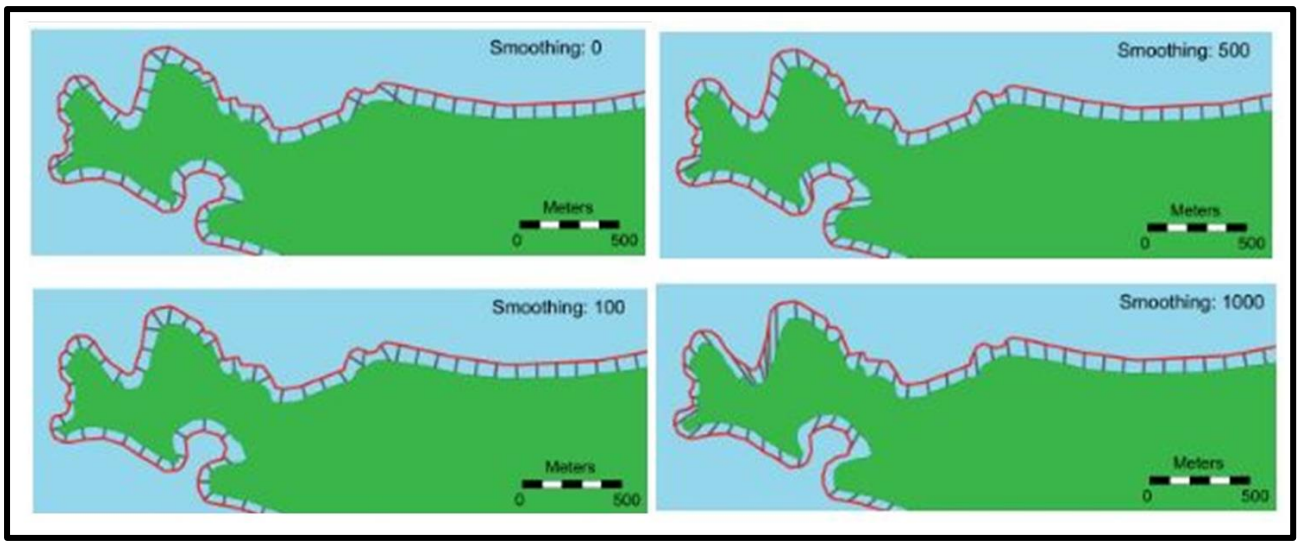

Figure 14 DSAS smoothing tolerance settings

Although the maximum search distance was set to 500m from the baseline, it is the actual position of the shorelines that restricts the transects and where a transect intersects with any shoreline an intersection point is created. Once the transects were cast, the rates were calculated at a confidence interval of 90% based on linear and weighted regression. The statistics calculated here are based on the change in intersect position over time. Table 5 explains the difference between these two regression methods and their discrepancies are further discussed with the results in Chapter 5 on page 87.

Table 5. DSAS Regression Methods Comparison

LINEAR	WEIGHTED
Fits least square regression line over intersection points.	Weight distribution is based on the variance of the shoreline uncertainty values.
All data are used.	Only intersection points with smaller uncertainty are used.
Purely computational, statistically sound, and easy.	Greater weight is given to the more reliable intersection points.

The calculated rates were automatically added within a new transect feature class and these transects can be altered for visualization purposes. Shorelines for 2031 and 2041 were also forecasted using the Kalman filter through the DSAS Beta forecasting tool. It combines

observed and modelled shoreline positions to estimate future positions including uncertainties. The final DSAS maps and statistics are fully discussed in chapter 5 on page 101.

4.2.6 ACCURACY ASSESMENT

In the context of this study, accuracy is determined based on how close a calculated measurement or position is to its actual value. There are several sources of errors that such as satellite orbital variation and digitization (Malthus &Mumby, 2010). The shorelines here are derived based on how well we can distinguish between land cover classes and establish a land-sea boundary. Therefore, confusion matrices are used to determine the accuracy of designated land cover classes. The positional accuracy of the shorelines is determined through the shoreline position index whilst the uncertainty of the DSAS statistics is calculated through the End Point Rate (EPR) (Himmelstoss et al., 2018).

4.2.6.1 CONFUSION MATRICES

The best measure of classification accuracy is confusion matrices. Using the kappa coefficient along with producer-user statistics helps to determine the level of user error based on training samples (Bahari et al., 2014). Land cover changes can be determined through thematic change detection statistics to assess the effectiveness of this methodology. Academics have criticized using overall accuracy because it simply sums the correctly classified pixels and divides them with the total number of pixels whereas the Kappa coefficient has been thought to be a more precise measure of classification because it includes both the used and omitted pixels from the equation:

Equation 4 Kappa coefficient equation

$$K = \frac{N \sum_{i=0}^{n} m_{i,i} - \sum_{i=0}^{n} (G_i C_i)}{N^2 - \sum_{i=0}^{n} G_i C_i}$$

Where:

i= Class number

N=Ratio of classified values to truth values

$M_{i,i}$ = *values belonging to both the* i^{th} *truth and classification class*

C_i =*Total number of predicted values in the* i^{th} *class*

G_i = *Total number of truth values in the* i^{th} *class*

The classification accuracy results are discussed in section 5.3 page 100.

4.2.6.2 SHORELINE MOVEMENT ERROR CALCULATION

The uncertainty of shoreline change measurements is calculated based on the EPR using the following equation that sums the shoreline uncertainties and divides them by the time interval:

Equation 5 DSAS Shoreline Uncertainty Equation

$$EPRuncy = \frac{\sqrt{(uncyA)^2 + (uncyB)^2}}{date\ A - date\ B}$$

Where uncyA= youngest shoreline uncertainty

UncyB=oldest shoreline uncertainty

date A= Most recent shoreline date

date B= Oldest shoreline date

The statistical accuracy of the DSAS tool is based on both weighted (WSE) and linear (LSE) regression. They are both based on predicting shoreline positions from the typical best fit equation:

Equation 6 . Best Fit Linear Equation

$$y = ax + b$$

Where: y= predicted distance from baseline

a= rate of change

b= y intercept

Based on this, the standard error is determined by the difference between the actual and predicted shoreline positions:

Equation 7 DSAS Standard Error Equation

$$LSE\backslash WSE = \sqrt{\frac{\sum(y - y')}{n - 2}}$$

Where y= known shoreline distance

y'=predicted shoreline distance

n=number of shorelines

The statistical uncertainty results are presented in section 5.4.5 on page 109.

4.2.6.3 SHORELINE POSITIONAL ACCURACY

To determine the effect of factors such as spatial resolution or satellite orbit geometry on the extracted shorelines, a shoreline position index (I) was used which is calculated with the following formula in *Equation 8* (Zollini et al., 2020):

Equation 8. Shoreline Position Index equation

$$I = \frac{\Delta A}{L}$$

Where:

ΔA = Area between the reference shoreline and the extracted shoreline

L = Length of reference line

For the purpose of this study, the reference shoreline was from the waterline boundary of the topographic survey described in section below on page 81. The extracted shorelines from Sentinel-1, Sentinel-2 and Landsat 8 were used as the variable shorelines. The lower the index value, the more accurate the shoreline position.

4.3 DATUM-BASED BEACH PROFILING METHODS

This section addresses three elevation modelling methods for the purposes of observing coastal observation. Subsection 2.1.1 on page 9 has highlighted the fundamental aspects of coastal systems and that its general profile is the result of geomorphological processes such as erosion and accretion. For the context of this study, a beach profile can be described as a

cross-section of the beach area from the shoreline to the backshore (Lee et al., 2019). Including this in the study gives a better understanding of how the beach landscape has evolved both temporally and spatially, as well as its potential ecosystem influences.

The following techniques are as a direct prescription from past authors and data availability (Amaro et al., 2014; Mason et al., 1999; Parker, 2003; Salameh et al., 2020; Song et al., 2013). This study goes on to compare and discuss these methods in section 5.6 on page 117:

1. **Waterline Method**: Tide gauge data is used to level radar generated waterlines and they are interpolated into an elevation model.
2. **Differential Interferometry Synthetic Aperture Radar (DInSAR)**: Amplitude and Phase differences between SAR images are used to generate an elevation model.
3. **GPS Topographic Survey**: A continuous Real Time Kinematic (RTK) survey is used to capture the beach area and this point data is later interpolated into an elevation model.

LiDAR data are introduced as a normalizing factor to attain absolute heights. The accuracy of the waterline method and Differential Interferometry are calculated through Root Mean Square Error (RMSE) by comparing them to the ground truth data of the topographic survey in Kommetjie.

4.3.1 MATERIALS AND DATASETS

Microwave satellite data are an easily accessible means for elevation modelling. Sentinel-1 was launched in 2014 and its Single Look Complex (SLC) data is used to create DEM's through Differential Interferometry (DInSAR) whilst the Ground Range Detected (GRD) data is used to create a waterline extracted DEM. Tide gauge data are used as a referencing mechanism through sea level observations and whilst its vertical component is referenced to the Lowest Astronomical Tide (LAT) tidal datum, it is converted to the Hartebeesthoek94 spatial datum for a uniform analysis. The permission to use SANHO data has been included under SANHO Data Release Form on page 164.

As discussed in section 2.2.3.3 on page 27, SLC products have both phase and amplitude components embedded within them whilst GRD products do not have phase information, are multi-looked and ground range projected (Filipponi, 2019). The GRD extracted DEM was

adjusted to absolute height through the Mean Difference calculated when compared to an airborne LiDAR survey. The accuracy of these beach profiles is deduced at the pixel level through a Root Mean Square Error (RMSE) assessment based on ground truthing, terrestrial based RTK survey methods as shown in the workflow in Figure 15 on page117 and as described in section 4.3.7 on page 84. Study constraints excluded the use of UAV's thus an RTK GPS survey was conducted to capture the current state of the beaches and produce beach profile models to validate the DEM's produced from the Waterline and DInSAR techniques. Section below on page 82 goes on further to explain the field data collection at 5m intervals and its interpolation into a DEM.

Table 6. Integrated datasets for waterline method implementation

DATA TYPE	INSTRUMENT	TIME FRAME	RESOLUTION		
			Temporal	Spatial	Spectral Usage
RADAR	SENTINEL-1	2016-2021	12 days	SLC=3.5x22 m GRD=20x22 m	C-Band SLC and GRD Interferometric Wide (IW) VH, VV Polarization
SEA LEVEL	TIDE GAUGE	2016-2021	1 hour	Cape Town	-
GPS POINTS	RTK GPS	2021	1 day	±5m	GPS Points
LIDAR POINTS	ALS	2018			Multi-return dense cloud points

4.3.2 FUNCTIONAL COASTAL INDICATORS

Beach profiling is ultimately intended to understand the terrain of the shoreline which introduces elevation as the main extracted coastal indicator. The coastal indicator used in the Waterline method can be described as a virtual reference line because the nature of Radar images means the shorelines are extracted based on interferometric image processing to determine the shoreline maximum intensity as described by Toure et al. (2019). These shorelines are used to infer tidal limits for the necessary calculations and interpolation,

however actual instant tidal levels and datums are introduced by way of including tide gauge data.

Due to the variation of tidal range because of seasonal changes, the actual tide data introduces a tidal datum in this case the Lowest Astronomical Tide (LAT) as discussed in section 2.2.4 on page 28, to account for vertical variations in the beach face which assists with creating georeferenced models and an unbiased comparison between remotely sensed images (Rongxing Li &F, 2001). A datum conversion is required because satellite images and GPS coordinates are referenced to ellipsoidal datums whilst tides are based on tidal datums. DInSAR was used to digitally extract elevation from radar images whilst the High-water line wetting boundary was used as the starting point for the RTK GPS survey (Salameh et al., 2020).

Ideally, the time and date of image acquisition should be known to ensure tide synchronization for as accurate of an assessment as possible (Rongxing Li &F, 2001). This ascertains the positional accuracy of the shorelines to generate elevation models. The tidal datum is incorporated by intersecting a specific vertical elevation with a coastal profile (Mason et al., 1999). The subjectivity of visual interpretation is the reason we consider datum-based indicators; however, these are more applicable for more current as opposed to historical studies due to data limitations (Gens, 2010). To further confirm the satellite-based analysis, a site inspection was conducted as well.

Although several more indicators can be incorporated, the workflow depicted in Figure 15 on page 73 below summarizes how these chosen indicators are pertinent to the perspective of this study based on the objectives and aim. The datasets, as well as their associated extraction techniques are identified and further discussed in section 4.3.3 below.

4.3.3 SOFTWARE AND TOOLS

The Sentinel-1 data was pre-processed in SNAP[2] and the elevation models generated in ArcMap whilst Microsoft's Excel was used to prepare the Sea Level data to be modelled in the Python programming platform Spyder through the Pytides and UTide modules. The beach survey was conducted using Trimble's R8 receiver system. The GPS points were imported in ArcMap for spatial interpolation. A similar approach was used for the LiDAR data. Spatial

[2] Sentinel Application Platform software from ESA

interpolation is achieved by simply using known, sampled data points with an associated location to estimate unknown values at other locations (Gimond, 2022).

There are several interpolation techniques that can be classified as either deterministic, statistical or random. The most appropriate technique depends on the type of data being used and the expected outputs. For example, with Kriging, data must have a normal distribution and be random (Gis Resources, 2021; Tan &Xu, 2014). Data variance is used to interpolate and determine the error of prediction. Inverse Distance Weighted (IDW) on the other hand is ideal where the sampling density is the same as the variability. It assumes that each data point has a local influence that reduces with increased distance from the sampled location (T.Sutton; O. Dassau; M. Sutton, 2009). Splining reduces surface curvature by ensuring the surface passes exactly through the sampled data points and is not suitable for dense data points (Gimond, 2022). The Topo to Raster technique creates a hydrologically corrected elevation model from vector data.

These few interpolation examples are linked to spatial data based on the underlying theory of spatial autocorrelation that says closer things are more similar than those farther apart (Gimond, 2022). IDW is more ideal to use in the context of the collected GPS and LiDAR points because the data is dense enough to calculate local surface variation (T.Sutton; O. Dassau; M. Sutton, 2009). In this instance a variable search distance was used and because the study area was quite small, the power parameter that determines the influence of the measured points on those that are interpolated was left as default with a power of two (Esri, 2016). Regarding the implementation of the Waterline method, Topo to Raster is more appropriate because the extracted waterlines act as contours. Their implementation is shown in Figure 15 below which shows corresponding data acquisition, pre-processing and information extraction for modelling. The expected report deliverables are highlighted in grey and further reported in section 5.6 on page 117, whilst the different datasets are color coded. The subsections that follow the workflow delve deeper into these different components.

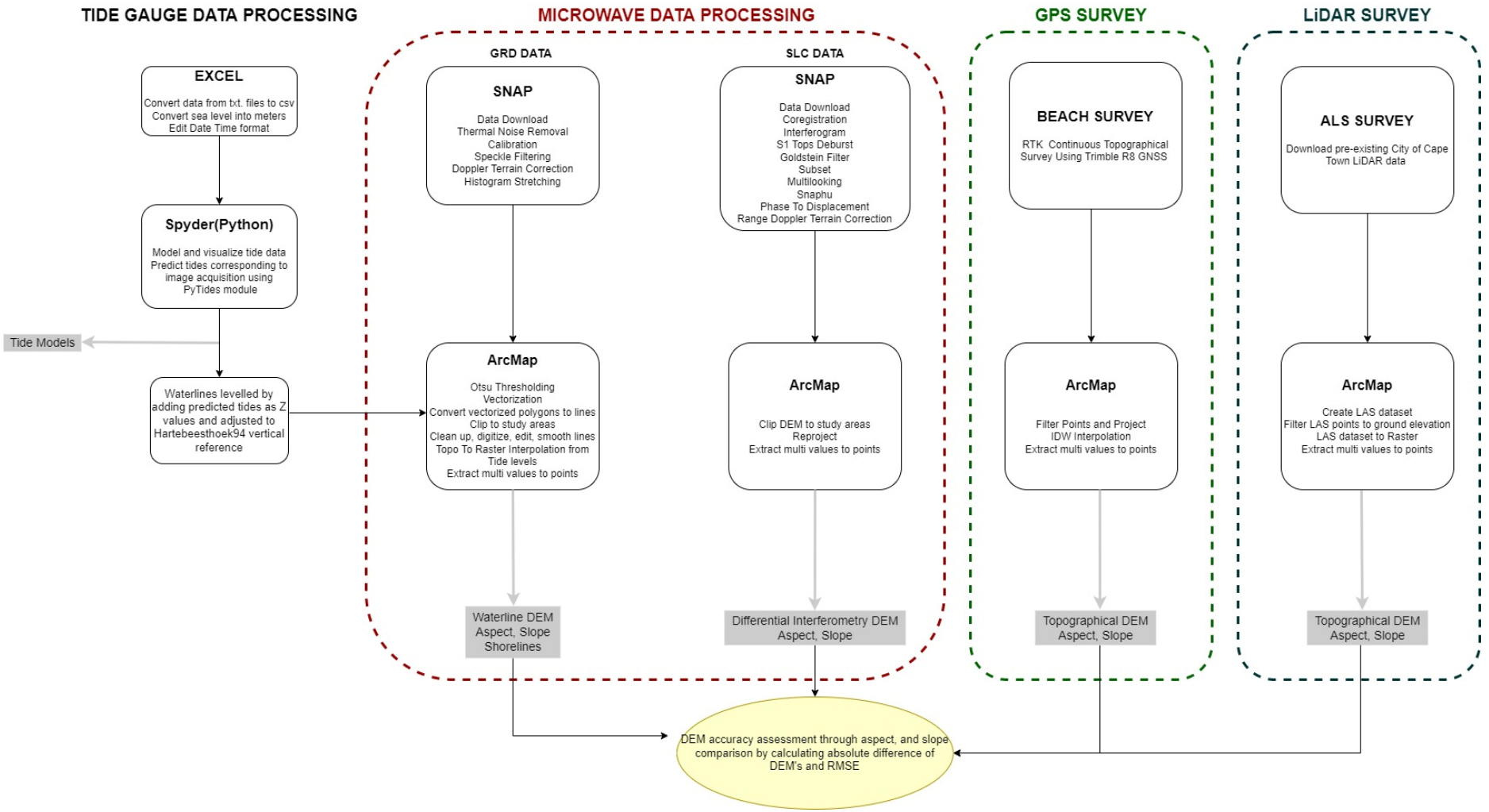

Figure 15 Beach Profiling methodology

4.3.4 APPLICATION OF WATERLINE METHOD FOR ELEVATION MODELLING

The Waterline method requires the integration and uniformity of two datasets, the tide data, which accounts for the change in sea level relative to a particular vertical datum and the position of shorelines derived from spatial data related to its own datum. The tide levels are added to the shorelines for interpolation into a DEM. The extraction of the shorelines is elaborated on from the perspective of edge detection using radar data.

4.3.4.1 PREPARATION OF TIDE LEVELLING DATA

The Sentinel-1 shorelines extracted as described in the 4.3.4.2 on page 76 were used as the waterlines whilst the tide gauge data was modelled and used to adjust the elevation of the waterlines. The tide data were acquired in the form of .txt files and had to be converted to .csv through Excel™. To be compatible with Python, the appropriate date-time format (dd/mm/yyyy hh:mm) was used, and the sea level data was converted to meters. The final data format used for tide modelling is shown in Figure 16 below.

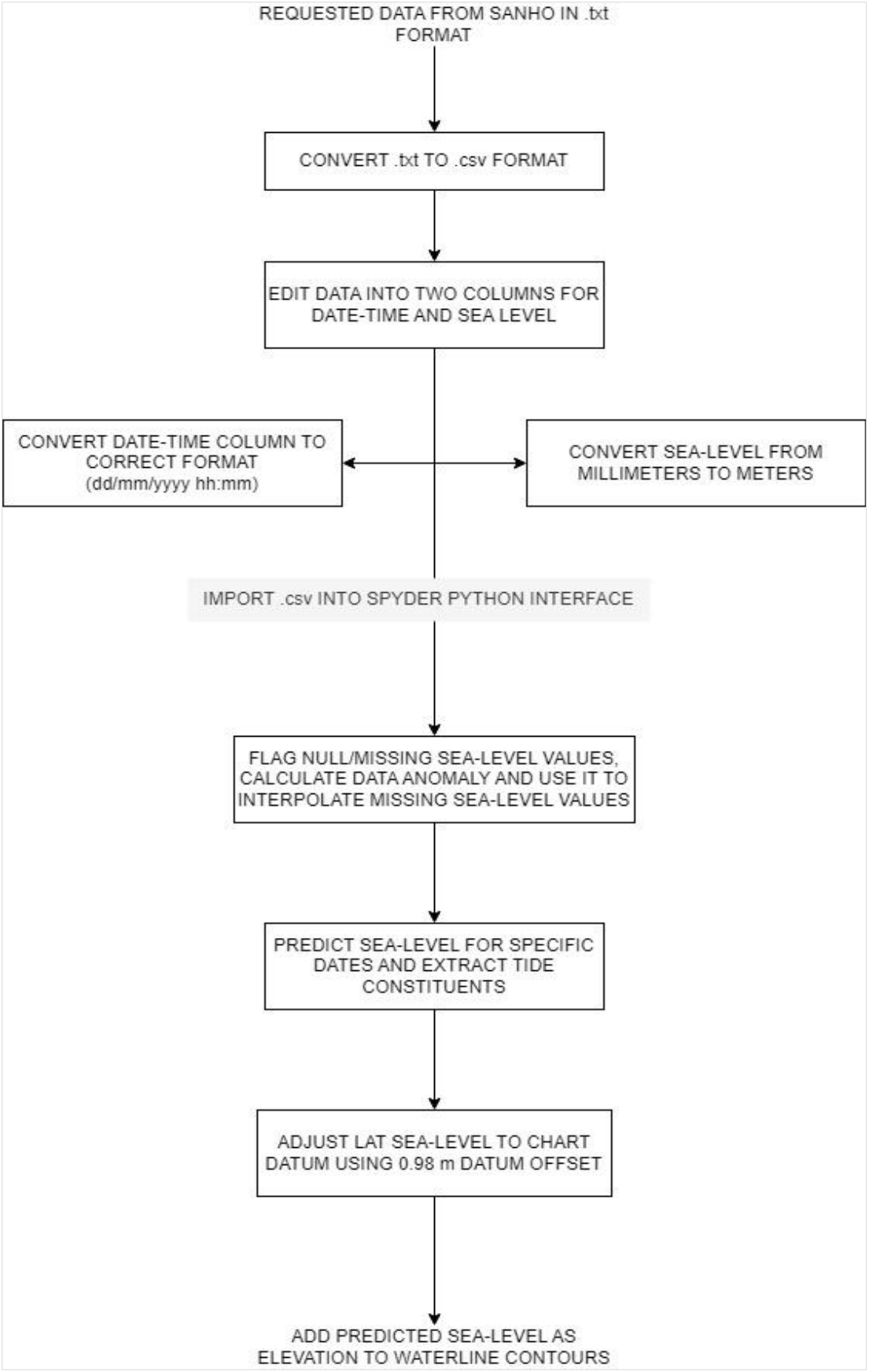

Figure 16 Tide gauge data pre-processing

The sea level data were used to lend vertical accuracy to the deduced elevation model. The Waterline method assumes equal elevation and topography along a waterline, as such the derived DEM was regulated to the sea level by stacking the waterlines and comparing only their varying tidal conditions (Mason et al., 1999). The satellite data were processed based on a land-based datum and so it is necessary to convert the sea level data from its original Lowest Astronomical Tide (LAT) vertical reference to the Hartebeeshoek 94 datum. Ultimately this requires a calculation that accounts for the offset between the hydrographic and land based datums. This was achieved by simply adding the chart datum offset for LAT in Granger Bay of -0.98m to the predicted sea level. As such, the Python module, Pytides was used to create a model of the tide data and used to predict the sea level coinciding to the satellite image acquisition time and date as shown in the PyTides data prediction summary in *Table* 20 on page 154 in the appendices. The predicted sea level was then added as a Z elevation value to the vectorized shorelines, which are also smoothed and clipped to the study sites before being interpolated.

4.3.4.2 EDGE DETECTION BASED LAND SEA SEGMENTATION FROM RADAR SATELLITE DATA

As previously stated, backscatter is dependent on factors such as wavelength, incidence angle and polarization (Orlikova &Horak, 2019). For this process, the Sentinel-1 data was downloaded as Ground Range Detected (GRD) because its ground range projection means it has already been corrected to have less speckle and its phase information removed whilst only its amplitude remains for spectral analysis (Orlikova &Horak, 2019). The horizontal component is required for accurate shoreline positioning whilst its vertical component was determined based on the tide levelling data. The pre-processing in SNAP as depicted in Figure 17 (B) on page 77 included thermal noise removal to reduce the additive noise from image sub-swath discontinuities (Filipponi, 2019). To radiometrically correct the images, the calibrate tool was used to convert intensity values into sigma nought (σ^{o}) to quantify the image backscatter as discussed in the theory chapter. The only available polarizations for the Cape Town region are VH and VV. Past researchers have used both sigma and beta for coastal monitoring studies and as such a comparison of the two was conducted in section 5.1.2.2 on page 94 to determine the most suitable for land-sea segmentation (Miranda et al., 2015; Orlikova &Horak, 2019; Zollini et al., 2020).

Cape Town's hilly, fynbos vegetated landscape affects the surface backscatter captured by satellite sensors as is discussed in the spectral analysis section of chapter 5 on page 87.

Granular noise from wave interference of surrounding scatterers was reduced by applying the Refined Lee filter to preserve edge information whilst smoothening the images through the Speckle filter tool in SNAP (Orlikova &Horak, 2019). Distortions from the side-looking geometry of the sensor such as foreshortening were addressed by Range Doppler orthorectification using the SRTM 1sec HGT elevation model (Filipponi, 2019). To properly make use of the backscatter coefficient (σ^{o}), it was converted to decibels through a logarithmic function as shown in Figure 17 (B) on page 75 below.

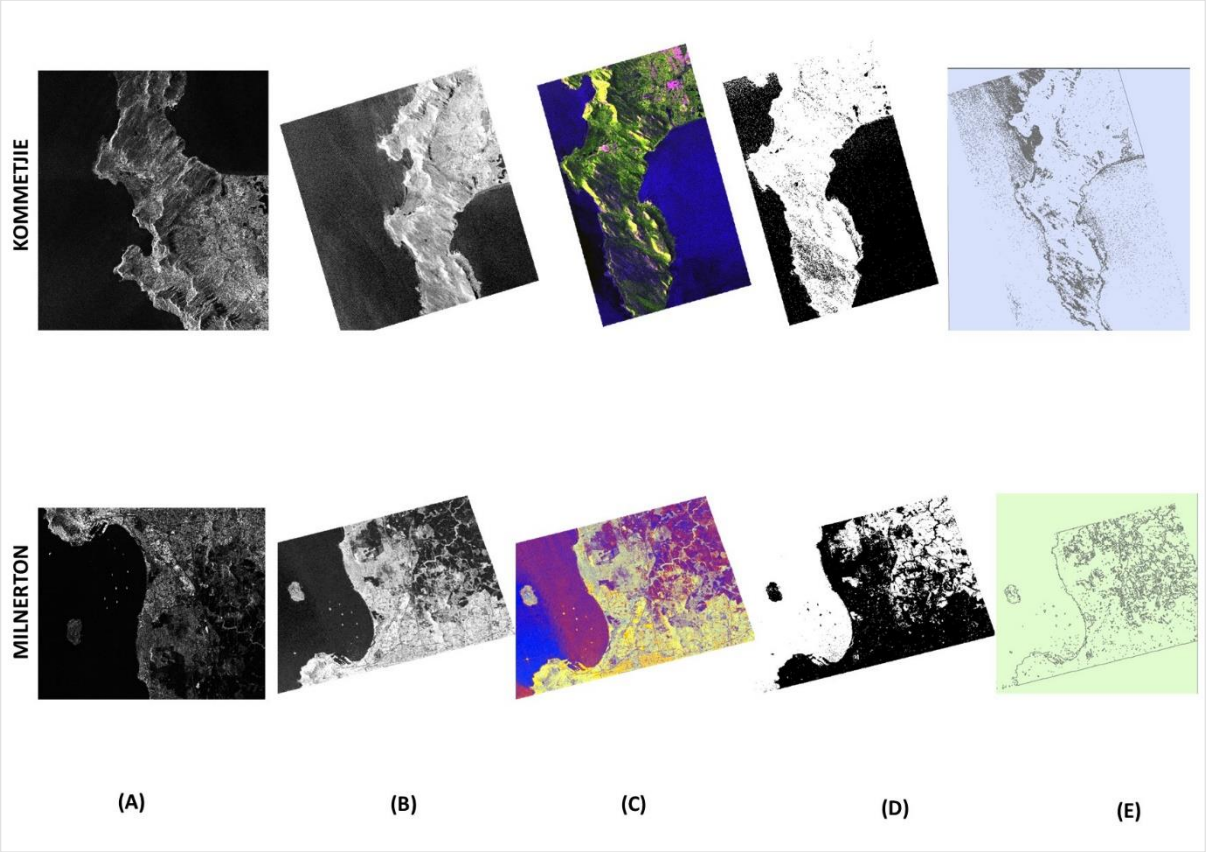

Figure 17 Sentinel-1 GRD processing outputs

Histogram stretching was applied to the backscatter histograms of the pre-processed images to indicate the transition from water to land along the coastal areas after which, the Otsu thresholding technique was applied to them in ArcGIS as in Figure 17 (D) to improve segmentation. It operates by separating data by maximizing pixel intensity variance between pixel classes and thus the result is a binarized image (Bangare et al., 2015). As shown in Figure 17 (E), the threshold boundaries were then vectorized to represent waterlines before

being levelled by the tide data in ArcGIS to create a beach DEM. To adjust the waterline DEM's to absolute values, LiDAR data were used to compare coinciding elevation points and the mean difference between the two datasets was used as the adjustment factor. The resultant DEM's and corresponding accuracy graphs are discussed under section 5.6.2 on page 123.

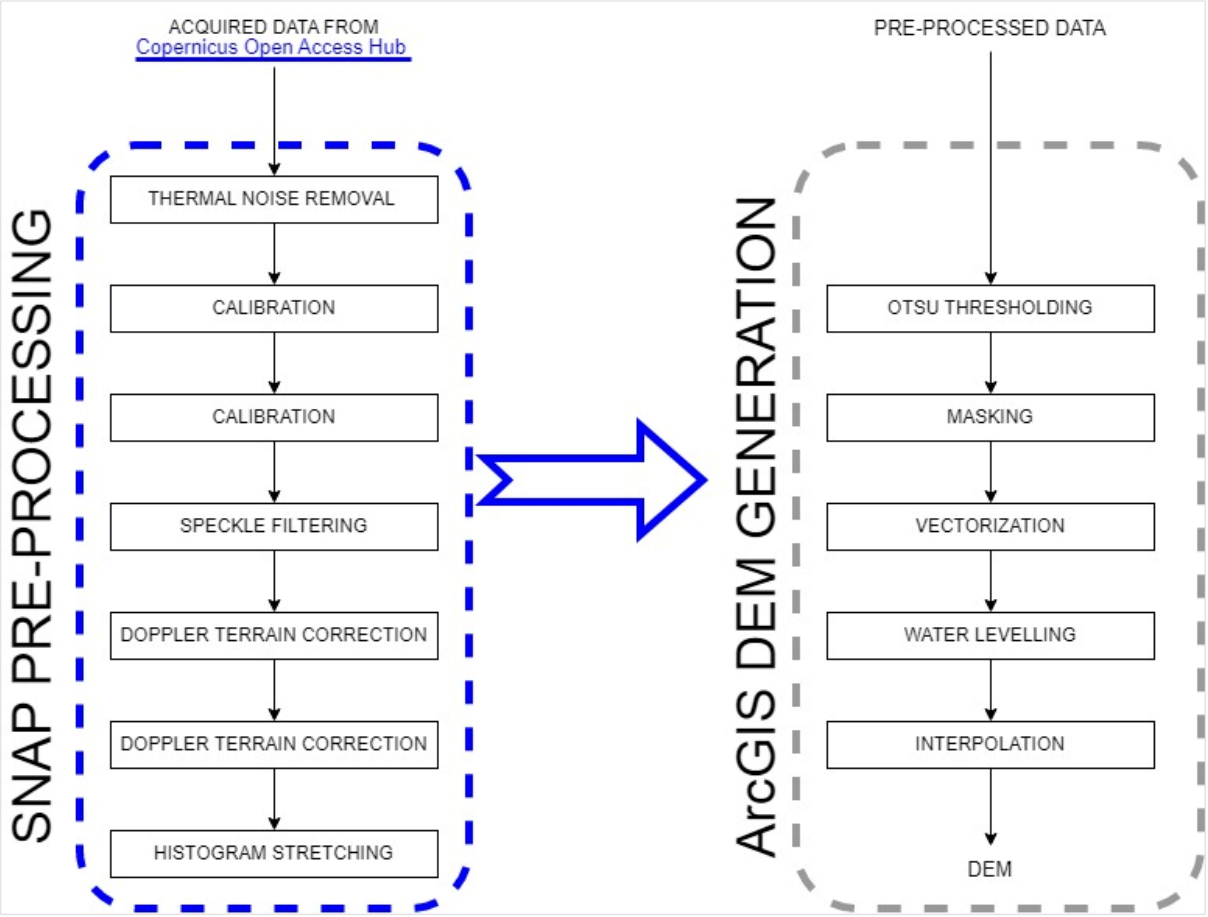

Figure 18 Sentinel-1 GRD waterline extraction process

The amount of usable data for the Waterline method was thinned out due to cloud cover and geographical coverage. Although overlaying Sentinel-1 and Sentinel-2 images by collocation was considered, not enough coinciding images were available. Past literature advises at least 8 to 10 waterlines be used which is why Sentinel-1 was the best option (Salameh et al., 2020). The waterlines were then assembled and interpolated to produce a DEM. The Topo to Raster tool in ArcGIS affords the capability of interpolating line data because of the hydrographical precision of the data and the software assumes the waterlines to be contour lines.

4.3.5 DIFFERENTIAL INTERFEROMETRY (DInSAR)

The prescribed workflow for working with Sentinel-1 Single Look Complex (SLC) data for the purposes of generating an elevation model is depicted in Figure 19 on page 80 below (Veci, 2015). Two images were used with the best available temporal baseline of 12 days and over the specified geographical area. The image obtained earlier acted as the reference image and the other, captured at a slightly different sensor position, was the secondary image. The initial visual state of the images was incomprehensible and presented as a static filled image as shown in Figure 20 (a) on page 81. Both amplitude and phase are preserved in SLC images and the phase difference between the two images is the factor required to deduce elevation (Braun, 2021). This means the two images had to be stacked through coregistration which is a SNAP tool that encompasses splitting the images based on the sub swaths of interest, adjusting the misregistration between the two images through the Sentinel Precise vector that accounts for sensor orbit changes and back geocoding the images with the assistance of the 30m bicubic resampled, SRTM 1Sec HGT elevation model (Grandin, 2015).

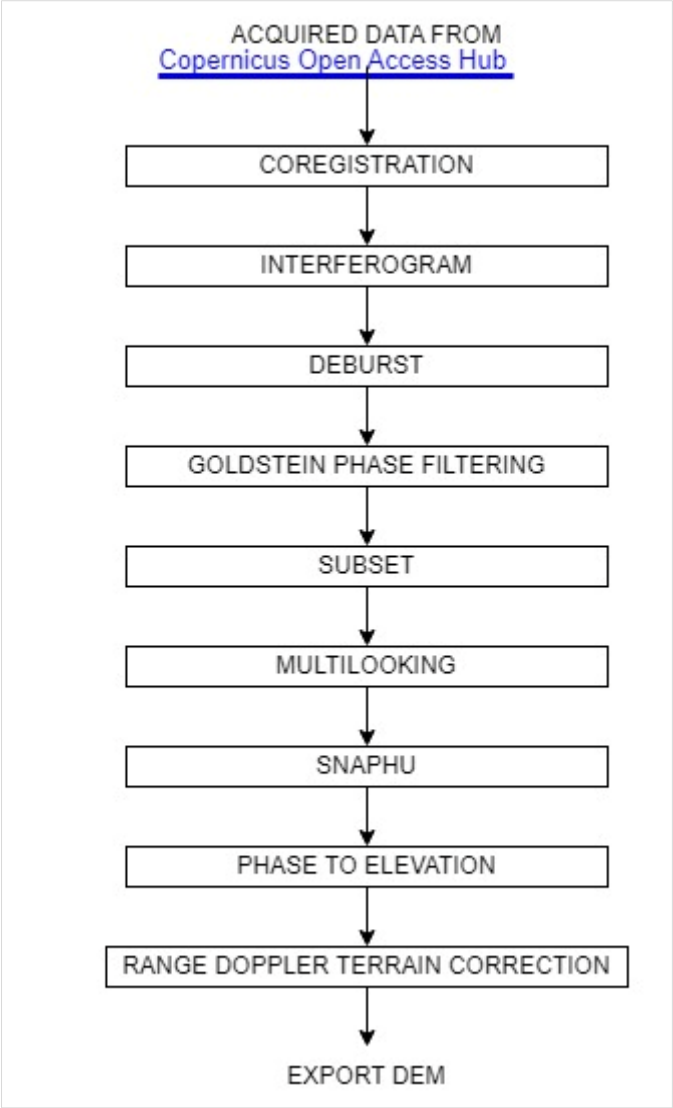

Figure 19 Sentinel-1 SLC data processing

Once the secondary image was shifted to align with the reference image at the sub-pixel level, an interferogram was generated by cross-multiplying the amplitudes whilst differencing the phases between the two images (Veci, 2015). The interferogram presented in the form of seemingly random-colored fringes as in Figure 20 (c) on page 78, however inferences such as regular spaced fringes representing flat land or the distinction between water and land surfaces can be made (Ferretti et al., 2007). The deburst tool was then used to merge the splits between sub swaths. To reduce the effect of decorrelation on interferogram fringes, the Fast Fourier Transform (FFT), Goldstein filter was also applied to produce Figure 20 (d) below (Grandin, 2015). The processing strain during phase unwrapping was reduced by subsetting the image to the Kommetjie and Milnerton areas.

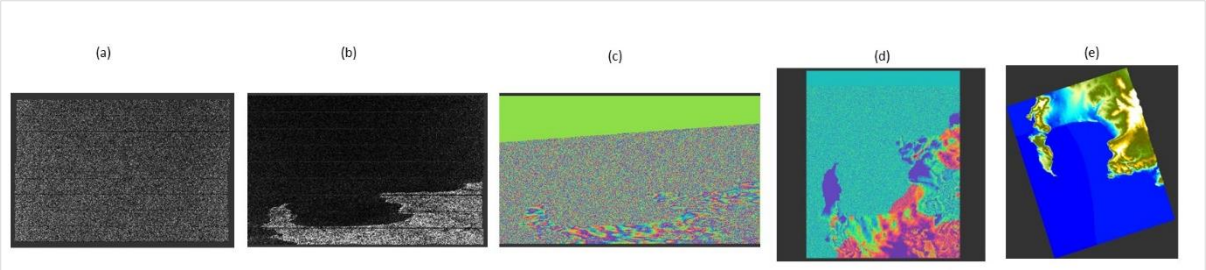

Figure 20 Differential Interferometry process outputs

The external Snaphu tool converted the obscure interferogram into a recognizable topographic format based on the phase change between adjacent pixels (Veci, 2015). This occurred through 3 steps: exporting, external product unwrapping and importing the product back into SNAP. The product was exported with the Deformation mode because Sentinel-1's main purpose was subsidence detection and not so much for topographic modelling (Braun, 2021). This was due to the technical conditions imposed by a narrow Earth-fixed orbital tube, which ensures repeatable surface coverage but leads to an unfavorable temporal and perpendicular baseline and thus phase decorrelation (Prats-Iraola et al., 2015).

This can cause errors in interferometry, but the expected output was the smoothened interferogram as in Figure 20 (d) above where the shape of the Cape Peninsula began to emerge meaning there was still a need to convert the radian units into metric units through the Phase to elevation tool in SNAP thus creating the DEM. Figure 20 (e) above depicts the final terrain corrected DEM, which was converted from the slant range to planar coordinates again with the assistance of the global SRTM 1Sec HGT elevation model due to terrain induced errors such as foreshortening. The DEM was then imported into ArcGIS and reprojected from the WGS84 reference system to Hartebeesthoek94. Whilst there was uncertainty caused by decorrelation elevation values were relatively within the range of the ground truthed data. The DEM's were then used for volumetric analysis and the generation of derivative products.

4.3.6 REAL TIME KINEMETIC (RTK) BEACH SURVEY

The information extraction presented above highlights the multiple levels of data manipulation required, and to capture the current state of the beaches, a ground-based survey with a higher resolution was used to fulfill objective 2; Objective 2: Assess and classify the Kommetjie and Milnerton coastal areas through field work to validate satellite results. on

page 6 to ultimately validate the satellite data. There are several approaches to coastal surveying such as aerial imagery, resection fixes or traverses. Whilst a UAV approach was considered, flight permission constraints were a hindrance and an RTK survey proved to be most appropriate. Geomorphological mapping requires detailed preparation, which includes review of literature, historical, topographical, and geological imagery. This ensures a clear, concise plan that considers all factors pertinent to data acquisition. An appropriate planning strategy was employed based on the following:

1. Size of area under investigation
2. Data resolution
3. Topography of the study site
4. Remoteness and accessibility of the study site
5. Weather conditions
6. Availability of equipment, financial scope, and time frame

Although excursions were made to both sites, due to budgetary and manpower limitations, as well as ensuring an overhead satellite on the day of the survey, only the Kommetjie site was surveyed. A small-scale stretch of beach ranging between 1-2 Kilometers was observed through a Real Time Kinematic (RTK) continuous topographic survey. The Kommetjie shoreline is an urbanized coastal area and for the most part exhibits homogenous gentle slopes with dunes that mark the back shore, as well as an alternation between a sandy and rocky shoreline. Figure 21 on page 83 is an image of the actual scanned area. The spatial resolution used is based on the phenomenon being observed and the available equipment (Lee et al., 2011). The dataset with the lowest resolution in any GIS based study dictates the data limits. In this case, the 30m resolution of the Landsat data and 10m of the Sentinel-2 data mean that any ground truthing data must have a better resolution. The Waterline, as well as the DInSAR derived DEM’s were thus compared against this survey as a form of validation.

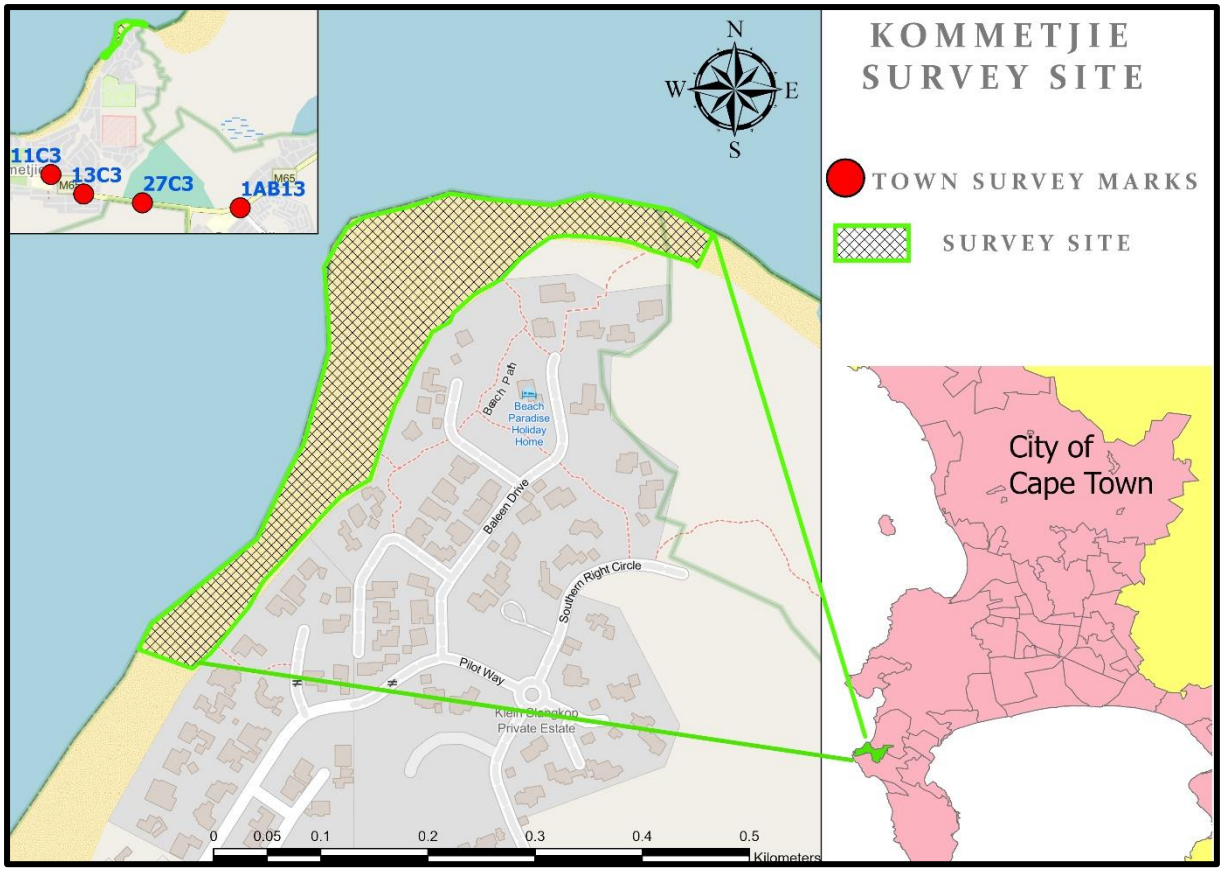

Figure 21 Kommetjie survey site

The Trimble R8 GNSS/ R6/ 5800 system shown in Figure 22 (a) on page 84 was supplied by the UCT Geomatics Division. The GPS system works as an on the pole rover and GPS receiver through Bluetooth whilst real time corrections are made through TrigNet system making this survey method efficient. The 4 town survey marks (11C3, 13C3, 27C3, 1AB13) depicted in Figure 21 above and as illustrated in Figure 22(b) on page 81 were used to calibrate the GPS within the Hartebeesthoek94 coordinate system before the survey. To ensure homogenous kinematic GPS transects and coverage of the site, two surveyors, approximately 5m apart, walked along the beach, perpendicularly to the shoreline with the rover in hand as in Figure 22 (c) on page 81. The wet/dry waterline boundary was marked, as well as rocks and measurements concluded at the backshore dunes but could not go beyond due to restricted access of private property in the area.

Figure 22 (a) R8 Trimble GPS equipment (b) Surveying a TSM (c) Beach RTK survey

The collected data were filtered and cleaned up to reflect only the general beach profile before using Inverse Distance Weighted (IDW) interpolation to create a DEM. A resolution of 1.838m^2 was achieved. The beach survey acted as the ground truthing aspect of this study and elevation points were chosen along 12 transects to determine the accuracy of the other beach modelling methods discussed above.

4.3.7 DEM ACCURACY ASSESSMENT

The quality of an elevation model is often deduced through the Root Mean Square Error (RMSE) by comparing the DEM to the true values of ground control points from another dataset (Wang et al., 2015). The errors associated with any DEM vary with the topography of the area under investigation. For instance, a more rugged terrain is more likely to produce more errors. There are other factors that affect accuracy assessment such as the distribution of the GCP's; however, the error values can be used to adjust or orthorectify elevation (Wang et al., 2015). Table 7 below is a synopsis of the parameters that govern the original data used here. The difference in ellipsoids and datum are major contributing factors to the results presented in section 5.6.2.7 on page 131.

Table 7 Beach profiling original data comparison

	RTK (GPS)	SENTINEL-1 SLC	SENTINEL-1 GRD
HORIZONTAL DATUM	Hartebeesthoek94	WGS84	WGS84
ELLIPSOID	WGS84	EGM96	ellipsoid earth model WGS84
SPATIAL RESOLUTION	±5m	5x20m	20x22m

Models are approximations of reality and can lead to a false Earth Superficial Shape (ESS), which means there is a need to account for the difference between the generated and true elevation values (Satge et al., 2016). To confirm positional accuracy, the elevation values were observed at the pixel level. All the elevation models were extracted at varying resolutions and using different techniques. They were interpolated to the topographic survey scale and elevation points were compared along transects. Difference of DEM's (DoDs) were used to determine volumetric changes between 2016 and 2021 whilst DEM derivatives such as slope and aspect classification were included for error assessment because they can be better at detecting artefacts (Wang et al., 2015). The models produced from waterlines can be considered as having relative heights, however the higher resolution City of Cape Town's LiDAR data are used as a geodetic benchmark to adjust the models to absolute heights using error approximation.

4.3.7.1 VERTICAL ADJUSTMENT TO ABSOLUTE ELEVATION

2020 City of Cape Town LiDAR data was used to create DEM's at a resolution of 0.52m. 30 points at each study site were selected and their corresponding elevations from the LiDAR and Waterline DEM's were extracted for comparison. Because there were no LiDAR data that coincided with the waterline imagery, it was decided that the 30 points would reflect permanent ground features such as roads, intersections and parking lots that existed in both 2016 and 2021. The heights for the 30 points were differenced and the difference mean was then used to vertically adjust the DEM's using a simple raster calculation. The vertical adjustment tables can be found in Appendix E.

Equation 9 Pixel Height Mean Difference

$$Mean\ Difference = \frac{\Sigma_{30}(L_n - W_n)}{30}$$

Whereby:

L_n= elevation value at nth point in LiDAR DEM

W_n= elevation value at nth point in Waterline DEM

The results are visually depicted in section 5.6.2.3 on page 127.

SUMMARY

The methodology presented here has drawn from the work of past authors and has been further streamlined by data and tool availability. It showcases a GIS based approach to quantifying coastal erosion through 2 different shoreline monitoring approaches. The first elaborates on the use of waterlines as visually extracted proxies to observe shoreline propagation. This movement is related to erosion because landward migration depicts erosion whilst seaward migration indicates accretion of coastal sediments. The second technique is a highly technical approach that uses datums as a proxy for beach profiling.

Two techniques were compared. The waterline method combines principles of marine science and remote sensing to interpolate tide levelled waterlines into elevation models. Differential interferometry applies the phase difference of remotely sensed radar images to create elevation models. These models were compared to a current state beach profile model captured by means of a topographic survey. The incorporation of theoretical considerations around the application of remote sensing towards coastal morpho-dynamics and hydrodynamics have been showcased here and their importance becomes clearer in the results chapter that follows. The results highlight interesting shoreline extraction observations through spectral analysis, discuss shoreline movement measurements and elevation modelling accuracy.

5 RESULTS and ANALYSIS

Whilst the methods section has conveyed the practicality of this study approach, this chapter consolidates the observations and various outputs from the above executed methodology framework to determine shoreline changes in Kommetjie and Milnerton. The results are sectioned to address the analytics that went into both pre-processing and finalizing the results. The spectral properties of coastal areas and land cover changes as discussed in section 2.2.1.1 on page 18 are demonstrated here both statistically and visually. The same approach is used to address the various parameters associated with multidecadal shoreline changes, as well as an effective comparison of the different coastal elevation modelling techniques towards capturing coastal zone geomorphological changes.

5.1 SPECTRAL ANALYSIS

Deciding on suitable image processing techniques requires an understanding of the satellite data and how land cover responds within different wavelengths. Ultimately, indices are band ratioing calculations and the wavelength bands with the biggest contrast are most ideal to capture pixel variations (Asmadin et al., 2018). Based on past works, the 4 indices discussed in section 2.2.1.2 on page 19 were tested to determine the ideal one for the purposes of this study (Mcfeeters, 1996). The comparison of these indices fulfills objective 4; Objective 4: By process of elimination, determine the most applicable and accessible satellite data processing methods for shoreline extraction on page 7 in determining appropriate geo-processing techniques for shoreline extraction.

5.1.1 MULTISPECTRAL BAND SELECTION FOR CLASSIFICATION

The spectral profile depicted in Figure 24 on page 89 with its corresponding table below compare Landsat-8 satellite bands and their land cover responses of a transect over the coastal area of Kommetjie in Figure 23 on page 83.

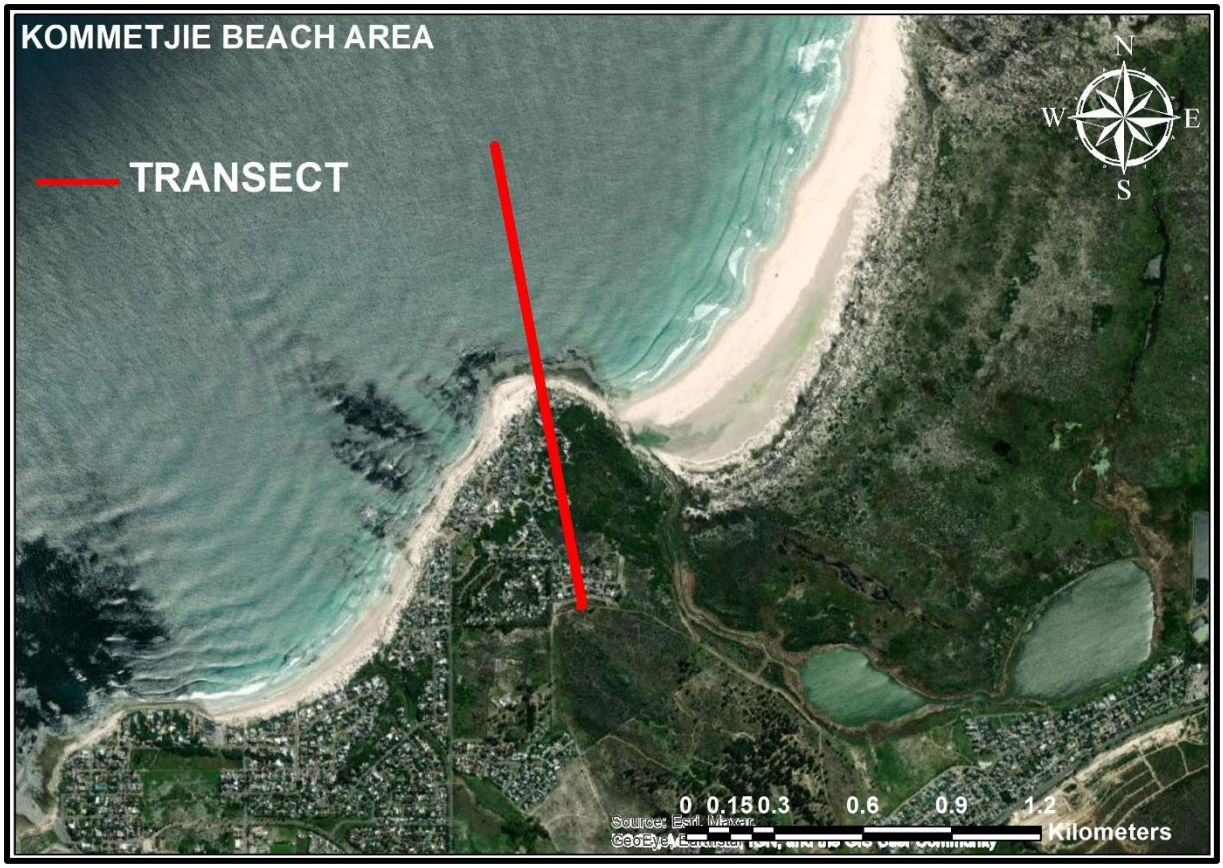

Figure 23 Spectral transect over Kommetjie

Aerial imagery source: City of Cape Town 2018

Evidently all the bands can detect land cover change to differing extents. The Short-Wave Infrared (SWIR) band has the lowest reflectance of four over water whilst the opposite is true reaching a maximum of 144 as it transitions over land. The Green and Near Infrared (NIR) bands can detect more subtleties in the shallow coastal area than the SWIR band. They also detect the beach area at pixel 8 as opposed to SWIR's pixel 9. Both the Green and NIR bands reach their maximum within the beach area at pixels 74 and 97 respectively, however, because they have the same general profile and the difference between them remains consistent, using them together in an index may not give the best contrast in land cover changes. At pixel 13, the profiles all level off and this could be a response from vegetation or buildings in the area.

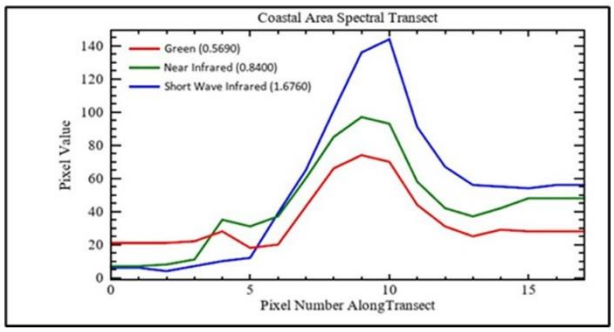

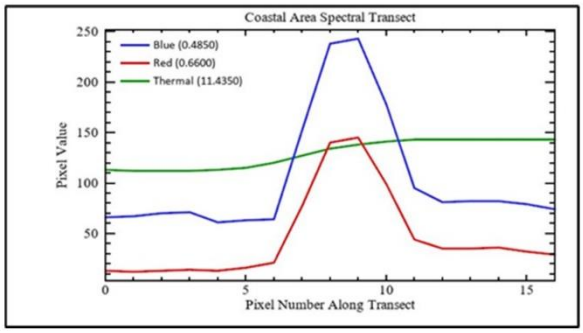

Land Cover	Pixel Number Along Transect	Land Cover	Pixel Number Along Transect
Ocean	0-5	Ocean	0-5
Shallow Coastal	5-8	Shallow Coastal	5-7
Beach	8-10	Beach	7-12
Mixed land	10-17	Mixed land	12-17

Figure 24 Example of Landsat TM spectral signatures

The second graph in Figure 24 compares a different group of bands along the same transect. The little variation in the thermal band suggests poor change detection capabilities, which is to be expected with it lower spatial resolution, however, it was designed to detect temperatures, which coincides with its slight increase as land cover changes from water to beach at pixel 6 like the blue and red bands (Chander et al., 2009). All the bands have a consistent lower response over the ocean with the Red band having the lowest reflectance of 12 whilst the Blue band achieves a high of 243 over the beach area. Again, it is clear that the Blue and Red bands have the same general profile which again brings into question whether they would be compatible in an index calculation

5.1.1.1 SPECTRAL INDEX SELECTION

The 4 indices tested were Normalised Differential Vegetation Index (NDVI), Normalised Differential Water Index (NDWI), Bare Land Index (BLI), Bare Soil Index (BSI). Before assessing their suitability, the 3 variations of NDWI, which is used to distinguish waterbodies in remotely sensed imagery, specified in the literature review were first investigated (Mcfeeters, 1996; Nguyen et al., 2021; Xu, 2006).

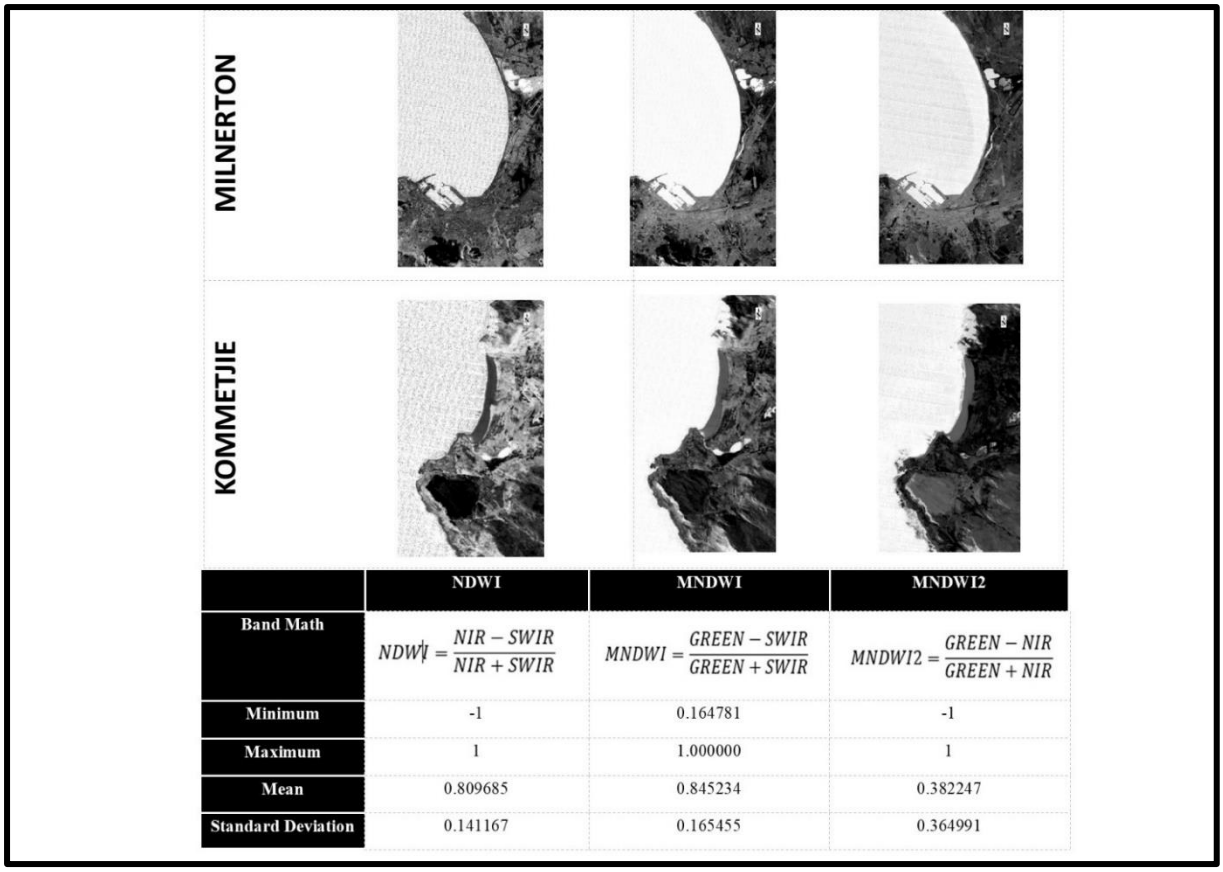

	NDWI	MNDWI	MNDWI2
Band Math	$NDWI = \frac{NIR - SWIR}{NIR + SWIR}$	$MNDWI = \frac{GREEN - SWIR}{GREEN + SWIR}$	$MNDWI2 = \frac{GREEN - NIR}{GREEN + NIR}$
Minimum	-1	0.164781	-1
Maximum	1	1.000000	1
Mean	0.809685	0.845234	0.382247
Standard Deviation	0.141167	0.165455	0.364991

Figure 25 Comparison of NDWI formula variations

The visual and statistical effects of interchanging image bands in a differential index formula for the detection of water bodies are depicted in Figure 25 above. All three equations can differentiate between land and ocean components; however, their level of sensitivity differs. The MNDWI equation had clearly assigned all water bodies the same value of 1 whereas NDWI and MNDWI2 can detect wave fluctuations of the ocean leading to the speckled images which may lead to spectral confusion during classification. MNDWI2 depicts land surfaces such as the beach and mountain areas in a similar tone whilst the urbanized areas appear significantly darker, the opposite is true for NDWI. MNDWI2 had the highest standard deviation of 0.364991 however it was the closest to its mean of 0.382247 meaning the land covers were more correlated and harder to distinguish. The MNDWI1 equation reaffirmed the literature review by having the greatest divergence and was subsequently carried forward to compare it with the rest of the indices shown in Figure 26 on page 91.

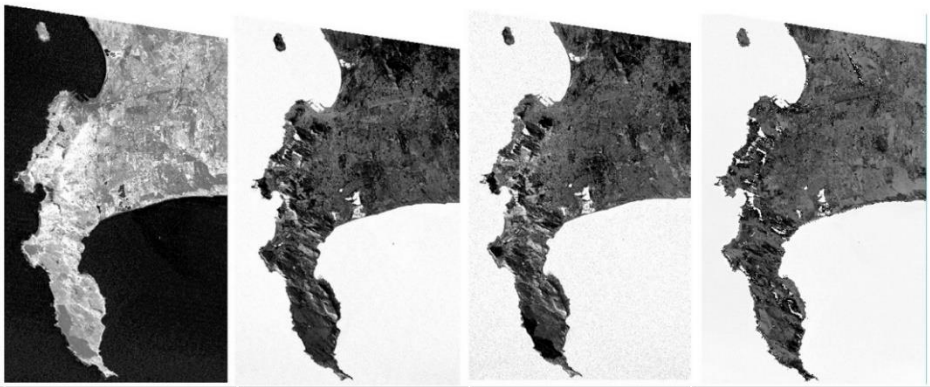

	NDVI	MNDWI	BLI	BSI
Equation	$NDVI = \frac{NIR - RED}{NIR + RED}$	$MNDWI = \frac{GREEN - SWIR}{GREEN + SWIR}$	$BLI = \frac{RED - TIR}{RED + TIR}$	$BSI = \frac{(RED + SWIR) - (NIR + BLUE)}{(RED + SWIR) + (NIR + BLUE)}$
minimum	-1.00	0.16	0.44	-132245.23
maximum	0.77	1.00	1.00	202041.19
mean	-0.29	0.89	0.96	0.039
Standard Deviation	0.28	0.15	0.05	188.20

Figure 26 Comparison of Indices

Figure 26 above takes a broader look at the Cape Town area to compare the indices. It is abundantly clear that they can all distinguish water and land components. The results echo the opinion of the literature review as the NDVI formula depicts vegetation or land as positive values whilst water is negative (Gao, 1996; Xu, 2006). The BLI was able to discern different land covers, however could not be used because Sentinel-2 data does not have already usable thermal bands and operate based on Land Surface Temperature (LST). For the sake of uniformity, this index was disregarded going forward. The BSI misclassified the mountain shadows as waterbodies and its deviation in contrast to its mean was too large, which was due to the use of the Blue band because as second image in Figure 26 indicates, it had the highest reflectance values overall. NDVI and MNDWI were the most viable indices to use, however statistically MNDWI was able to detect more land cover variability with a higher divergence between its mean and standard deviation. For these reasons and the recommendation of past research, MNDWI was the chosen index for this study.

5.1.2 RADAR BAND SELECTION FOR THRESHOLDING

As stipulated in section 4.3.1 on page 69, both variations of Sentinel-1 data have been used being GRD for shoreline extraction and SLC for differential interferometry (Ferretti et al., 2007; Filipponi, 2019). Coastal areas are highly complex areas, and the land cover backscatter responses of these datasets were again the basis for the research design along with literature-based advice. This section seeks to explore how the intricacies of radar data discussed in the theory chapter are considered for a comprehensive analysis of shorelines.

5.1.2.1 EFFECT OF POLARISATION ON LAND COVER BACKSCATTER

A transect was drawn over the Kommetjie coastal area of a backscatter image as shown in Figure 27. Figure 28 and Figure 29 on page 93 compare the effect of polarization on land cover response. The only polarizations available for the Cape Town area are VH and VV, which is a major limitation to this study. Land cover changes can be deduced as we move along the transect.

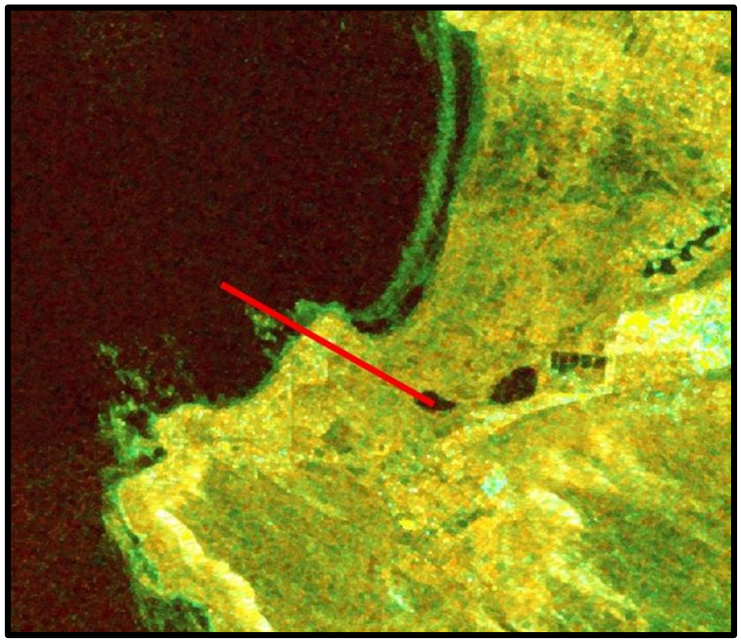

Figure 27 Radar spectral transect over Kommetjie area

The transect originates from the Wildevoelvlei Dam, transitioning to land at pixel 14.987(red arrow) and continues to fluctuate over land until pixel 117.624 where it transitions over the ocean as shown in Figure 28 by the black arrow.

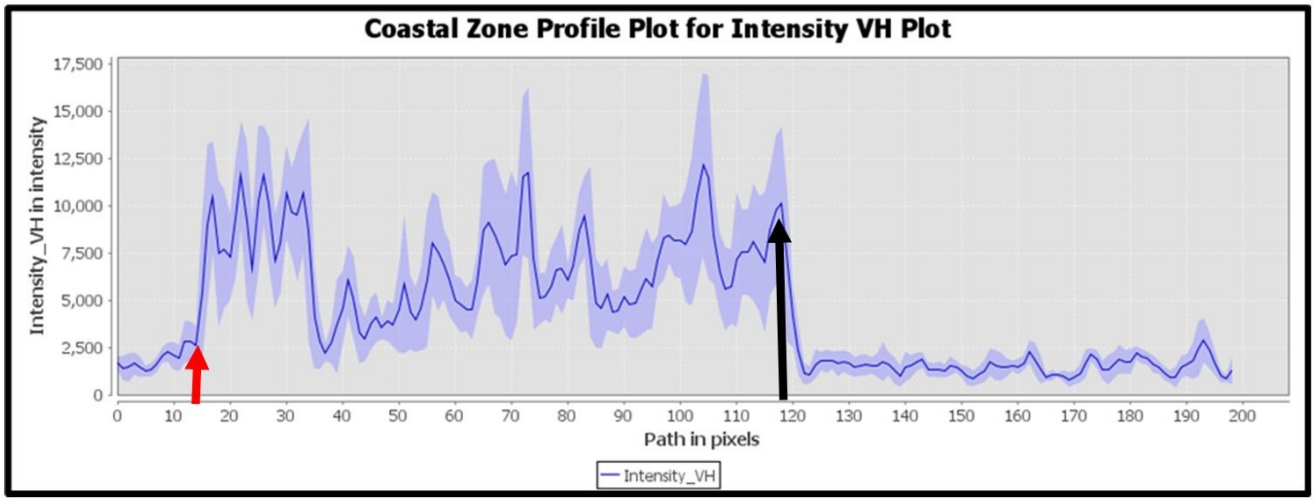

Figure 28 Spectral plot for Intensity VH band of Sentinel-1 data with change in land cover shown by arrows

The land cover changes are not as easy to note from the intensity of the VV Band because there are several fluctuations over both land and water in Figure 29, however again, the transition from Wildevoelvlei Dam to land begins at pixel 10 and the land portion occurs from pixel 18.166 until 115 where the beach occurs to pixel 123 and transitions over the ocean. These land cover transitions are indicated by the red arrows.

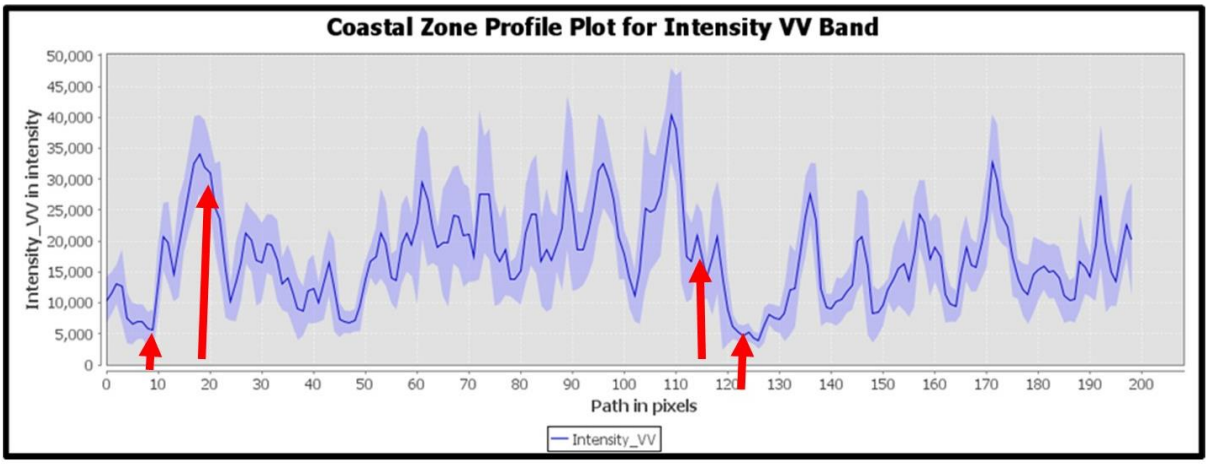

Figure 29 Spectral plot for Intensity VH band of Sentinel-1 data with change in land cover shown using arrows

Figure 28 and Figure 29 reiterate the theoretical concepts behind Radar-based remote sensing discussed in section 2.2.3.3 on page 27. The general expectation is for water bodies to have a lower intensity because they are flat surfaces as opposed to land components that are mixed and include volume scatterers (vegetation, buildings, soil, and roads among others.) (Schmidt et al., 2020). The fluctuations in Figure 29 over the ocean may be caused by the presence of rocks, seaweed, or wave peaks. The VV Band was clearly more sensitive than the VH band in detecting surface backscatter changes, which is more suitable for the complexity of the bio-optical properties of coastal zones to determine the most precise shoreline position, however, the VH band has a more clearly defined water-land transition. This contradiction could be better refined by combining radar and optical images.

5.1.2.2 RELATING CALIBRATION TO LAND COVER BACKSCATTER

Calibration was observed to further determine the most appropriate band. Radar data can be calibrated to either Sigma, Beta or Gamma based on the project expectations. Gamma calibration is simply a flattened, terrain corrected derivative of either Sigma or Beta calibrated data (European Space Agency, 2021).

The graphs in Figure 30 below depict the combined effect of polarization and calibration on land cover response measured in decibels. The same transect over the Kommetjie coastal area was used. All 4 variations were able to detect general land cover changes with landcover transactions indicated by the red arrows. Again, the graphs associated with the VV band were more sensitive and detected more backscatter over waterbodies. They all detected the transition from the Wildevoelvlei dam at pixel 10 and the graphs fluctuate over the urban land area before transitioning to the beach. The peaks that occur between pixels 120 and 135 can be attributed to the beach areas and there after the lower backscatter references the ocean.

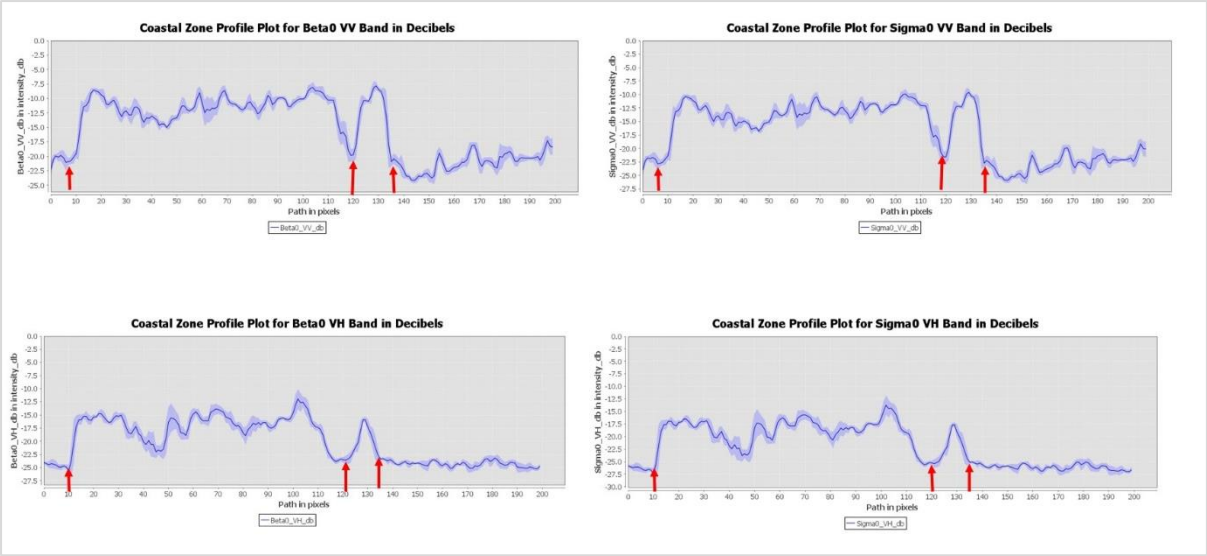

Figure 30 Comparing the combined effect of calibration and polarization on coastal area spectral plots

These graphs did not offer conclusive evidence on which calibration was applicable and so their histograms were observed as shown below. The choice to ultimately use Sigma calibration stems from literature, which emphasizes that Sigma is the backscatter coefficient whereas Beta is the Brightness coefficient, and we are interested in backscatter response in this instance (European Space Agency, 2021).

The histograms show that VH polarization was able to clearly differentiate better between land and water components regardless of whether sigma or beta calibration was used. Whilst the VV bands only had one intensity peak, the VH histograms had two peaks. The higher peaks signified the land components which had more pixels whilst the lower peaks were the waterbodies, again highlighting the expected lower backscatter from waterbodies (Salameh et al., 2020).

The ability to pinpoint the transition as indicated by the red markers between landcovers led to the initial assumption that the Sigma VH band was more suitable for thresholding because its histogram shows two clearly distinguished peaks for land and water components respectively. A closer visual inspection of the images concluded that the Sigma VV band was most appropriate.

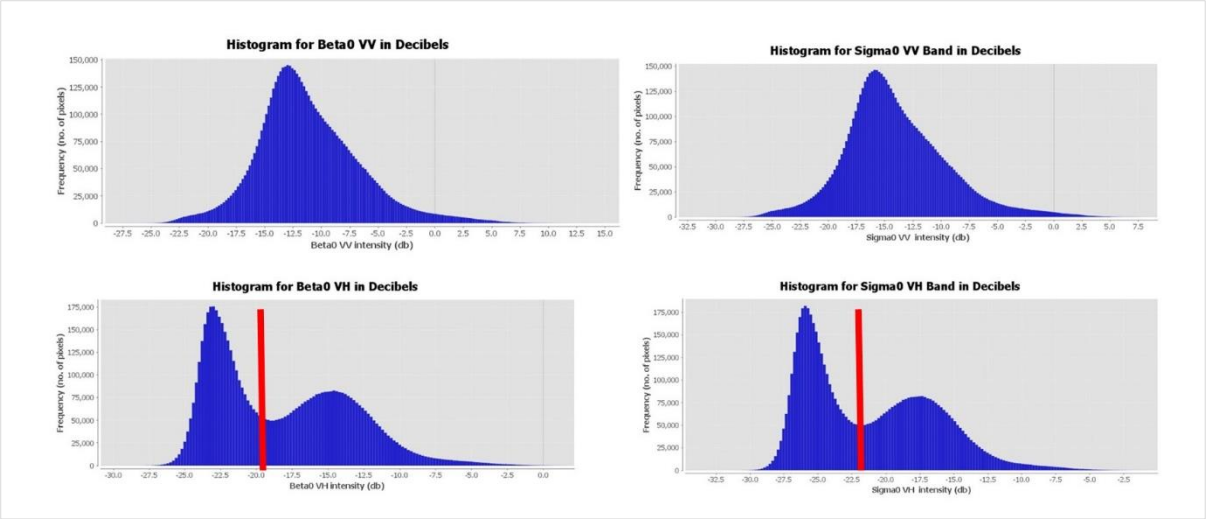

Figure 31 Comparing combined effect of calibration and polarization on spectral histograms

Figure 32 on page 97 shows an example of Sigma VH and VV backscatter images over the general Kommetjie area. Whilst they both have a clear delineation between the land and ocean, the Sigma VH band image on the left segments natural and urbanized land covers. It detects beach sand, rocks, and the ocean as one land cover leading to a false shoreline position. The Sigma VV band on the other hand is sensitive enough to detect the semi-submerged rock outcrops and the ocean wave run-up interaction with the beach leading to a more accurate shoreline position. This observation ultimately shows the value of using the VV band as opposed to VH and the discussion here reiterates the sentiments of subsection 2.2.3.3 on page 25 about the factors that determine backscatter detection in Radar imagery (Braun, 2021; Filipponi, 2019; Veci, 2015).

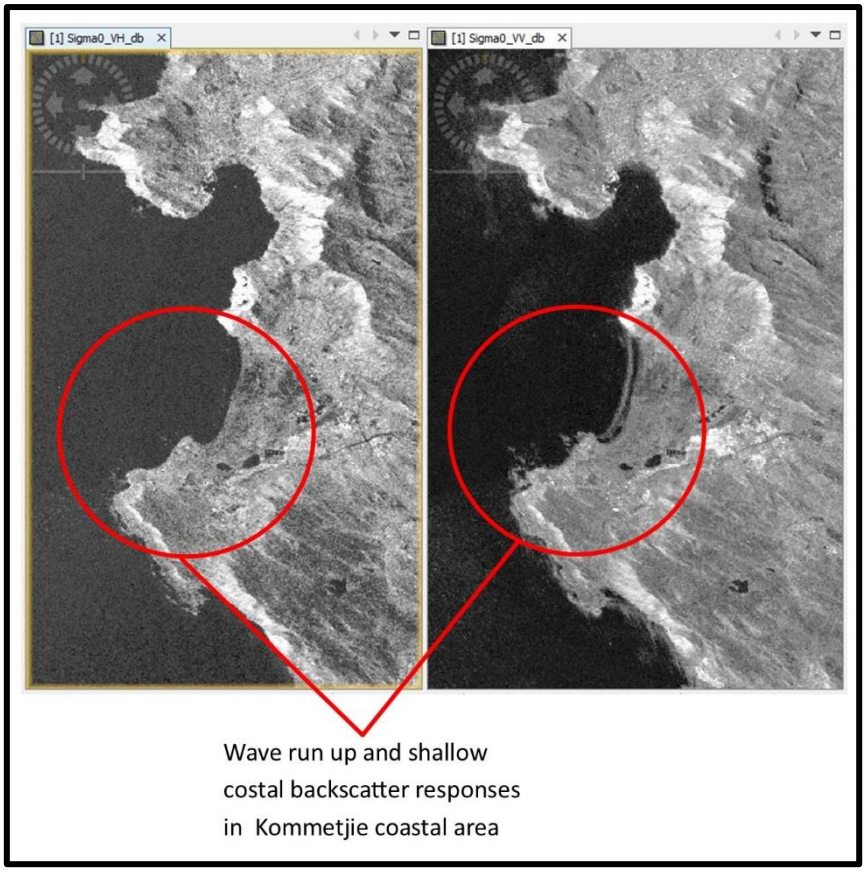

Figure 32 Comparing influence of polarization on coastal radar imagery

SUMMARY

The spectral analysis ultimately led to identifying MNDWI as an appropriate spectral index for optical image manipulation whilst applying thresholding to the Sigma VV band seemed appropriate for Radar data. The underlying theory of image segmentation is applicable for both datasets. As the earth surface undergoes both natural and anthropogenic changes, it is also reflected in satellite images. Based on pixel changes we can deduce and quantify land use land cover changes (Orlikova &Horak, 2019).

5.2 LAND COVER CHANGES

The land cover land use change (LULC) aspect was introduced in this study because as shown in the literature review Cape Town's coastal management is dependent on legislative urban planning, which is influenced by socio-economic needs, as well as environmental conditions. For example, within coastal areas specifically land cover changes between sand,

water and vegetation can help to infer the rate of sea level rise or deforestation. Sea Level rise would indicate a loss of land to the sea whilst deforestation leaves beaches further exposed to erosional processes. Urban sprawl can also be observed as a proxy for human influence. LULC was a challenge to deduce because the areas of interest, which were beaches had the lowest training samples for classification simply because even in the real world, beaches are small compared to other land covers. The images below showcase the output of support vector classification over the study sites, as well as the state of land cover changes 1991 and 2021 respectively, within both the Milnerton and Kommetjie coastal areas.

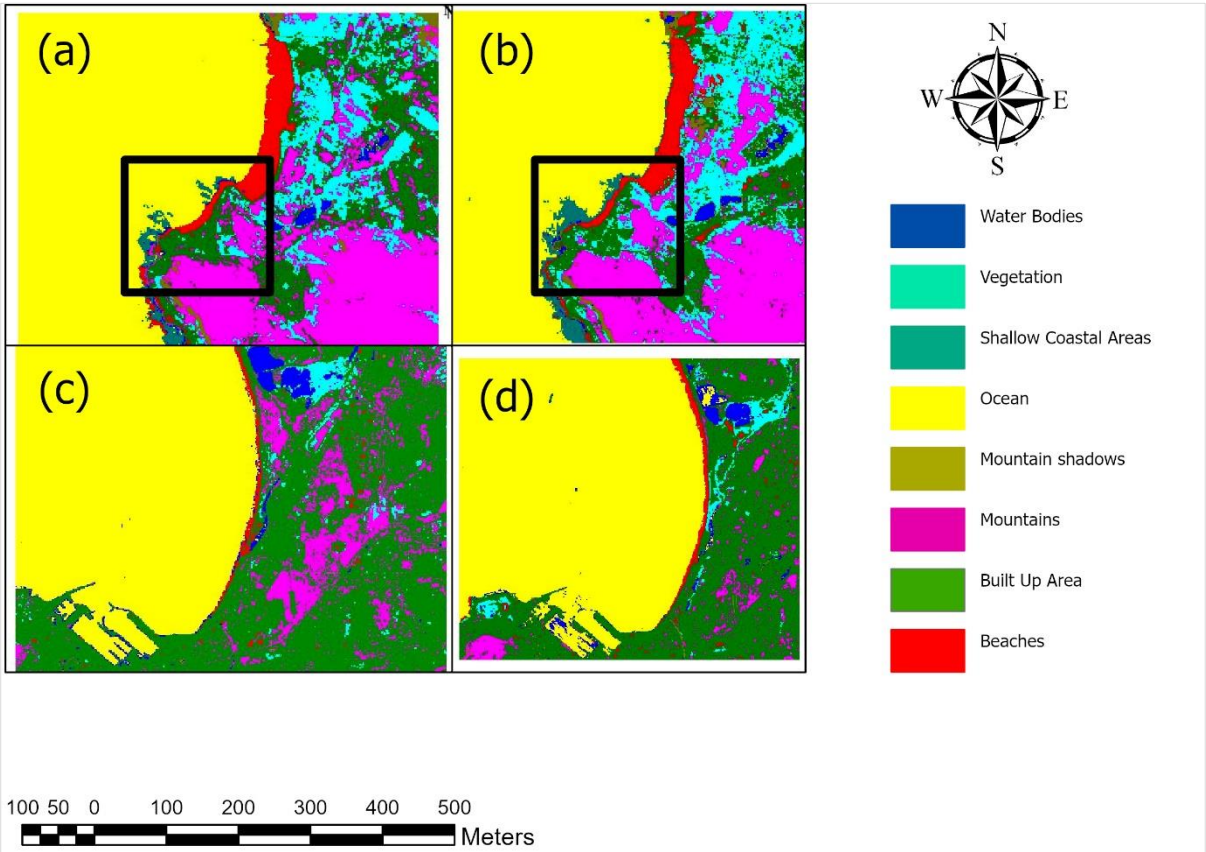

Figure 33 Comparison of land cover

(a) Kommetjie 1991, (b) Kommetjie 2021, (c) Milnerton 1991, (d) Milnerton 2021

The most notable changes along the Kommetjie coastline are the increased shallow coastal areas within the black square in Figure 34. They quantified in Table 8 on page 95 with a 62% significant increase from 1991 to 2021. Again, these areas could be a combination of seaweed

and rock outcrops. The increase may be due to increased seaweed floating at the surface of the water or it could be a simple case of a lowered water level that exposes the rocks at the time of image acquisition. As stated, Landsat satellites have generally passed over Cape Town at the same early morning time(7-8am), which is when Cape Town experiences its low tide. The classification scheme shows a clear discrepancy between land and water bodies, however urbanized land cover has increased whilst beach areas and vegetation have decreased. From the image change statistics derived from ENVI in Table 8, the Kommetjie area experienced a 7% increase in beach areas along with 14% for vegetation.

Table 8 Thematic Change Detection Statistics (%) for Kommetjie (1991-2021)

		INITIAL STATE								
FINAL STATE		Vegetation	Shallow Coastal Areas	Ocean	Mountain Shadows	Mountains	Built Up Area	Beaches	Row Total	Class Total
	Unclassified	0.000	0.000	0.000	0.000	0.000	0.000	0.000	0.000	0.000
	Water Bodies	0.361	4.016	0.027	9.043	0.187	0.200	-0.093	100.00	100.00
	Vegetation	50.642	0.000	0.000	7.553	10.514	28.767	2.109	100.00	100.00
	Shallow Coastal Areas	0.000	69.177	1.389	1.915	0.005	0.015	7.289	100.00	100.00
	Ocean	0.000	23.394	98.487	0.000	0.000	0.000	2.854	100.00	100.00
	Mountain Shadows	2.068	2.108	0.054	41.809	0.686	1.471	2.140	100.00	100.00
	Mountains	21.116	0.000	0.000	33.298	76.601	11.073	1.582	100.00	100.00
	Built Up Area	21.413	0.000	0.000	4.255	11.311	56.048	6.607	100.00	100.00
	Beaches	4.401	1.305	0.044	2.128	0.696	2.426	77.326	100.00	100.00
	Class Total	100.00	100.00	100.00	100.00	100.00	100.00	100.00		
	Class Changes	49.358	30.823	1.513	58.191	23.399	43.952	22.674		
	Image Difference	14.031	62.149	-0.696	14.468	-4.271	-9.009	7.010		

Interestingly, the classification can discern between the ocean (yellow land cover) and inland waterbodies (dark blue land cover). Whilst they both may have the same make up, their bio-optical properties are slightly different due to different environmental influences and thus are classed differently. Even though the Milnerton lagoon interacts with the ocean, it has still been classified as an inland waterbody. The ocean class has generally experienced the least amount of change overall whereas the Milnerton beach class increased by 38%, the built-up areas by almost 13% and vegetation by 16%. As opposed to the Kommetjie however, the Milnerton area has experienced a decline in shallow coastal areas.

Table 9 Thematic Change Detection Statistics (%) for Milnerton (1991-2021

		INITIAL STATE									
FINAL STATE		Water Bodies	Vegetation	Shallow Coastal Areas	Ocean	Mountain Shadows	Mountains	Built Up Area	Beaches	Row Total	Class Total
	Unclassified	0.000	0.000	0.000	0.000	0.000	0.000	0.000	0.000	0.000	0.000
	Water Bodies	50.608	3.923	30.952	0.503	12.941	0.770	0.902	1.507	100.00	100.00
	Vegetation	4.862	51.845	0.000	0.000	0.000	2.157	2.646	0.066	100.00	100.00
	Shallow Coastal Areas	0.608	0.000	2.381	0.011	0.000	0.000	0.003	0.131	100.00	100.00
	Ocean	19.109	0,047	30.952	98.917	8.235	0.031	0.101	6.815	100.00	100.00
	Mountain Shadows	3.410	0.187	11.905	0.050	9.412	0.760	0.606	0.262	100.00	100.00
	Mountains	0.439	5.138	0.000	0.001	3.529	17.594	5.821	2.425	100.00	100.00
	Built Up Area	16.205	38.533	23.810	0.231	51.765	77.722	88.080	26.606	100.00	100.00
	Beaches	4.760	0.327	0.000	0.286	14.118	0.965	1.841	62.189	100.00	100.00
	Class Total	100.00	100.00	100.00	100.00	100.00	100.00	100.00	100.00		
	Class Changes	49.392	48.155	97.619	1.083	90.588	82.406	11.920	37.811		
	Image Difference	-18.906	15.974	-28.571	-0.030	445.882	-57.724	12.759	38.270		

Although it is visually discernible that the shallow coastal areas have decreased in 2021 for Kommetjie, the beach areas (red land cover) look as though they are thinning out. The Milnerton coastline has seemingly widened slightly. It must be noted that the increase in beach areas is ultimately an increase in bare land, which is characterized by a soil spectral response. As such this increase may be a result of inland bare land increases as well. The Cape Town landscape is also well known for its hilly nature and the combination of rock faces, vegetation and bare soil land covers can lead to spectral confusion, which is why we use confusion matrices to establish how correct these classification schemes are. The Producer and User accuracy metrics can be found in APPENDIX A PRODUCER AND USER MATRIX FOR 1991 AND 2021 LANDCOVER CLASSIFICATION on page154.

5.3 CLASSIFICATION ACCURACY

As stated in the methodology, the suitability of both the support vector machine (SVM) and Neural network (NNC) classification algorithms were assessed through confusion matrices which incorporate aspects of omission errors and user accuracy. It was evident That SVM performed slightly better than NNC. A well classified image leads to more accurate shoreline extraction. Although 90% was the minimum overall accuracy exclusion value, all the shorelines used in the analysis achieved an accuracy of 94% and higher.

Table 10 below summarizes the classification accuracies for the extracted shorelines used in the DSAS analysis. The SVM classification performed better than the NNC achieving a

Kappa coefficient consistently over 0.8 and an accuracy over 94% whilst NNC ranged from 0.7. 2021 has the highest accuracy. This is probably because satellite sensor designs have progressively improved with time.

Table 10 Classification Accuracy Comparison

	Support Vector Machine (SVM)		Neural Network (NNC)	
	KAPPA COEFFICIENT	OVERALL ACCURACY (%)	KAPPA COEFFICIENT	OVERALL ACCURACY (%)
1991	0.8053	94.0057	0.7673	90.9242
2001	0.8308	94.2611	0.8267	94.1203
2011	0.8448	94.9670	0.7995	91.7149
2021	0.8485	95.1397	0.8458	95.0488

5.4 CALCULATION AND ASSESSMENT OF SHORELINE CHANGE RATES

A historical assessment of shoreline propagation through satellite observation is presented here. SVM classification was used to classify land covers and determine a line of transition between land and ocean components i.e., the shoreline. After the vectorization of the classification boundaries, the shorelines were further digitally cleaned up and smoothened by 50m to produce the following maps (Figure 34 to Figure 41) to better understand shoreline lateral movement. The shoreline captured for 1991 acted as the baseline for the study and a 10-year time interval was established for uniformity, as well as accommodating the slow rate of change of coastal systems and as such this study spans 40years (1991 to 2021). The results are presented for the Milnerton and Kommetjie study sites respectively

5.4.1 SHORELINE POSITION CHANGE

Figure 34 shows the Woodbridge area of interest in Milnerton. The shoreline evidently moved seaward between 1991 and 2001, maintained a similar range until 2011 and thereafter, the shoreline moved back landward by 2021 almost to its baseline position. Based on the transects produced between the shorelines by the DSAS tool, the maximum shoreline movement was 123.86m.

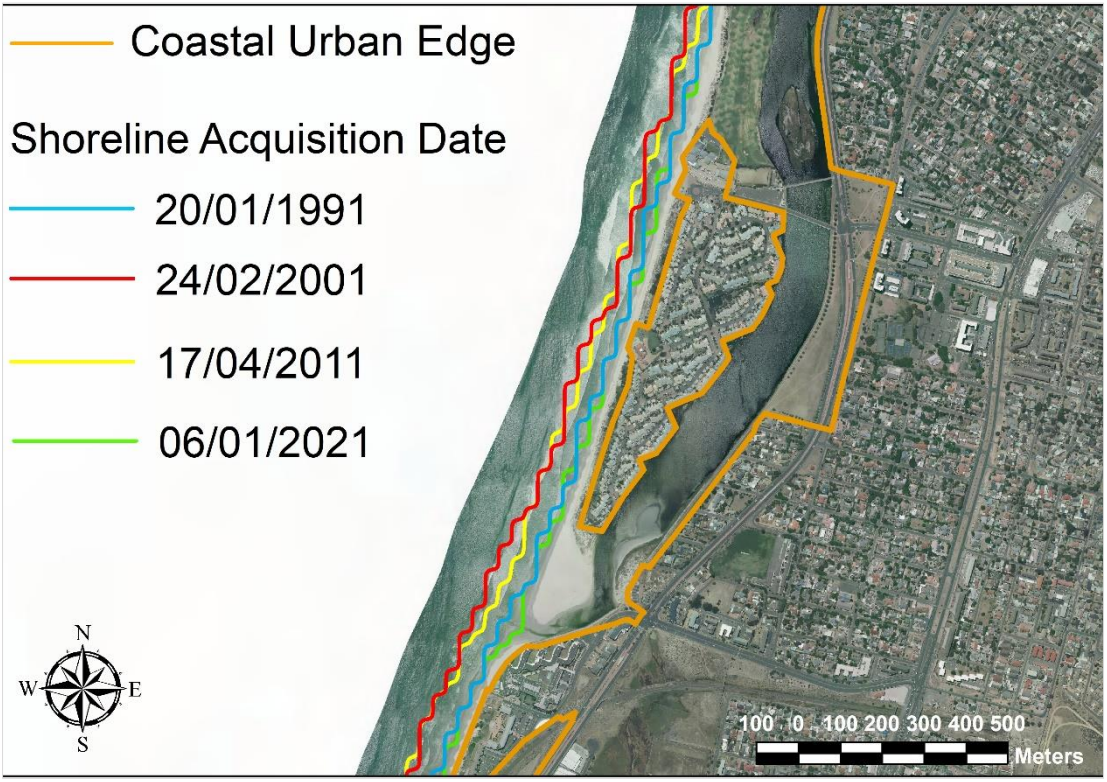

Figure 34 Shoreline change along Milnerton beach at 10-year intervals(1991-2021)

Aerial imagery source: City of Cape Town 2021

Figure 35 below of the Kommetjie shoreline shows a consistent landward motion over the 40-year period and its furthest movement was 150.94m. A shoreline moving land or seawards explains why the resulting statistics can be either negative or positive. Although it would be easy to assume that both stretches of beach would have a similar response over time because they occur along the Atlantic seaboard there are several environmental and anthropogenic forces that have shaped both these ecosystems. Table 11 on page 77 summarizes the DSAS measurements of these two coastal areas.

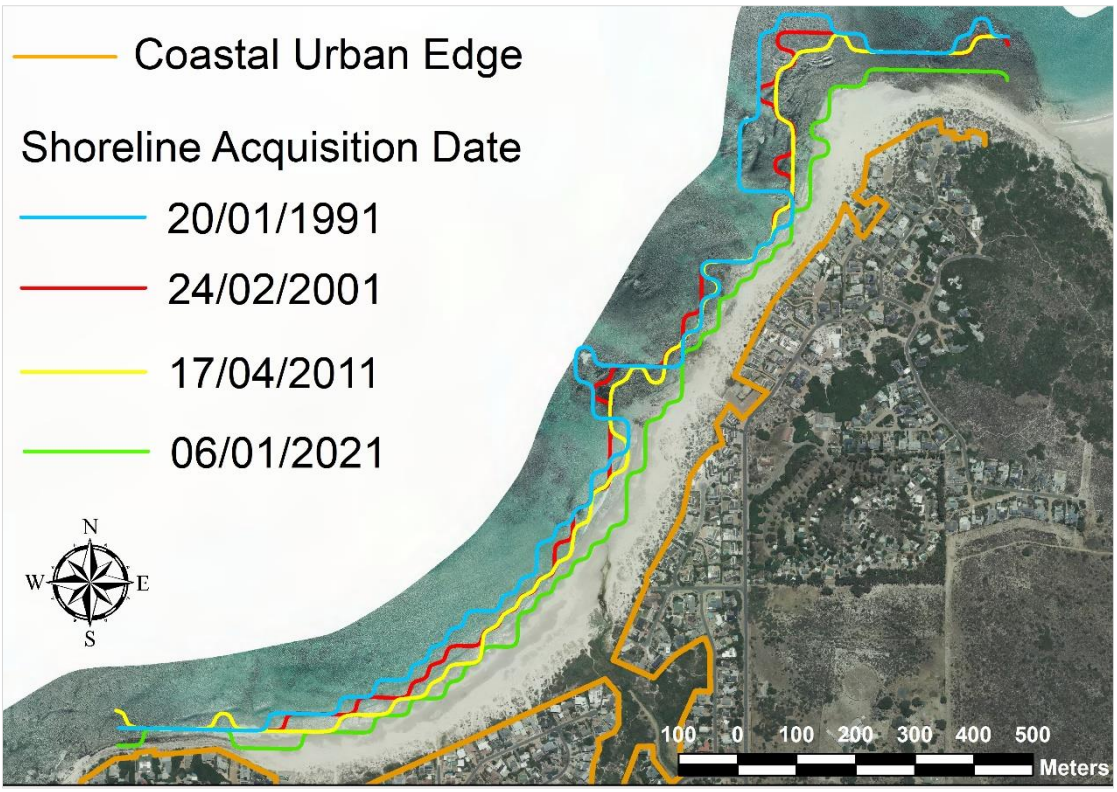

Figure 35 Shoreline change along Kommetjie beach at 10-year intervals (1991-2021)

Aerial imagery source: City of Cape Town 2021

DSAS allows us to quantify these coastal changes under the assumption that these lateral movements either indicate erosion or accretion of actual beach sediment and quantitatively this would be depicted as either negative or positive values (Oyedotun, 2014). As discussed in the methodology (section 4.2.3 on page 56) 3 measures of shoreline propagation (SCE, NSM and EPR) have been used to quantify erosion in this study (Himmelstoss et al., 2018). It is not enough to simply note these statistical changes without appreciating their underlying geography. Their associated maps will help to visualize where most change occurs. Understanding the locale also help to establish the reasoning behind the results.

5.4.2 SHORELINE CHANGE ENVELOPE (SCE)

The Shoreline Change Envelope simply measures the greatest distance moved by the shoreline irrespective of its acquisition dates (Himmelstoss et al., 2018). With an average shoreline length of 6.89km, the Milnerton shoreline used 1387 transects to deduce that the most significant change was observed at the Milnerton lagoon mouth where a maximum

change of 123.81m shoreline movement was detected as illustrated in Figure 36 on page 104. The shortest distance moved was 0.35m and ultimately the average distance moved was 49.35m. As expected, the fluctuating flow of the lagoon affects the transition zone to the ocean and the two opposing streams of flow accelerate erosion in the area.

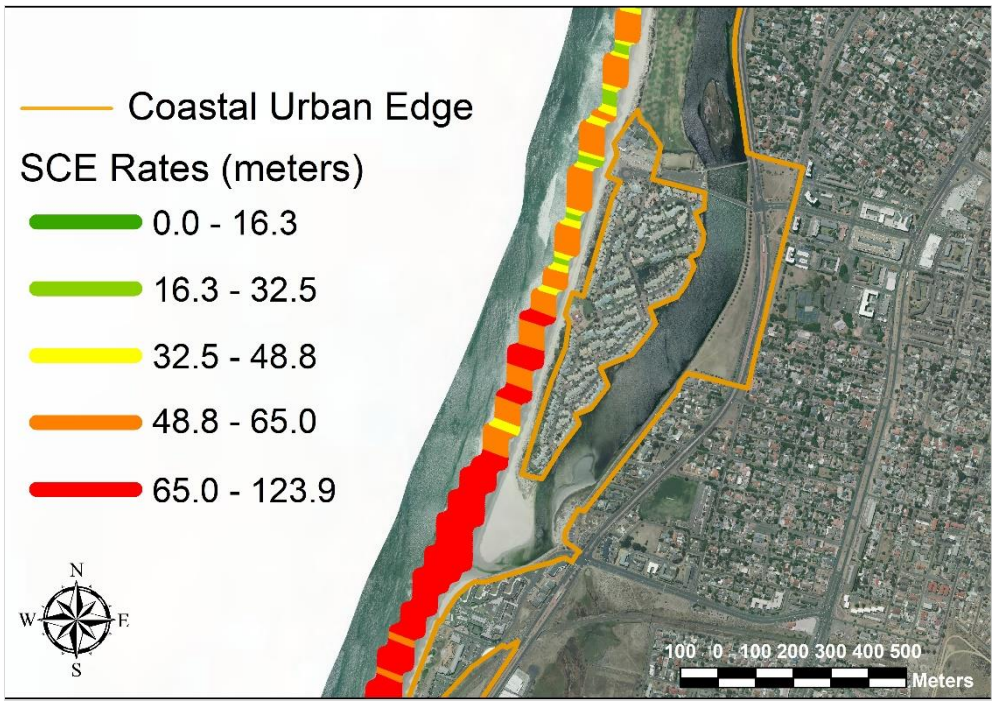

Figure 36 Shoreline Change Envelope (SCE) over Milnerton beach (1991-20212)

Aerial imagery source: City of Cape Town 2021

The Kommetjie Shoreline on the other hand was significantly shorter and only 578 transects were generated with an average shoreline length of 2.6km. Figure 37 below depicts the unexpected outcome of the areas with the most significant shoreline change occurring along the rocky portions of the beach with a maximum of 150.88m whilst a minimum of 0.2m was recorded. This averaged out the distance change to 51.77m. The drivers and implications of the statistics derived here are discussed under section 6.1 on page 136.

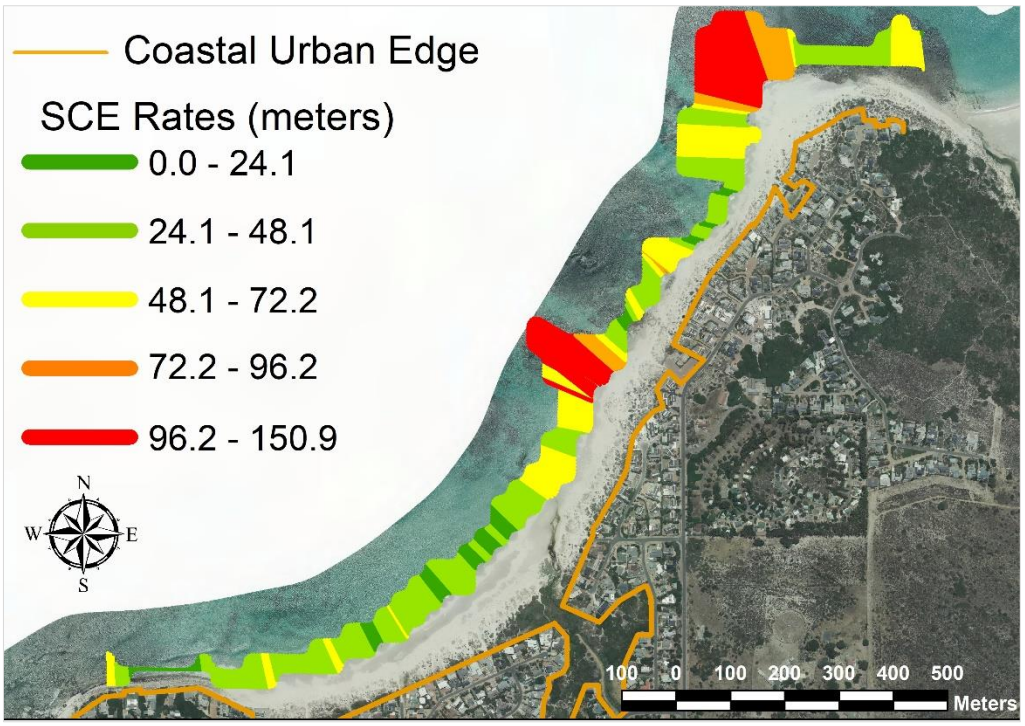

Figure 37 Shoreline Change Envelope over Kommetjie Beach (1991-2021)

Aerial imagery source: City of Cape Town 2021

5.4.3 NET SHORELINE MOVEMENT

This shoreline change parameter takes acquisition dates into consideration by to deducing the change between the oldest and youngest shorelines (Himmelstoss et al., 2018). 98.49% of the 1387 transects registered as negative or depicted landward movement along the Milnerton coastline. This means a maximum of 123.81m shoreline was eroded whilst only 0.49m of accretion was recorded. Again, these erosion statistics coincide with the locale of the Lagoon mouth indicated by the red arrow in Figure 38 on page 106. The shoreline erosion was averaged to 46.61m.

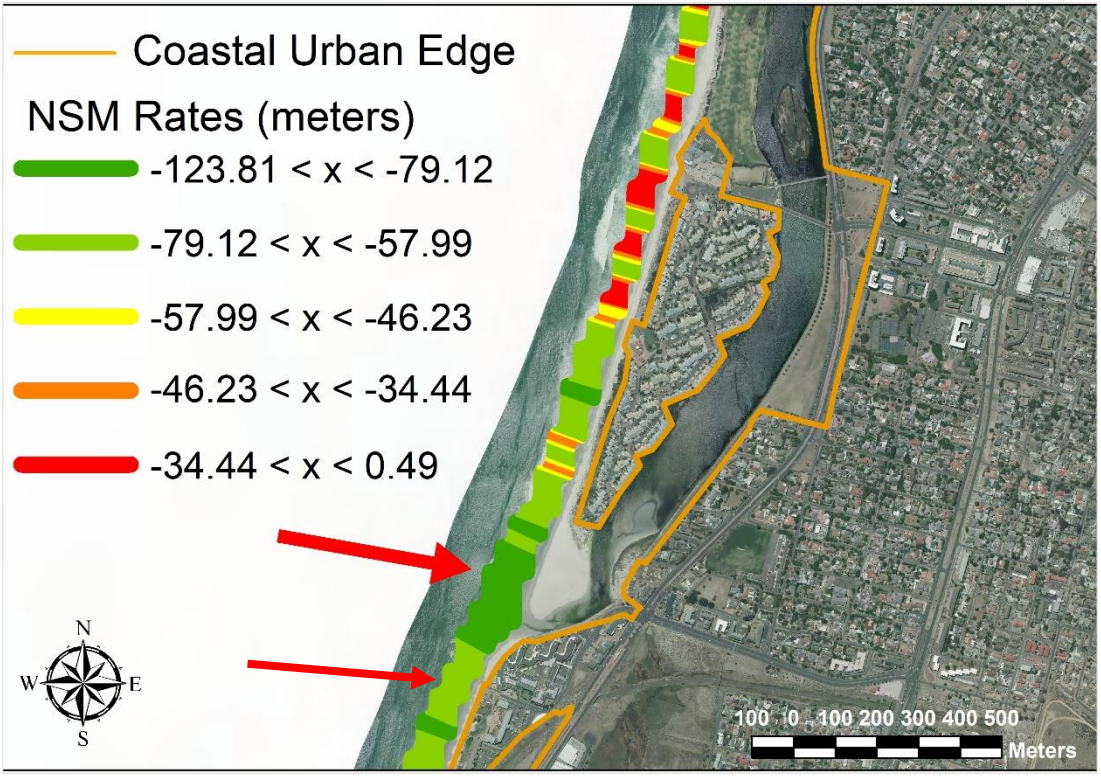

Figure 38 Net Shoreline Movement between 1991 and 2021 along Milnerton Beach

Aerial imagery source: City of Cape Town 2021

A general assumption would be that the Kommetjie shoreline experienced a slightly lower level of erosion with 95.16% of its transects recording erosion, however a higher erosion distance of 150.88m and 21.4m of accretion were measured. The accretion was detected at the mouth of the Bokramspruit estuary as indicated by the red arrow in Figure 39 on page 106 and southwards of it whilst the erosion occurred along the rocky curved portions jutting out into the ocean as shown below. An average of 53.52m of shoreline erosion was recorded along with 1.71m of accretion which led to an overall shoreline sediment deficit of 50.84m.

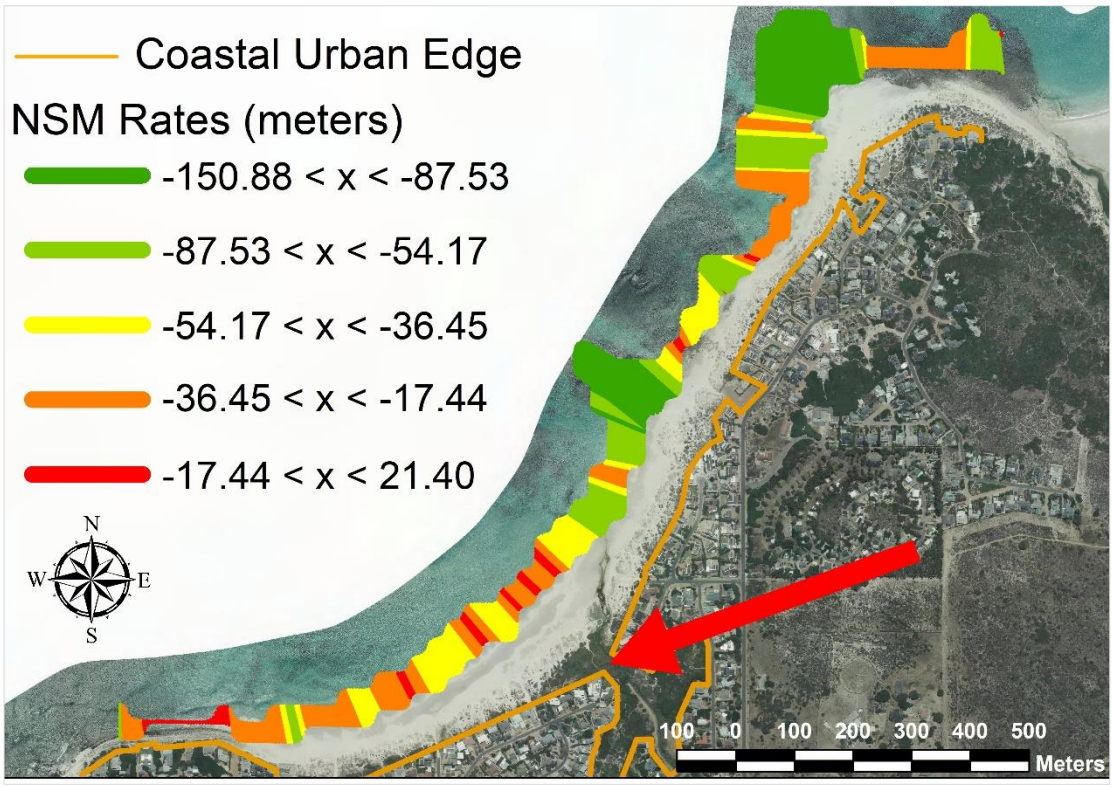

Figure 39 Net Shoreline Change between 1991 and 2021 along Kommetjie Beach

Aerial imagery source: City of Cape Town 2021

5.4.4 END POINT RATE

The End Point Rate calculates the rate of shoreline change by dividing the total shoreline distance moved by the time that has elapsed (Himmelstoss et al., 2018). There are portions of the Milnerton beach that have erosion rates of up to 6.23 m/yr. whilst only an accretion rate of 0.02m/yr. was recorded. The average of the accretion and erosion rates calculates to 2.35m/yr. This is cause for concern because the inference is that at an estimated average beach width of 49.503m and with the same level of coastal intervention, it would take 22 years for the Milnerton foreshore to be completely eroded. Again, as indicated by a red arrow in Figure 40 on page 108, the highest EPR is observed at the mouth of the Milnerton lagoon.

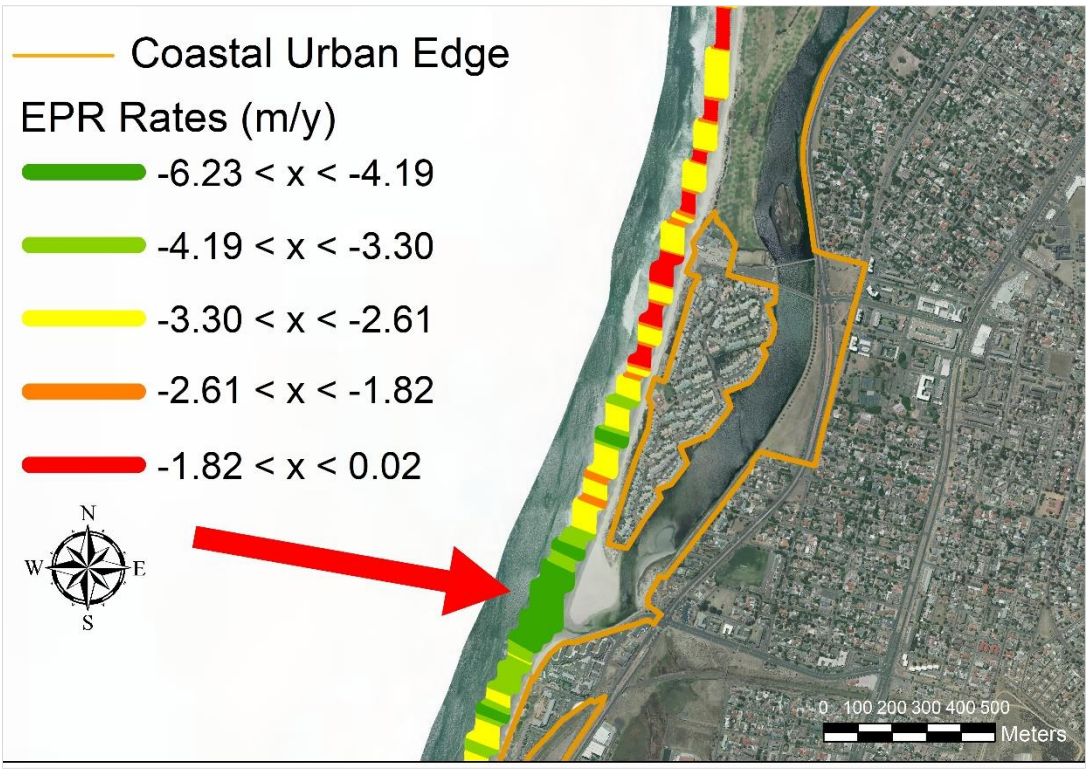

Figure 40 Rate of Erosion between 1991 and 2021 along Milnerton Beach

Aerial imagery source: City of Cape Town 2021

The maps shown in Figure 40 above and Figure 41 on page 109 illustrate the change in EPR along the Milnerton and Kommetjie shorelines respectively. The maximum rate of erosion along the Kommetjie shoreline is higher with 7.59m/y and with a maximum accretion rate of 1.08m/y it averages out to 2.56m/y of overall erosion. Whilst the statistics presented here can be daunting, the effectiveness of the assessment lies in its statistical significance.

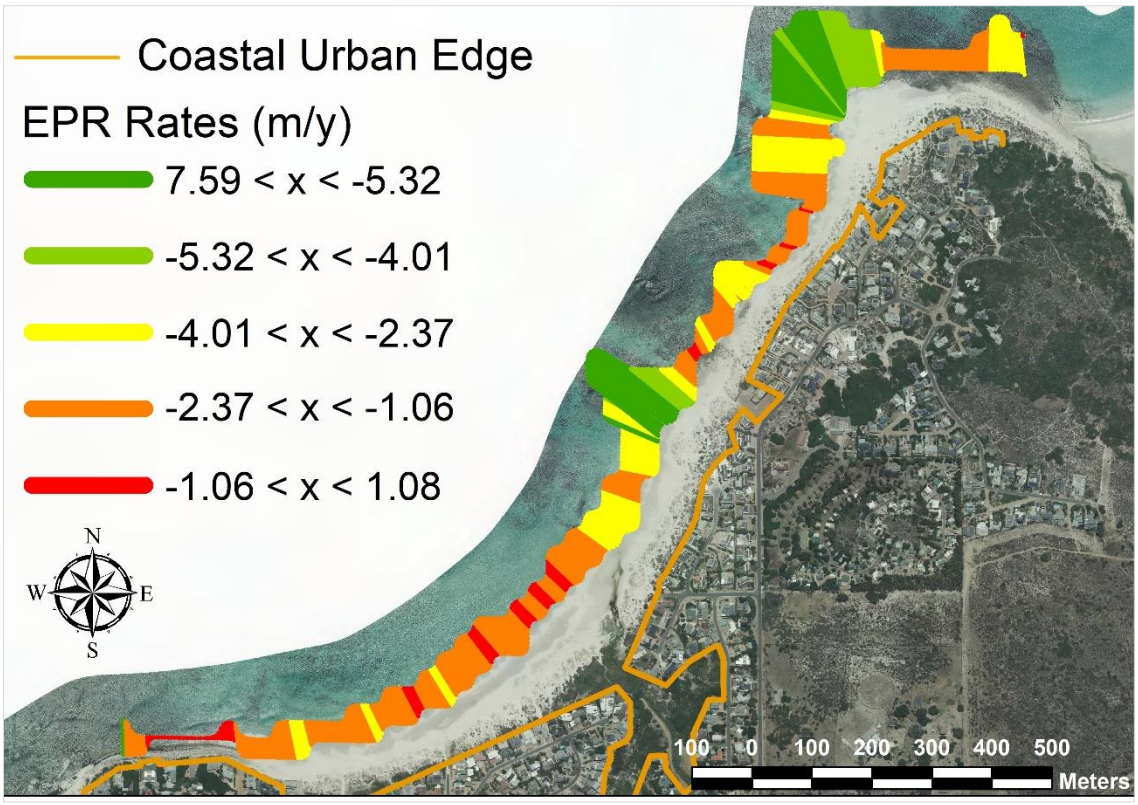

Figure 41 Rate of Erosion between 1991 and 2021 along Kommetjie Beach

Aerial imagery source: City of Cape Town 2021

5.4.5 STATISTICAL UNCERTAINTY

As previously stated, there are several sources of error when processing satellite data such as sensor orbital changes or atmospheric factors. Based on Equation 5 *DSAS Shoreline Uncertainty Equation* on page 67, the EPR uncertainty was concluded to be ±2.14m/yr. for both the Kommetjie and Milnerton Shorelines. This means that their overall average erosional rates were -2.56 ±2.14 m/yr. and -2.35±2.14m/yr. respectively between 1991 and 2021. It must also be noted that the DSAS was able to conclude that only 46.37% of erosion was statistically significant in Milnerton whilst it was 47.37% for Kommetjie.

Both the LSE and WSE achieved the same statistics and established the erosion rates to be -2.34±1.69m/yr. with only 15.16% erosional significance for Milnerton and -2.55±1.57m/yr. for Kommetjie with 11.98% significance. The implications of these errors are further

addressed in the discussion chapter, whilst the shoreline change results are summarized in Table 11 below.

Table 11 DSAS Results Summary

		KOMMETJIE					MILNERTON				
Acquisition Date	Satellite Sensor	Shoreline length(m)	No. of Transects	SCE average(m)	NSM average(m)	EPR average(m/y)	Shoreline length(m)	No. of Transects	SCE average(m)	NSM average(m)	EPR average(m/y)
20/01/1991	TM	2891.979728	578	51.77	-50.84	-2.56	7057.910078	1387	49.35	-46.61	-2.35
24/02/2001	ETM	2637.595482					6831.297266				
17/04/2011	TM	2532.22485					6721.224853				
06/01/2021	OLI	2378.436606					6944.826493				

5.5 FIELD OBSERVATIONS

Both the Milnerton and Kommetjie beaches are more elongated than wide, however due to time and financial constraints the areas of interest were limited to a 1-2 km range. Whilst they are both urbanized coastal areas, they exhibit different morphologies and as such the effect of erosional processes will differ. Milnerton can be characterized as having a narrow, undulating beach. The area of interest was Woodbridge Island because the proximity of the Milnerton Lagoon presented an interesting case study as to how effective satellite capture could be in detecting the shoreline at its mouth especially because effluent has altered the lagoons bio-optical characteristics as shown in Figure 42(a) below.

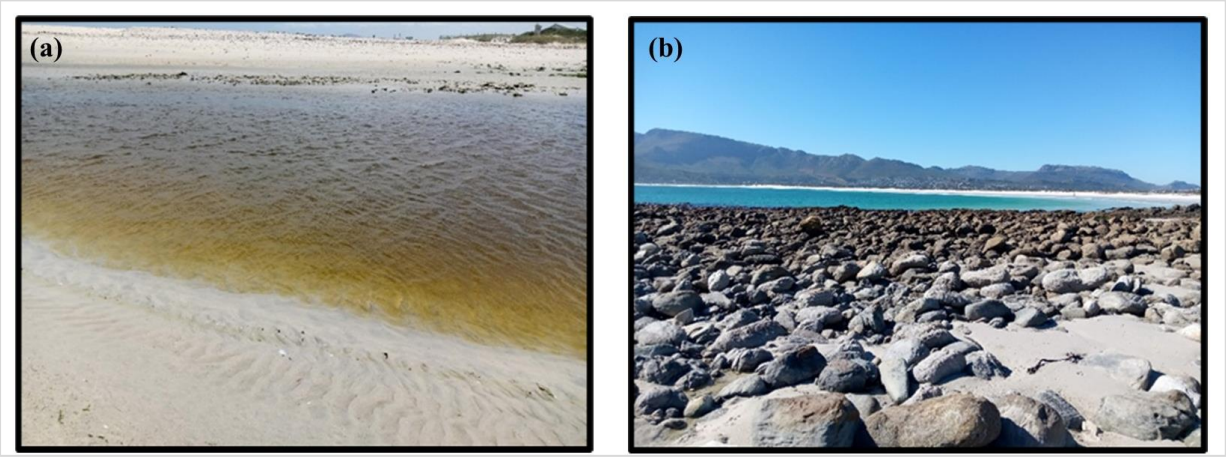

Figure 42 (a) Milnerton Lagoon Mouth (b) section of Kommetjie beach covered by boulders

The Kommetjie coastline is wider than Milnerton's and exhibits homogenous gentle slopes with dunes, vegetation and private residential buildings that mark the back beach. Semi-submerged rock outcrops were also observed as shown in Figure 42(b) above which was a point of interest in shoreline extraction as well.

Figure 43 (a) Beach sand constituents (b) sand ripples along beach (c) water ripples within intertidal zone

The two beaches exhibit the same general biogenic sand profile with white fine beach sand mixed with broken down shells as shown in Figure 43(a) above. The influence of aeolian erosion was also prevalent at both beaches as depicted by the sand ripples in Figure 43(b). Wave ripples were also observed within the swash zone as in Figure 43(c). Bedding was observed in Figure 44 (a) whilst wave action is clearly exploiting their lines of weakness and striations were also observed in Figure 44(b). Rock bedding or stratification is associated with sedimentary rocks and is simply the layering of sediment as they settle out of suspension and are compressed over time (Zhou et al., 2021). Rock striations on the other hand are lines of weakness or faults on a rock surface, they are linked to glacial abrasion (Burningham &Knight, 2020). The force from waves as they move up and down a coastline turns these faults into cracks through hydraulic action or abrasion.

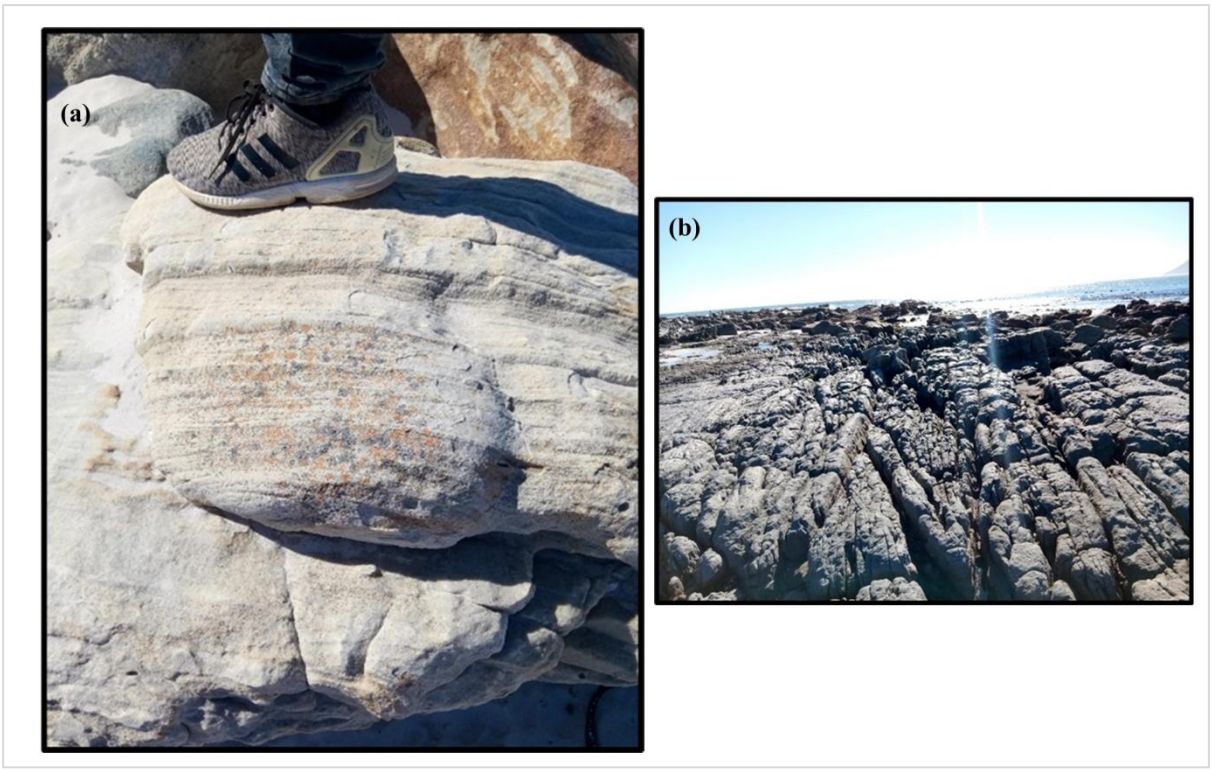

Figure 44 (a) Rock bedding (b) Rock striations

These rock outcrops and kelp beds along the Kommetjie shoreline act as protection against coastal erosion as they absorb majority of wave force as opposed to Milnerton that has no form of natural coastal defense (Lafferty et al., 2019; Nové-Josserand et al., 2018). The amount of seaweed awash was substantially more in Kommetjie with a brownish color and powerful stench whilst in Milnerton far less bits of green seaweed were observed as shown in Figure 45 on page 115. It could be argued that this flotsam could be used as a shoreline proxy as it coincides with waterline movement, however it is far too unreliable. Dune rehabilitation using re-vegetation was also observed along the backshore and in between private properties in the areas.

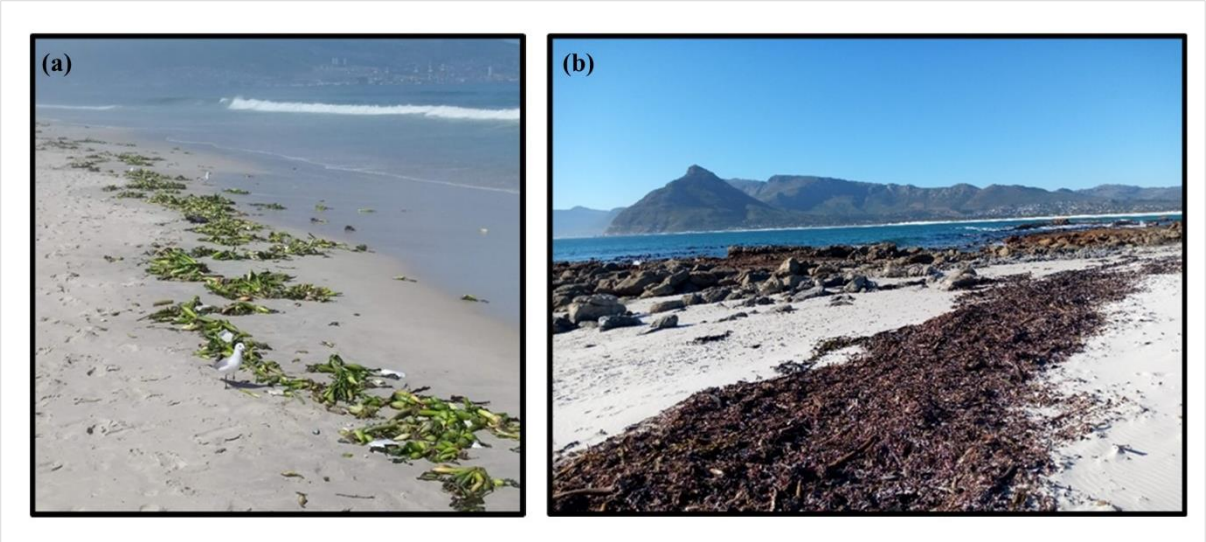

Figure 45 Comparison of Seaweed flotsam along (a) Milnerton Beach and (b) Kommetjie Beach

The field excursions helped to rationalize the DSAS results and expected coastal erosion processes were observed. Both wind and water are active erosion agents in the areas. The force from wave action acts as a form of physical erosion and it was apparent that with enough force the sea water could move boulders more so during storm surge events. This became apparent with the presence of an almost 6m log lodged amongst the boulders as shown in Figure 46 that many locals noted was moved during high wave events.

Figure 46 Wave dislodged log and boulders at Kommetjie beach

Figure 47 Water movement cutting into beach face at Kommetjie Beach

Figure 47 also shows how the water is actively cutting into the sand at the shoreline. Biochemical erosion is driven by the water infiltrating rock cracks and the presence of the shells indicates the influence of organisms on the soil profile and explains the white sands are derivative of the carbonate rich shells as expected from the geology discussed on page 45. Erosion is a slow process, however over the 40-year observation, the accumulation of erosive processes may be the reason why the Kommetjie shoreline fluctuates the most along its rocky portions. Observing the fluctuations of the Milnerton lagoon's current also confirms why it is the area with the highest level of erosion.

5.6 BEACH PROFILE ANALYSIS

The shoreline movement analysis discussed above is dependent on visual interpretation and the influence of the ocean. Beach profiling has been introduced into this study to observe beach topography and sediment volumetric changes. It also encompasses all the potential erosion influences including aeolian sand movement, river sediment flow, human intervention, or extreme weather effects. Elevation is introduced to create an effective profile model. Because waterlines are the primary coastal indicator used in this study, their associated sea levels act as a datum-based proxy for their elevation values, and they are predicted through tide modelling.

5.6.1 TIDE MODELS

The tide models produced reinforce the oscillatory theory discussed in section 2.1.3 on page 14. Figure 48 on page 118 depicts the actual tidal range from the Granger Bay tide station for the entirety of 2014, which was the most complete dataset acquired from SANHO. The tidal amplitude is within the expected 2m whilst the shortest tidal ranges occur in January and the longest occur in May which is to be expected with the influence of winter storms. Figure 49 on page 116 takes a closer look at our specific study interval (January to April) and the Figure 50 on page 116 shows the daily tidal movement.

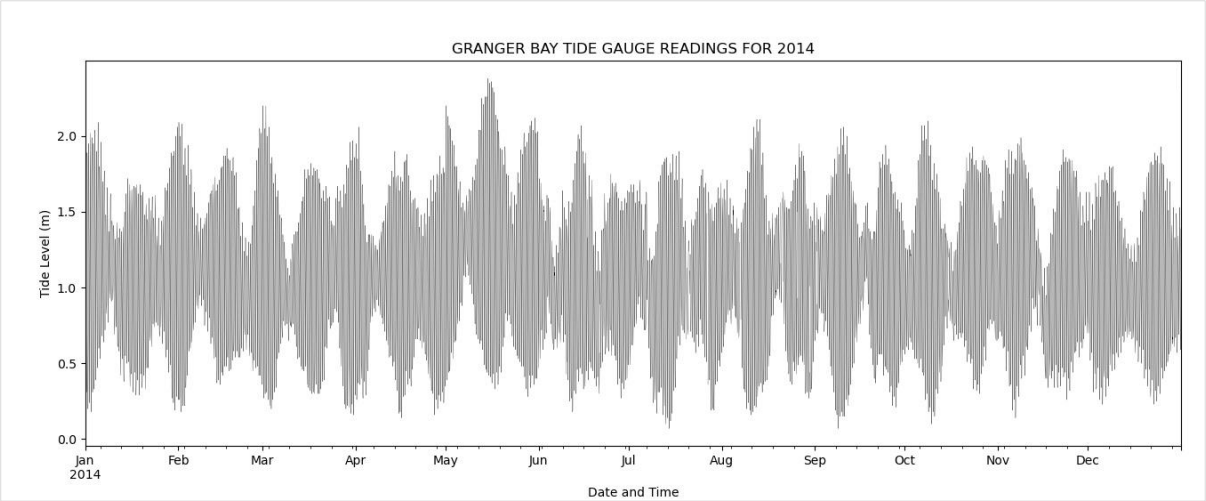

Figure 48 Tide model for Granger Bay Station (2014)

There were concerns that the waterline elevations would all be the same because the satellites pass over Cape Town at roughly the same time; however, the tide graphs show that the tide levels vary monthly. This is because of the astronomical tide generating forces from the proximity and phase of the sun and moon. Tides rise and fall continuously over several hours covering and uncovering the intertidal zone of beaches.

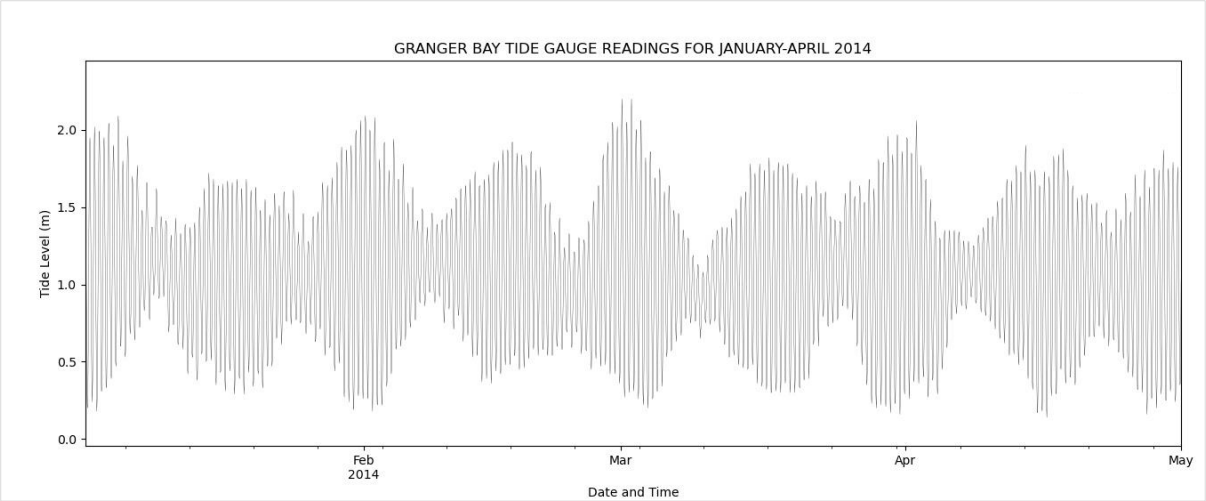

Figure 49 January-April 2014 Tide model for Granger Bay

The daily tide model in Figure 50 on page 116 allows us a closer look at the oscillatory tides observed along the Cape Town coastline. The effects of solunar changes are evident and indicate a semi-diurnal tide for Cape Town with 2 tide cycles a day at approximately 12-hour intervals.

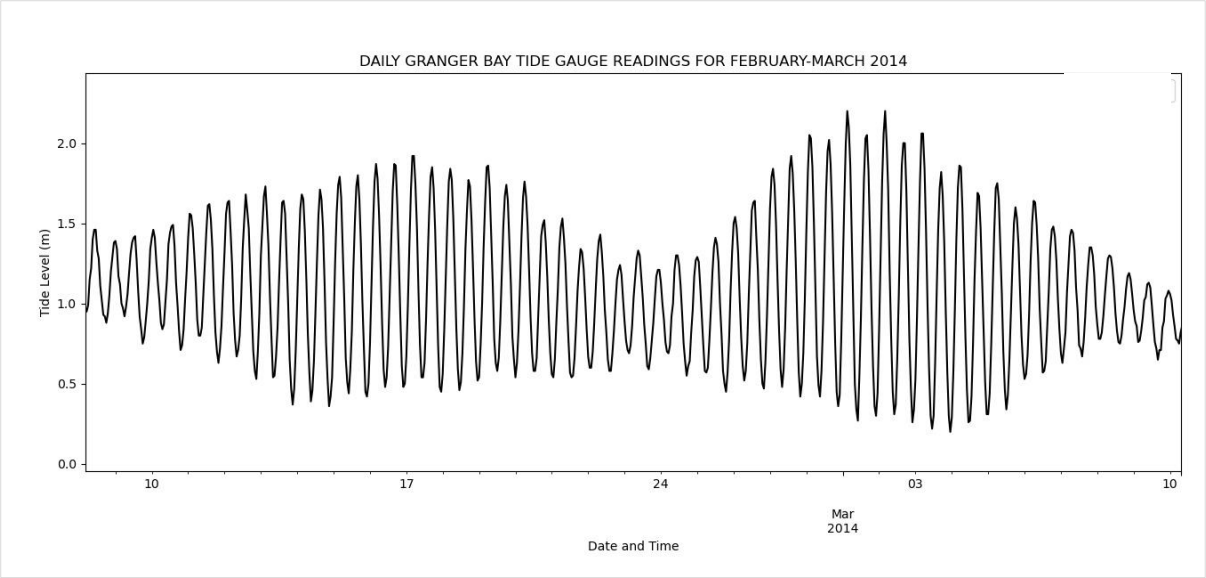

Figure 50. Daily Tide Movement as per Granger Bay Station

Whilst a semi-diurnal tide is observable, its mathematical components are required for a more definitive inference. Based on the tide models above, the following main tide constituents as discussed in section 2.1.3 on page 14 were derived:

Table 12 Harmonic Constituents Generated from 2014 SANHO data

Constituent Index	Amplitude	Phase
M2	0.5178	261.0773
S2	0.2303	176.9912
K1	0.0552	158.5324
O1	0.0129	67.1532
N2	0.1132	105.7109
K2	0.0424	150.4487
P1	0.0125	170.4509

These constituents act as the basis for harmonic analysis of tides because as stated tides are natural oscillatory occurrences. M2, S2, and N2 amplitudes are larger than those of K1 and O1, which reinforces the semi-diurnal classification observed in the tide models above. The full harmonic constituents table can be found in Harmonic Constituents For Granger Gay Tide

Gauge In 2014 on page 164. The tide data observed here shares the same consensus as past literature that Cape Town experiences a micro-tidal, semi-diurnal tide.

5.6.1.1 TIDE PREDICTION

The 2014 tide data were used to predict the tide levels that correspond to the acquisition time of the Radar images. The model shown in Figure 51 below is the actual tide levels for the first week of 2020 compared to PyTides prediction of the same time frame as measured from the Lowest Astronomical ide (LAT). 2020 was the most recent data available from SANHO and was used as a benchmark to determine the error associated with tide prediction. The residuals were also calculated to determine a prediction offset for as accurate of an analysis as possible. The residuals between the actual and predicted tides are shown in red on Figure 52 on page 122. The complete Python code that incorporated the PyTide library can be found in APPENDIX D PYTIDES PREDICTION PYTHON CODE on page 167.

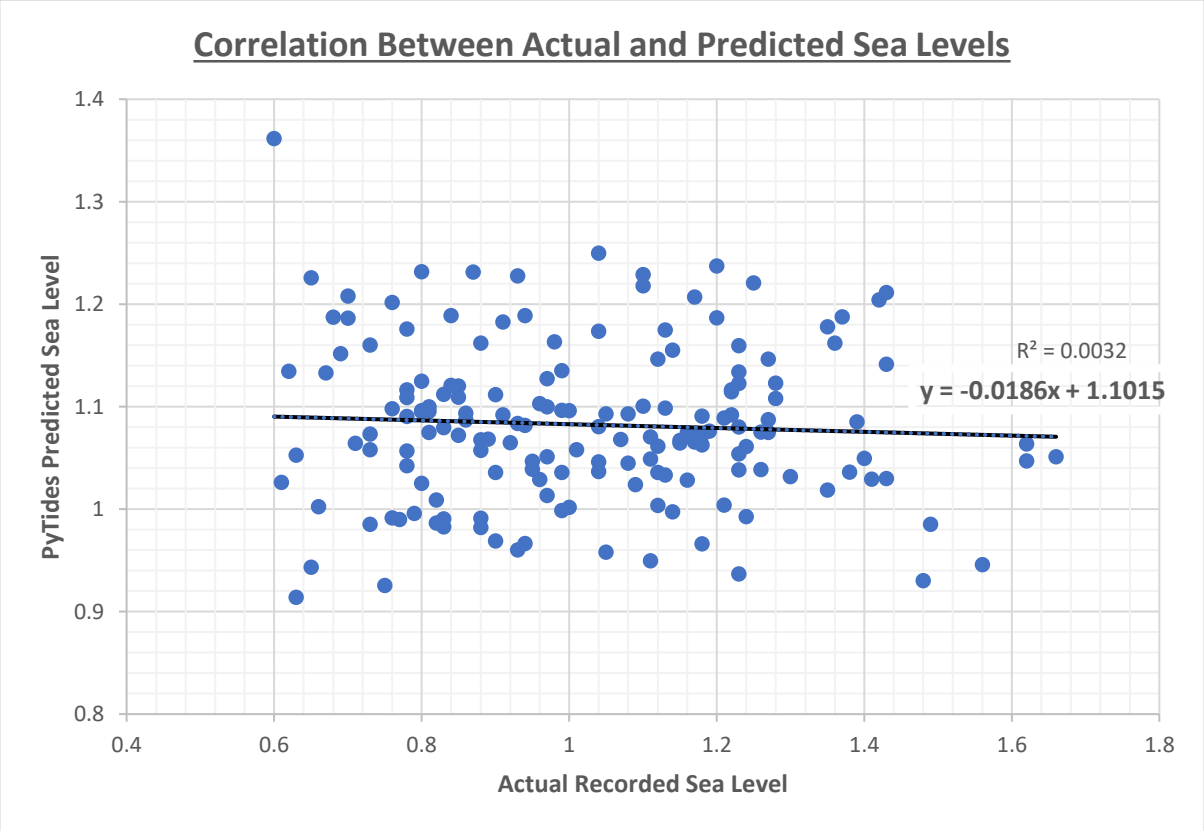

Figure 51 Comparison between Actual and Predicted Sea Levels

The residual is the difference between the actual and predicted values. From the line of best fit equation deduced above, there is a negative, almost negligible correlation between the predicted and actual values. This is because tide analysis is not a typical predictive model but is dependent on harmonic constants. To account for any anomalies, the data were also demeaned because PyTides fits the amplitude and phase of tide cycles through a least squares function.

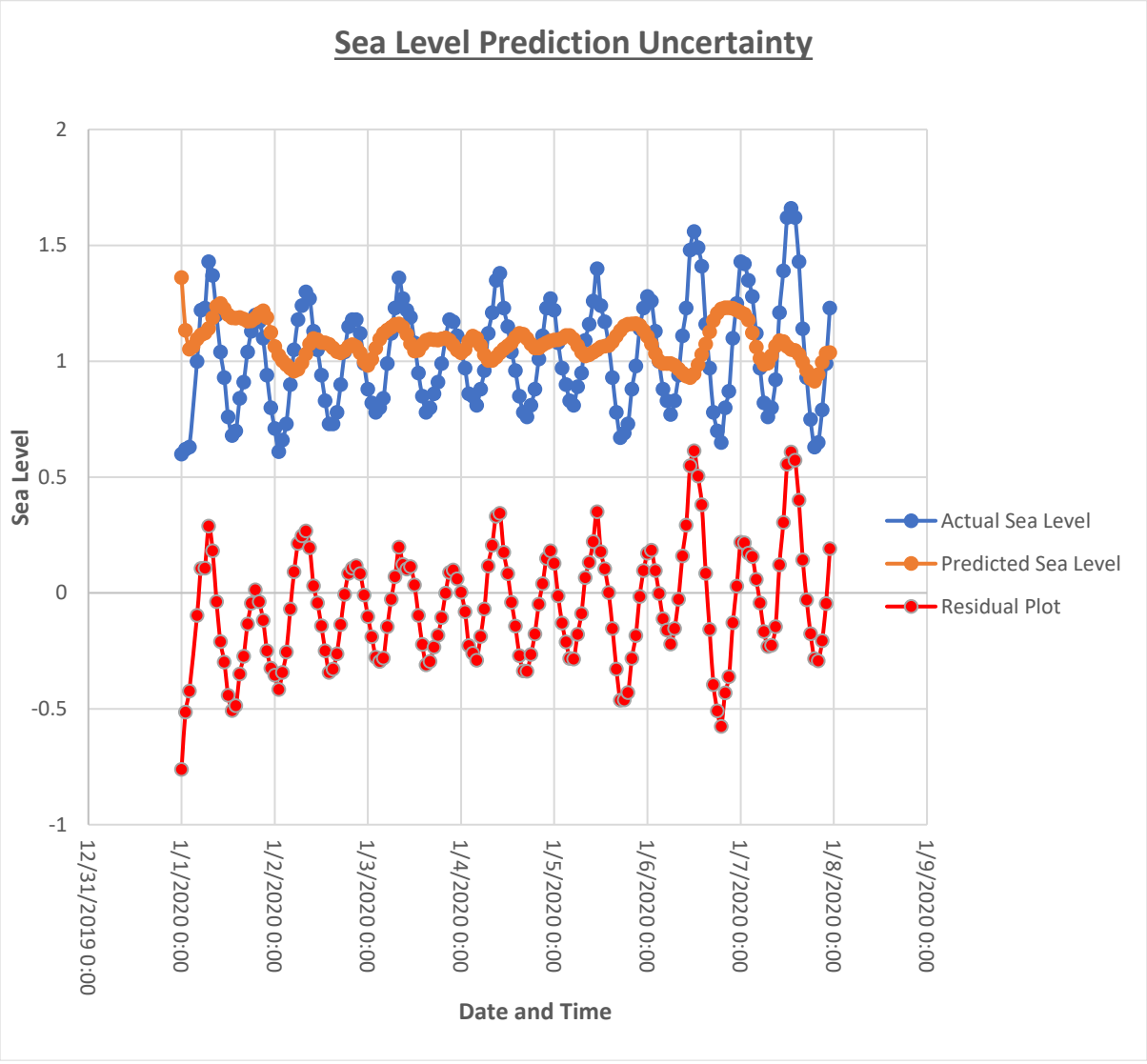

Figure 52 Errors associated with PyTides prediction

From Figure 52 above, PyTide predictions consistently undershoot the actual tide values as depicted by the residual errors. The tide predictions corresponding to image acquisition dates and times can be found in Table 20 of the appendices.

5.6.2 ELEVATION MODELS

As stated in section 4.3 on page 68, three elevation modelling techniques were used to profile the beaches. These results are further elaborated on using maps and statistical analysis. Elevation is used as an extracted measure of the beach profiles. The general assumption is that a decrease in elevation indicates sediment erosion whilst an increase is accretion. A volumetric analysis based on the elevation and area of a DEM can determine how much coastal sediments are being eroded. This approach is widely used in geomorphic studies. Differencing DEM's can thus determine sediment volumetric change and thus model erosional changes.

5.6.2.1 WATERLINE DERIVED DEM's

The waterlines as indicated in Figure 53 on page 124 were extracted from Sentinel-1 images through the image processing described in section 4.3.4 on page 74. The waterlines were assigned a height derived from tide level data. Whilst the expectation is to extract waterlines that indicate the interface between the beach and water, other land cover features such as rocks and vegetation affected the land-sea segmentation process. The waterlines are color coded based on their dates. For reference, the background image used was acquired in 2018, however some waterlines delineate sections of fore dune vegetation. Again, the influence of rock outcrops at Kommetjie is observable. Its waterlines for 2021 show a rock outcrop extension into the water within the same area as observed during fieldwork excursions. The only assumption can be that the images may have been captured at low tide because majority of the waterlines occur over the sandy area.

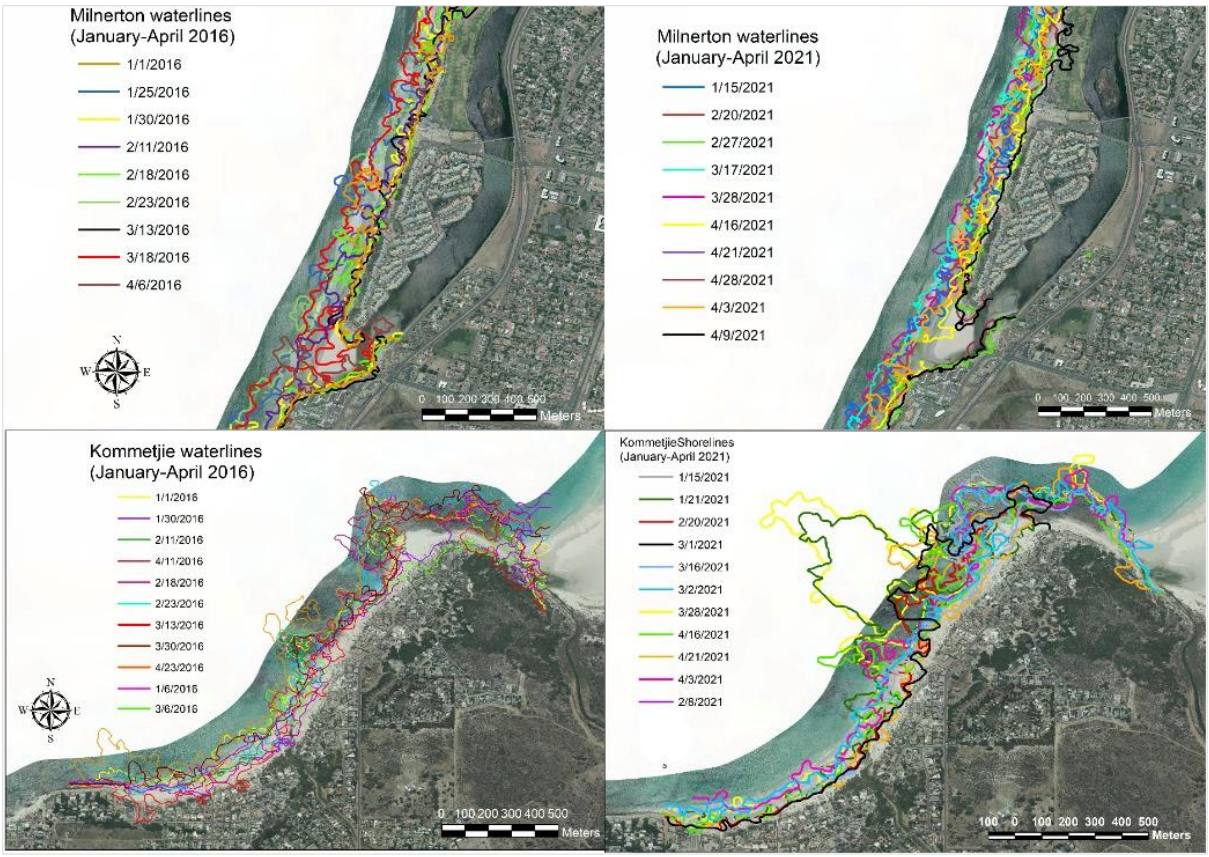

Figure 53 Sentinel-1 SLC Extracted Waterlines for Milnerton and Kommetjie

Aerial imagery source: City of Cape Town 2021

The Milnerton Beach waterlines on the other hand, were consistently along the shoreline. Whilst there was influence from vegetation, there were also spatial variations caused by the opening of the Milnerton lagoon. The flow of the lagoon fluctuated with the tide. A higher tide means less beach can be detected and as such it is difficult to deduce a definite shoreline at the mouth of an estuary. These waterlines were merged and interpolated using the Topo to Raster tool in ArcMap. The waterlines are assumed to be hydrographically corrected contours and their assigned elevations are used to interpolate them into an elevation raster surface as shown in Figure 54 below.

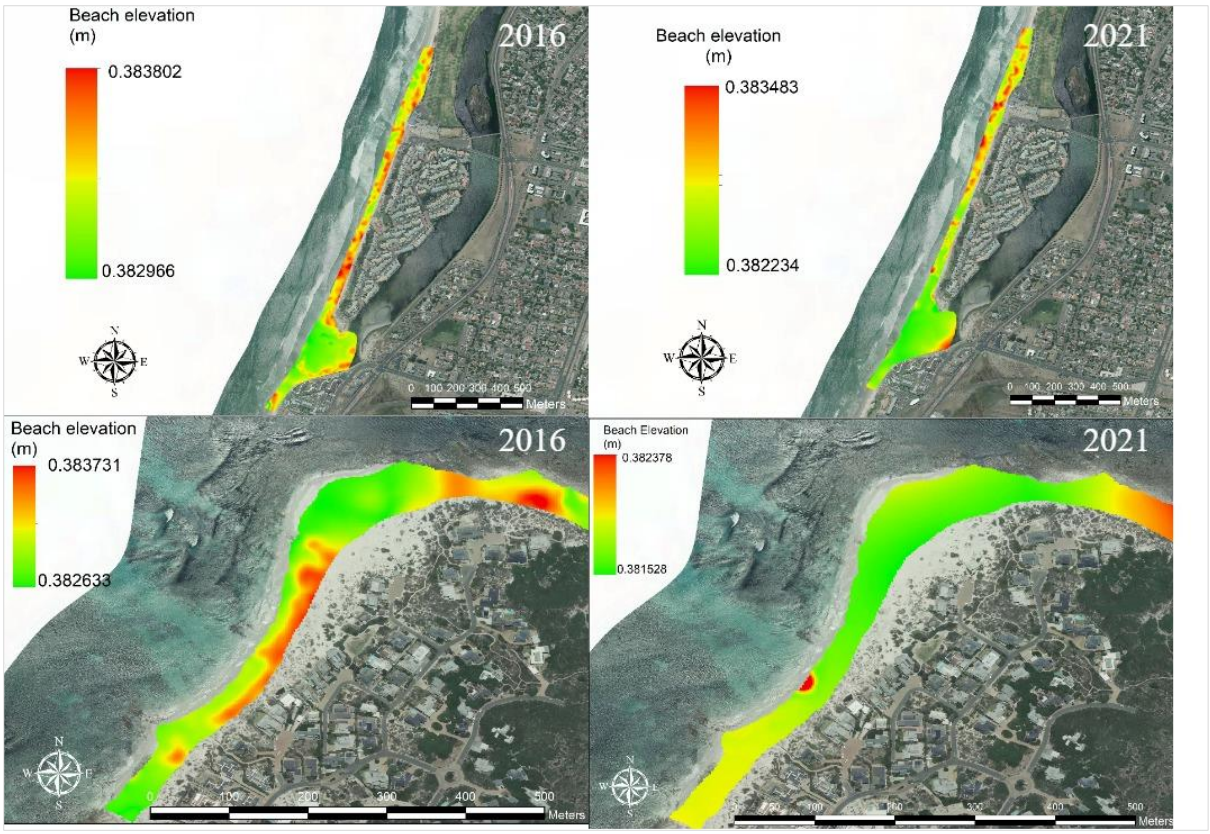

Figure 54 Initial Waterline extracted DEM's for Kommetjie and Milnerton

Aerial imagery source: City of Cape Town

The spatial distribution of the waterlines is a major factor in generating the DEM's. Where contours are closer, generally would indicate a steeper terrain thus higher elevation. Therefore, spatial resolution of the satellite imagery is important, for as accurate of a shoreline position as possible. The 2016 elevation model for Kommetjie agrees with the general beach profile expectation. The higher elevations are observed along the back beach whilst the lower ones are along the shoreline. Interestingly, the Milnerton DEM's consistently show lower elevations at the boundary of the lagoon and ocean. Their combined water action is actively eroding the sediment at a higher rate whilst patches of higher elevation are observed along the rest of the narrow beach.

5.6.2.2 DIFFERENTIAL INTERFEROMETRIC ELEVATION MODELING

As stated, the accuracy of Differential interferometry is observed through the coherence statistics in Table 13 on page 126. To maintain consistency with the topographic beach survey, which was conducted on the 5th of May 2021, the acquired Sentinel-1 images were approximated for the same date. The major sources of error in interferometry are

decorrelation and atmospheric interference. Decorrelation differs with land cover and is higher with a larger temporal baseline or a shorter perpendicular baseline

Table 13 Interferometric Coherence

	KOMMETJIE		MILNERTON	
Dates	03 May 2021 15 May 2021	05 May 2016 17 May 2016	03 May 2021 15 May 2021	05 May 2016 17 May 2016
Temporal Baseline (days)	12	12	12	12
Perpendicular Baseline (m)	68.304	38.284	68.929	38.513
Coherence	0.928	0.956	0.932	0.957

Whilst the image acquisition dates may be similar, it is important to note that ground coverage of the two study areas is not the same and thus the viewing angle of the sensor will not be the same, which will in turn be reflected in the baselines. The images from 2016 have a shorter perpendicular baseline and as such are more likely to produce a more accurate DEM.

Water surfaces are in constant motion and are more likely to have stronger temporal decorrelation, when compared with surrounding non-water related land surfaces that don't experience much change over time such as buildings, rocks or bare soil which have a higher coherence, water surfaces can easily be detected (Grandin, 2015). The same cannot be said in the case of vegetated areas that experience seasonal change. This is why temporal baselines are important and why the rugged, vegetated nature of Cape Town and surrounding areas is not a favorite for interferometry (Gesch et al., 2016). Interferometry can only be used to infer changes on the ground because it can be difficult to distinguish actual geophysical changes from the influence of sensor geometry errors. Whilst interferometry decorrelation is interesting, it goes beyond the scope of this study. The temporal changes between the beach faces using interferometry are exemplified in Figure 55 on page 127.

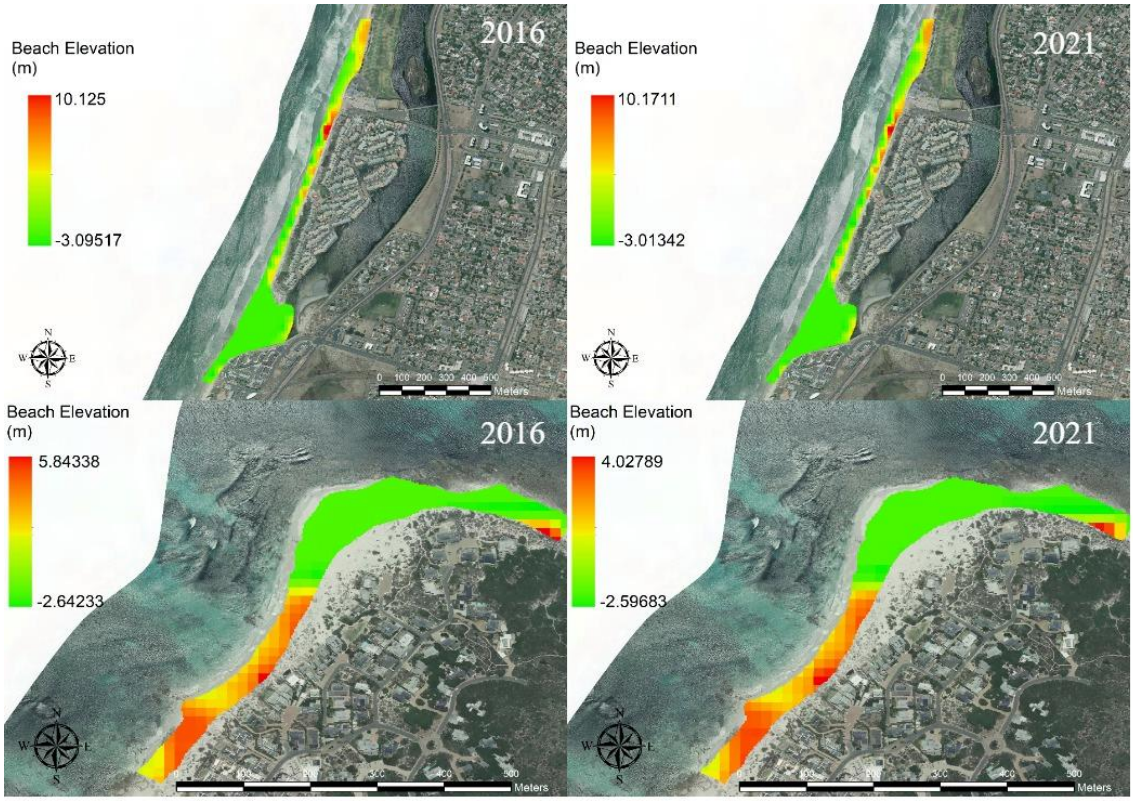

Figure 55 Interferometry derived DEM's for Kommetjie and Milnerton

Aerial imagery source: City of Cape Town 2021

The DEM's produced here have a similar spatial distribution to those of the waterline method with the back beaches having higher elevation. Again, the curve along the Kommetjie beach has the lowest elevation and the same can be said along the opening of the Milnerton lagoon. Interestingly, whilst they have the same spatial distributions, their elevation values are quite different. The waterline DEM's have significantly lower elevations restricted by the highest and lowest predicted sea levels whilst decorrelation effects in interferometry are assigning negative elevation values. Seemingly, the Interferometry produced results more similar to the ground truthed data discussed below. For this reason, as previously stated, LiDAR data were introduced as a normalizing factor to adjust the waterline elevation models more especially because the tide prediction tool performed poorly.

5.6.2.3 WATERLINE DEM ADJUSTMENT

A mean difference of ±2.737m for Milnerton and ±6.873m for Kommetjie were used in Equation 9 to adjust the DEM's. The resultant adjusted DEM's for the Waterline method can be found in Figure 56 on page 128. Whilst the elevation values have been changed, the range of the values is still the same. Therefore, the effectiveness of elevation modelling is often observed through its derived products such as slope, aspect and difference of DEM's, which are described in section 5.6.2.6 on page 130.

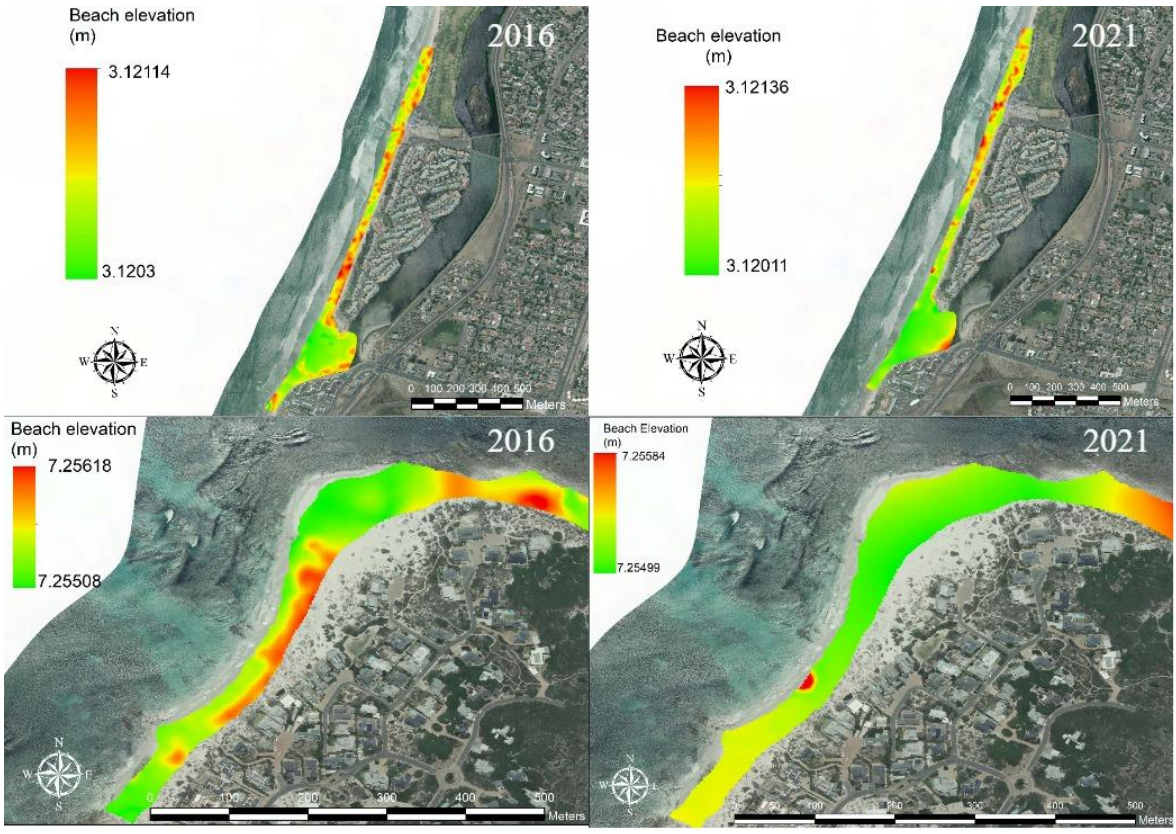

Figure 56 Waterline DEM 's adjusted by City of Cape Town LiDAR data

Aerial imagery source: City of Cape Town 2021

5.6.2.4 TOPOGRAPHIC BEACH SURVEY

As discussed in the methodology, a topographic survey was conducted in Kommetjie as a means of ground truthing to validate the satellite derived beach DEM's. The GPS points collected along transects were interpolated into the resultant DEM in Figure 57 through IDW. This DEM went through the least amount of processing and as such was used as the truest depiction of the current state of the beach and was used to determine the RMSE errors of the Kommetjie 2021 models.

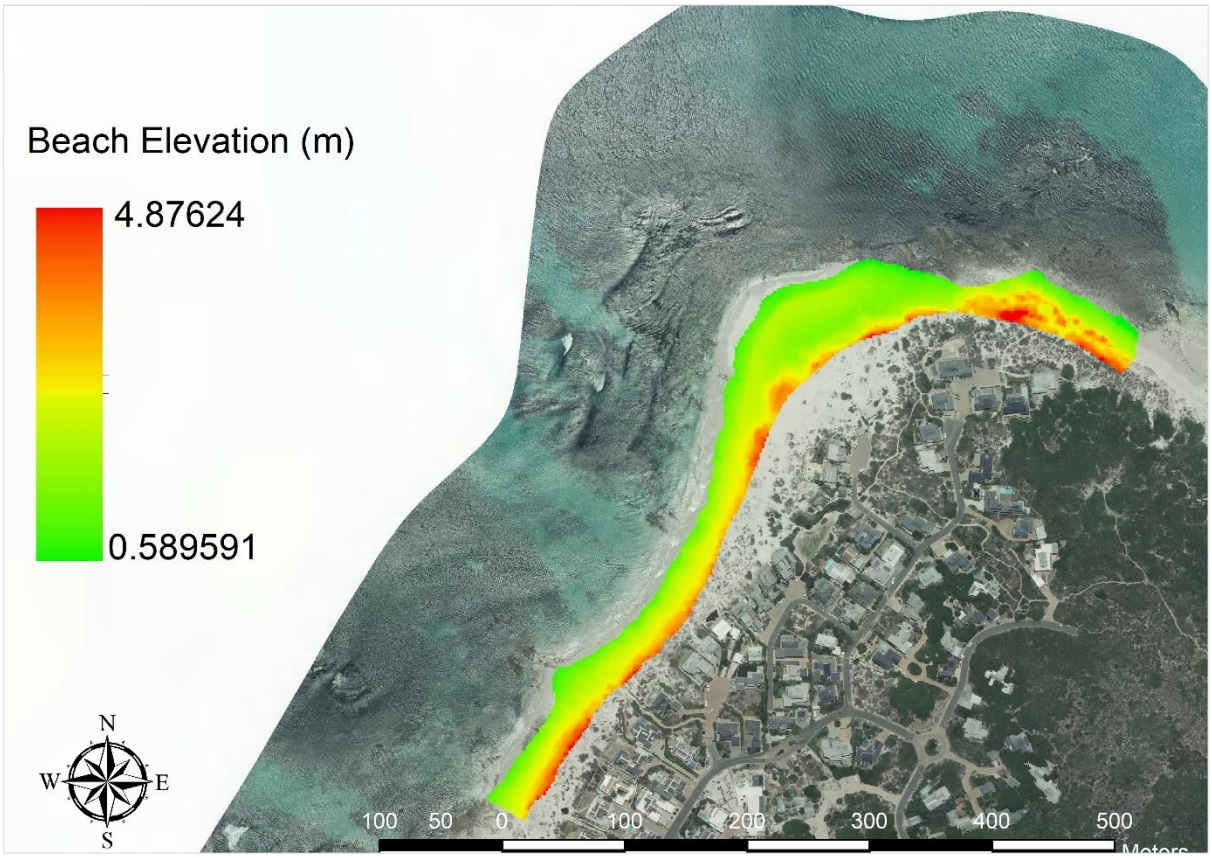

Figure 57 RTK Topographic Beach survey DEM

Aerial imagery source: City of Cape Town 2021

5.6.2.5 VOLUMETRIC CHANGES

The main objective with including beach profiling in this study was to determine whether satellite data could conclusively detect and quantify coastal erosion. In order to determine an overall volumetric change over the five-year observation period, a simple Difference of

DEM's (DoD's) calculation was conducted between the 2016 and 2021 DEM's. Positive values indicate deposition whilst negative values indicate erosion. Any discrepancies are a result of the difference in techniques applied.

Table 14 Coastal erosion volumetric changes between 2016 and 2021

	KOMMETJIE		MILNERTON	
	WATERLINE METHOD	DIFFERENTIAL INTERFEROMETRY	WATERLINE METHOD	DIFFERENTIAL INTERFEROMETRY
2016	10.478	58598.346	32.885	241639.093
2021	3.152	58384.105	38.873	244793.233
CHANGE IN SEDIMENT VOLUME (m^3)	-7.326	-214.242	+5.988	+3154.139

Evidently the volume changes differ, however, they are proportional to their individual data ranges. Both methods are of the same consensus that over the 5-year period, Kommetjie has experienced erosion whilst accretion has been prevalent along the Milnerton Beach. As indicated in Table 14 above. The waterline method shows a sediment deficit of $7m^3$ along Kommetjie whilst accretion of $6m^3$ was detected along Milnerton. Differential interferometry on the other hand indicated a deficit of roughly $214m^3$ in Kommetjie and accretion of $3154m^3$. These results echo the same conclusion as the shoreline change analysis in section 5.4 on page 101, interestingly, more erosive change is evidently being detected along the Kommetjie coastline regardless of the method of detection.

5.6.2.6 ELEVATION MODELLING DERIVATIVES

Whilst the DEM's are ultimately referenced to Hartebeesthoek94, the original data was pre-processed based on different ellipsoids. This is important because ellipsoids act as a theoretical reference for any geodesic calculations. The differences in ellipsoidal surfaces may be a contributing factor to the elevation differences. As such DEM slopes and aspects were also included in the analysis. Slope and aspect are important coastal geomorphologic characteristics because they also inform the shoreline's ability to refract or diffract oncoming waves which in turn affects wave heights (Merwe, 2017). Only the 2021 Kommetjie DEM's

were compared in Table 15 because there is no ground truthed RTK survey for 2016 or for Milnerton.

Table 15 Beach Profiling Data Derivatives Comparison

	DInSAR	RTK	WATERLINE
Minimum elevation(m)	-2.5968	0.5896	7.2550
Maximum elevation(m)	4.02789	4.8762	7.2558
Average(m)	-0.4738	2.1305	7.2551
Minimum slope(°)	0	0.0445	2.6280e-06
Maximum slope(°)	48.1986	20.3509	0.004214
Average(°)	2.5087	3.7825	0.0001312
Minimum aspect	-1 (Flat)	0.005778(North)	0 (North)
Maximum aspect	359.9547 (North)	359.9444 (North)	359.2152 (North)
Average	65.05292 (North-east)	234.4590(South-west)	163.8011 (South)

Differential interferometry is clearly more accurate than the Waterline method as evidenced by how similar it's elevation and slope ranges are to the RTK survey, however, there are discrepancies with their aspects. The RTK survey confirms an expected southwesterly aspect whilst North-east is observed for differential interferometry. Whilst the data range for the waterline DEM may differ a southerly aspect is deduced. The next section delves further into the accuracy of these elevation modeling techniques based on the RMSE that compares the actual (RTK survey) to the predicted (Waterline and Differential interferometry) values.

5.6.2.7 ACCURACY OF ELEVATION MODELLING

This section addresses objective 5; Objective 5: Determine the effectiveness of satellite-based beach profiling. on page 7 on how effective the above presented profiling techniques are. There are several contributions to the inaccuracies observed in the beach profiling results such as:

1. The use of different interpolation techniques. IDW was used to interpolate the waterline and topographic survey DEM's whilst bicubic interpolation was applied through differential interferometry on the radar data.
2. Resampling of the elevation models for an unbiased comparison at the pixel level.

3. The application of different ellipsoids
4. Discrepancies in tide data predictions

Whilst the actual source of errors can only be inferred, we can confirm the degree of inaccuracy through RMSE. A total of 36 Points were chosen along beach transects and used to extract multiple elevation values across all three elevation models. The full tabulation can be found in APPENDIX F ELEVATION MODELLING ACCURACY on page 170, however ultimately a mean error of 2.198 m and RMSE of 3.038m was determined for the elevation model deduced through differential interferometry. The waterline method on the other hand had a mean error of -5.047 m and an RMSE of 5.112 m. Differential interferometry achieved a much higher accuracy because there is less deviation between the RMSE and mean error, the waterline profiling method was hindered by the poor prediction of the PyTides tool.

5.6.3 RESOLUTION EFFECTS ON SHORELINE EXTRACTION

As indicated in the methodology an array of satellite datasets was considered for this study. The major distinctions were the electromagnetic wavelength applied for remote sensing and the resolution of the data as summarized in the table below. The current state of the Kommetjie beach was captured by an RTK survey that also marked the shoreline benchmark. As shown in the map below, this reference shoreline overlaps with the satellite derived shorelines. Visually it is clear that the shorelines follow a similar trend, however the Sentinel-1 shoreline juts out over the water due to the rock outcrops. As discussed in section 2.2 of the theory chapter on page 15, the land cover detection sensitivity varies by the instrument used.

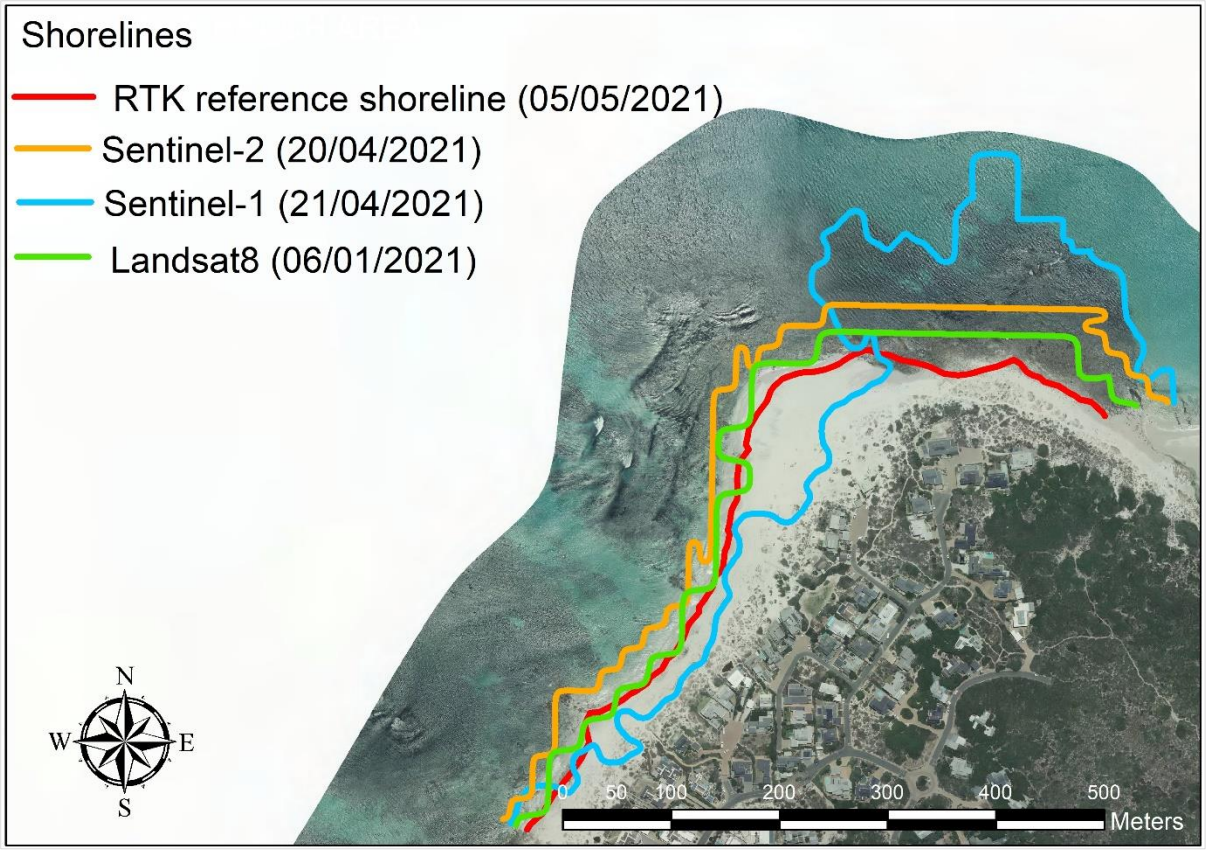

Figure 58 Comparison of Extracted Waterlines from different satellites

Aerial imagery source: City of Cape Town 2021

The visible spectrum data from Landsat 8 or Sentinel 2 is manipulated by using bands that specifically highlight the difference between land and water components by incorporating MNDWI and later applying Support Vector Machine (SVM) classification, however the same cannot be said for Sentinel-1 data, which may be why its derived shorelines trace the rock outcrops. An alternative explanation may be the influence of tide levels at the time of image capture. It is also worth noting that Radar has the ability to penetrate water surfaces to certain depths which also explains why its extracted waterline juts out over the water. The difference in backscatter between wet and dry sand may also be a contributing factor.

Table 16 Waterline Extraction Resolution Comparison

DATASET	RTK Survey	Landsat-8	Sentinel-2	Sentinel-1
RESOLUTION (m)	1.837772	30	10	14.07
SHORELINE LEGNTH (m)	835.518947	1015.073057	1136.936645	1566.523882
AREA FROM REFERENCE SHORELINE (m^2)	0	13813.966502	32809.29254	56244.064131
SHORELINE POSITION INDEX (I)	0	16.53340	39.26816	67.31632

The Shoreline Position Index (I) equation as described in section 4.2.6.3 on page 68 was used to determine the most accurate of the satellite sensors used in this study. Interestingly, whilst Sentinel-1 and -2 had better temporal correlation with the RTK survey, the Landsat extracted shoreline had the lowest shoreline position discrepancy, making it the most accurate. Similar bands from Landsat 8 and Sentinel-2 were processed in the MNDWI calculation. Landsat 8 had the coarsest resolution of 30m and still outperformed Sentiel-2 with 20m resolution. This leads to the inference that spatial resolution may not be as major of a factor as spectral resolution in coastal remote sensing. This further reinforced by the fact that Sentinel-1 is able to detect shallow areas better than multispectral sensors and is more sensitive to subtle changes in the electromagnetic reflection of land surfaces, as such radiometric resolution should also be considered in sensor selection. This also proves the synergy that can exist between remote sensing platforms. The results showcased here are further discussed under the following Chapter.

5.6.4 BEACH PROFILE MORPHODYNAMICS CLASSIFICATION

This results chapter concludes by synthesizing the literature review, fieldwork, and analysis to classify the two study sites as per the objectives stipulated to determine the current state of both Kommetjie and Milnerton beaches. The beach widths are the averaged lengths of the transects generated from the DSAS analysis and the averaged slope for Kommetjie was deduced by applying the slope 3D analyst tool on the RTK generated elevation model and the interferometry DEM for Milnerton was used as an approximation.

Table 17 Coastal Classification of Study Sites

BEACH CHARACTERISTIC	KOMMETJIE	MILNERTON
AVERAGE BEACH WIDTH (m)	69.204348	49.502943
BEACH SLOPE	3.782507 ^{O} (gentle)	4.981293^{o}(gentle)
BEACH EXPOSURE	Sheltered	sheltered
TIDE CLASSIFICATION	Semi-diurnal, micro-tidal	Semi-diurnal, micro-tidal
SHORELINE TYPE	Dissipative	Dissipative

Milnerton is considered sheltered because of the influence of development at the foreshore, as well as the presence of Robben Island reducing the impact of wave motion. Kommetjie is also sheltered because of the Hout Bay headland, which also reduces the influence of wind on wave run-up. These beaches have been classified as sheltered also based on literature review. As stated headland-bay systems tend to create pockets of beaches (Van Zyl, 2019). Coupled with the presence of seaweed rock outcrops, it is well shielded from the full force of ocean swell. The observations reinforce the fundamental theory that fine beach sand is associated with gentle slopes exposed to low energy waves (Merwe, 2017).

6 DISCUSSION

6.1 SHORLINE MOVEMENT ANALYSIS DISCUSSION

By using a transect spacing of 5m and a search distance of 500m from the Baseline, it is abundantly clear from the maps above (Figure 35 to Figure 41) that the observed portion of the Milnerton coastline is significantly longer than that of Kommetjie, however over time Kommetjie has had more significant changes in length of up to 513m. A longer shoreline means more transects are used for calculations, however the difference between the averaged change statistics in this instance occurs within a similar range. For example, the average SCE is 51.8m in Kommetjie and 49.36m in Milnerton whilst overall shoreline movement has been generally negative with an EPR of -2.85m/yr. in Kommetjie and -2.35m/yr. in Milnerton. All the measured parameters indicate that there has been slightly more shoreline movement in Kommetjie over these 40 years.

Whilst Milnerton is a sandy beach, Kommetjie has an alternation between rocks and sand at its shoreline. The extracted shorelines from the Kommetjie beach may have been influenced by wave action over the shallow coastal areas at the time of image acquisition. If the water was shallow enough, the wet rocks covered by seaweed or sand may be interpreted as the water limit. There is also the general expectation that over the 40-year period, hydraulic force from wave action has caused the erosion of these rocky outcrops and lowered them further below the water level, however these are countered by the uplift of rocks due to tectonic forces (Compton, 2004). As discussed in section 2.1 on page 9, coastal environments are complex to understand because of the many exogenic forces acting on them.

Another instance of environmental influences is the fact that both these coastlines have inland waterbodies within their immediate vicinity, the Milnerton lagoon and the Bokramspruit estuary in Kommetjie. The extent of their influence is visible in the maps (Figure 34 to Figure 41) presented above with the Milnerton Lagoon opening having the most significant influence on the shoreline with the highest erosion range of 6.23 to 4.19 m/yr. The same could be expected for Bokramspruit, however its smaller areal extent and the fact that its opening is shrouded by vegetation have lessened its impact with an erosional rate of 2.37 to 1.06 m/yr. There are also instances of accretion around the Bokramspruit opening of up to

1.08 meters per year whilst in Milnerton accretion of up to 0.02meters per year occurs further away from the Lagoon opening.

River sediment load is transported and deposited along the river. Whilst they deposit sand and gravel into the sea, the finer sediment from the riverbed load is transported by sea currents in the form of plumes (Merwe, 2017). The river source is the most important factor in river sediment load coupled with the activities within the general catchment area. Catchment sediment yield modelling, which is beyond the scope of this study is most appropriate to determine sediment load. Hughes, reinforced the findings of CSIR that the mouth of the Milnerton lagoon indicated a bimodal sediment transport system with a northwards sediment movement estimated at 100 000m^3/yr. (Csir, 1972; Hughes, 1992). His study also concluded that south of the mouth experienced a sediment deficit and was being actively eroded.

It must be noted that the statistical significance associated with the EPR is poor. For example, the uncertainty was determined to be -2.35 ±2.14 m/y. for Milnerton. This means that within a year, the shoreline will be eroded within a range of -4.49 m to 0.21 m. The minimum is negative and therefore erosional whereas the maximum is positive, indicating accretion. Because the shoreline cannot definitively be classified as accretional or erosional, the rates of erosion should be considered as insignificant (Himmelstoss et al., 2018). This is not an issue of the relevance and usefulness of DSAS but rather the availability of data. The best improvement to these results is to extract more shorelines, perhaps use 5-year intervals instead of 10 years.

The general hypothesis was that Milnerton would have experienced more shoreline erosion due to being narrower and having no coastal defenses however, even with the presence of kelp beds and rock outcrops, the Kommetjie coastline seemingly experienced its most significant erosion along its rocky portions probably because of lower water levels at the time of image acquisition as well as how far the rocks had been eroded. *Table 11* on page 111 summarizes these sediment movement statistics whilst the full DSAS summary reports can be found in APPENDIX B DSAS SUMMARY REPORTS on page 156. Past authors have also indicated that the construction of the Table Bay harbor has greatly reduced erosional rates in the Woodbridge Island area especially because dredging removed significant sand reservoirs (Hughes, 1992; Quick &Roberts, 1993).

Whilst there are no pertinent studies on the Kommetjie shoreline, there are some studies on the Milnerton shoreline that reinforce the findings of this study. The Milnerton beach experienced much of its shoreline change where the Milnerton lagoon meets with the ocean. Hughes (1995) is the only study on record that has conducted a comprehensive shoreline analysis in Milnerton, and it echoes the same findings of this study that there is significant influence from the lagoon. From the yearly shoreline positions most of the shoreline mobility occurs within this area. Hughes (1992) also echoed the same sentiments that erosion was less north of the lagoon opening as opposed to the south that had a sediment deficit.

6.2 BEACH PROFILING DISCUSSION

The three beach profiling methods described and implemented in this study were derived from literature and adapted to the available processing resources. All three have their limitations, the waterline method is dependent on accurate sea level data. The accuracy of differential interferometry is based on orbital baselines and whilst many researchers still emphasize the effectiveness of RTK surveys they can be tiresome and thus limited.

The intertidal zone is dynamic. The biggest hindrance to applying the waterline method in an African context is the lack of data availability especially because current satellite sensors are not designed to fully accommodate the Sub-Saharan landscape. The elongated shape of Africa means the Southernmost portions do not have the most optimum coverage. A higher number of images would greatly improve its accuracy whilst extending the time interval of observation beyond 4 months would reduce accuracy when considering the tide cycle. By ensuring all the data are collected within the same time frame, the variability introduced by seasonality is eliminated.

The Granger Bay tide gauge was the only freely available source of tide data and provided generalized tide levels for the entirety of Cape Town. Whilst the tide gauge is stationed in proximity to Milnerton, the same cannot be said for Kommetjie. As discussed, these two locales experience varying environmental conditions that may also affect tide levels and these discrepancies cannot be accounted for because only a single tide gauge is used. The temporal distribution of the waterlines must also be considered. In this case, 4 months was used as the observation time interval due to unavailability of data, however the waterlines are not evenly distributed over the 4-month period. For example, Milnerton had 3 shorelines extracted for

January in 2016 but only 1 in 2021. From the tide graphs in section 5.6.1 on page 117, tide varies monthly because of solunar changes, and this can ultimately affect the predicted elevations.

Whilst the DEM's are eventually referenced to Hartebeesthoek94, the original data are pre-processed based on different ellipsoids such as World Geodetic System 84 (WGS84) for the RTK survey whilst Sentinel-1 SLC data is processed based on the Earth Gravitational Model 1996 (EGM96). This is important because ellipsoids act as a theoretical reference for any calculations, thus, differences in ellipsoidal surfaces may be a contributing factor to the elevation differences

The accuracy of the elevation models is dependent on the following:

1. Spatial resolution of satellite images
2. Orthometric corrections
3. Intertidal slope
4. Accuracy of tide data

Whilst a simple RMSE calculation is acceptable in calculating individual DEM uncertainty, Salameh et al., (2020) cautions the need for a further assessment of the DEM of Differences (DOD's). He outlines the Level of Detection (LoD) thresholding method for this purpose by highlighting that because intertidal areas are usually small and flat, any slight volumetric changes can be over-exaggerated leading to large uncertainties (Salameh et al., 2020). The error assessment of the elevation models here is solely based on statistical calculations and does not consider spatial distribution of the Ground Control Points leading to the inclusion of elevation derivatives such as slope and aspect and more so because DoD's often have interpolation artefacts that can't be compared to geodetic benchmarks.

The rocks found along the Kommetjie beach clearly have an influence on coastline detection. Whilst fluctuating tides are seemingly the plausible cause for this, although beyond the scope of this study, vertical land movements through tectonic shifts and isostasy may also be a contributing factor. Whilst hydrodynamic models, influence of river sediment flow and anthropogenic defenses have been considered, perhaps a geological analysis would be a worthwhile contribution.

In the case of Milnerton occurs within a sediment starved embayment more so because the lagoon flows over hard bedrock such as granite and as such the sand supply is lessened (Woodborne &Flemming, 2021). This is also the result of its logarithmic spiral shape and typical of headland-bay systems, which form sediment traps that lead to pocket beaches and offshore sediment deposition (Woodborne &Flemming, 2021). Longshore drift generally transports sediment northwards from Duiker Point especially during storm events (Van Zyl, 2019). The major sources of sediment along the Atlantic seaboard are biogenic carbonate decomposition, Aeolian fine sands blown through the Karbonkelberg headlands pass and the weathering of the Table Mountain Group bedrock. Changes in sea-level and thus wave energy also determine the level of sedimentation and with the frequency of storm events increasing, more erosion can be expected (Van Zyl, 2019).

Using interferometry in observing intertidal zones has been criticized due to reduced coherence over sandy areas. Sand between two images may be wet or dry to different extents thus altering the level of coherence along with the fact that wet sand has a lowered radiometric response than dry sand. Interferometry is thus more suggested in areas with larger sediment sizes. This is why when compared to other techniques, interferometry will consistently have lower planimetric and vertical accuracy (Mason et al., 2000). There is a tradeoff between technical performance and cost where data availability is concerned and for this reason, ground surveys remain as the most accurate form of beach profiling.

Working with different datums is the biggest hurdle in remote sensing based multi-source data studies, which in this instance, have been overcome by simple arithmetic raster adjustments. Differential Interferometry has proven to be a viable remote sensing mechanism for coastal monitoring; however, it is clear that more robust tidal prediction tools are required in order to make the Waterline method GIS-user friendly.

This study has also discussed howt integral GIS has been in regards to the influence and controversy of Cape Town's Coastal risk governance (Mukheibir &Ziervogel, 2006). Whilst it is clear that legislature such as the ICMA are a step in the right direction, there is still much work to do. It has informed climate adaptation strategies, urban planning and can support further development of interactive coastal information systems. Past researchers have placed

an emphasis on the need to accommodate “knowledge-based, strategic decision-making processes” and less “bureaucratic administrative decision-making” however this unfolds differently for coastal cities in the global south (Desportes &Colenbrander, 2016). The growth of open-source software and tools has made this reality possible. Desportes and Colenbrander (2016) still go on to argue that GIS based applications are biased because they are generated from information that is deliberately collated to communicate a particular perspective and sway a specific audience. Risk modelling is indicative rather than conclusive (Colenbrander &Bavinck, 2017). Particularly with coastal areas where there are multiple anthropogenic, environmental, and hydrodynamic factors interacting over varying temporal and spatial scales.

There has yet to be a system that accounts for all of them. The CMU also still faces challenges imposed by the socio-spatial planning from the apartheid era (Colenbrander &Bavinck, 2017). Therefore, there is still bias towards coastal monitoring systems. And even with the implementation of such systems knowledge sharing is still limited because departments that should be collaborating are disjointed as shown under section 3.1 on page 43. Therefore, to date the best coastal risk management strategy in Cape Town has been the implementation of setback lines and overlay zones that encourage urban planning nodal growth zones (Celliers et al., 2015).

The combination of literature review, fieldwork, and tide modelling allowed for the geophysical characteristics of Kommetjie and Milnerton’s shorelines to be investigated. Whilst both Kommetjie and Milnerton are located along the Atlantic seaboard, they have different localized biophysical influences, which reinforces the consensus that whilst remote sensing saves time, is cost efficient and easily accessible, there is still a need to ground truth satellite data. This study proves how necessary it is to invest in multi-sensory and multi-proxy coastal monitoring research (Pollard et al., 2020).

7 CONCLUSIONS and RECOMMENDATIONS

This study has successfully applied remote sensing and GIS towards the assessment of localized shoreline propagation within a South African context to address the objectives re-listed below:

Objective 1: Combine coastal science and (optical and microwave) remote sensing principles for sediment change analysis by manipulating satellite imagery for volumetric change assessment of beaches.

In order to meet Objective 1, shoreline extraction has been synthesized to determine the landward or seaward movement of shorelines to infer sediment movement and thus coastal erosion. Two sections of the Cape Town coastline, Kommetjie and Milnerton along the Atlantic seaboard were analyzed separately. The statistics confirm that the Kommetjie and Milnerton beach areas are experiencing a sediment budget deficit and are dominantly erosional with 98.49% of transects generated in Milnerton calculated to be erosional and 95.16%. in Kommetjie. Shoreline change rates indicated a shoreline recession of 2.56±2.14 and 2.35±2.14m/yr. from 1991 to 2021 in Kommetjie and Milnerton respectively. This was a result of transect change rates ranging from -7.59 to 1.08 m/yr. in Kommetjie and -6.23 to 0.02m/yr. in Milnerton. These statistics are not definitive but must be considered as a best estimate because proxy bias cannot be confidently known without shoreline benchmark data which proved to be unavailable for past years. On the other hand, the beach profiling results showed that Kommetjie was erosional indicating sediment loss of -7.326m^3 using the waterline method and 2314m^3 using interferometry. Both methods agreed that Milnerton was accretional with and increase in sediment of 5.988m^3 using the waterline method and 3154.139m^3 using interferometry.

Objective 2: Assess and classify the Kommetjie and Milnerton coastal areas through field work to validate satellite results.

Field work observations reiterated literature on Cape Town's coastline. The Woodbridge Island beach in Milnerton proved to be a gentle, narrow beach backed by coastal dunes and private property. The Milnerton lagoon was also observed as an outflow of effluent. Kommetjie is a predominantly sandy beach, with a distinct rock outcrop that clearly affects the beaches spectral reflectance. These observations coupled with the PyTides analysis helped to classify these beaches as having a semi-diurnal, micro-tidal system.

Objective 3: Investigate the City of Cape Town's legal frameworks and how GIS has been adopted to mirror them for coastal area management.

The Integrated Coastal Management Act has been determined to be an instrumental tool towards inclusive coastal management more especially when combined with spatial planning guides.

Objective 4: By process of elimination, determine the most applicable and accessible satellite data processing methods for shoreline extraction.

The combination of the MNDWI spectral index and SVM classification was found to be effective for shoreline delineation. Differential Interferometry (DInSAR) was found to produce better beach profiling results than the coastal indicator-based waterline method.

Objective 5: Determine the effectiveness of satellite-based beach profiling.

Beach elevation modelling was included to evaluate short term (2016-2021) sediment volumetric changes by applying Differential Interferometry to Sentinel-1 SLC data and the Waterline method through a combination of Sentinel -1 GRD and tide gauge data. The accuracy, validation and correction of these elevation models was conducted at the pixel level by comparison to an in-field RTK GPS survey used to capture the current state of the beaches as described in section Size of area under investigation on page 81. Whilst the same could not be done for Milnerton due to limited resources, the results have proven to be an appropriate benchmark for beach profiling and that DInSAR is a effective in beach profiling.

As highlighted above, by emphasizing how the study met its objectives, the research, its design, its methods, and its findings therefore address the aims of the study.

The next chapter outlines areas of improvement or recommendation.

7.1 RECOMMENDATIONS

This section outlines the limitations of the current study and recommendations for improvement and further research.

There are several avenues of approach towards coastal erosion studies. The methodology presented here showcases remote sensing and GIS as a tool for geomorphology or geoscience. Working with large spatial datasets requires a large amount of storage and processing power. It is thus recommended that shoreline extraction and analysis be automated through computer vision and machine learning algorithms (Salameh et al., 2020). Data sharing platforms such as the newly launched Digital Earth Africa are making this possible by providing readily available datasets and algorithms specific to the context of Sub-Saharan Africa. To cut down on storage limitations, using web platforms such as Google Earth Engine which has the CoastSat Python toolkit may also be an alternative (Vos et al., 2019). Shortening the time interval of the DSAS analysis to perhaps 5 years may also offer more accuracy. To further understand the influence of seasonality on shorelines, a finer temporal scale such as a monthly analysis can also be conducted. Where Radar data are concerned, Persistence interferometry is also a worthy avenue to explore particularly in understanding coastline response to varying sensor orbital baselines (Almar et al., 2019). The study area examined here was restricted due to time, processing capabilities and financial constraints, however analyzing the entirety of the coastline would be greatly beneficial.

Whilst there is merit in using satellite data towards coastal management as shown in this study, a more digital or continuous approach may be required for the continuous capture of shoreline changes. For this, the set-up of video camera stations along shorelines can take it a step beyond static erosional analysis to understanding wave-run up dynamics. This approach is being well developed in countries such as New Zealand where researchers are developing the CoastSnap system (Harley et al., 2018). The City of Cape Town invests in yearly airborne LiDAR acquisition but there needs to be a specific and deliberate inclusion of the city's beaches for a yearly coastal erosion analysis. The combination of video and LiDAR would significantly improve the accuracy of any erosion analysis as it would allow for proxy bias calculations and comparing different shoreline or coastal defense modifications (Hart &Blenkinsopp, 2020). Perhaps also including Deronde et al.(2008)'s approach in collecting wet and dry beach sediment for a combined sediment type spectral classification and Radar polarization assessment would push shoreline assessments further in South Africa leading to web-based applications and automated systems (Deronde et al., 2008).

The recommendations highlighted here are logical, progressive and being implemented in other parts of the world, expectations must be managed especially with the South African context of climate change. Ultimately coastal erosion can be a slow climate change induced

process and therefore may be overlooked in countries like South Africa where the economic disparity leads to more investment and research towards more immediate concerns.

REFERENCES

ACHARYA, T. D., LEE, D. H., YANG, I. T. & LEE, J. K. 2016. Identification of Water Bodies in a Landsat 8 OLI Image Using a J48 Decision Tree. *Sensors,* 16.

ALMAR, R., BERGSMA, E. W., MAISONGRANDE, P. & DE ALMEIDA, L. P. M. 2019. Wave-derived coastal bathymetry from satellite video imagery: A showcase with pleiades persistent mode. *Remote Sensing of Environment,* 231**,** 111263.

AMARO, V. E., GOMES, L. R. S., DE LIMA, F. G. F., SCUDELARI, A. C., NEVES, C. F., BUSMAN, D. V. & SANTOS, A. L. S. 2014. Multitemporal Analysis of Coastal Erosion Based on Multisource Satellite Images, Ponta Negra Beach, Natal City, Northeastern Brazil. *Marine Geodesy,* 38**,** 1-25.

ANDRÉFOUËT, S., KRAMER, P., TORRES-PULLIZA, D., JOYCE, K. E., HOCHBERG, E. J., GARZA-PÉREZ, R., MUMBY, P. J., RIEGL, B., YAMANO, H. & WHITE, W. H. 2003. Multi-site evaluation of IKONOS data for classification of tropical coral reef environments. *Remote sensing of environment,* 88**,** 128-143.

ASHRAF, M. A., MAAH, M. J. & YUSOFF, I. 2011. Introduction to remote sensing of biomass. In Biomass and remote sensing of biomass. *IntechOpen***,** (pp. 129-170).

ASMADIN, A., SIREGAR, V., SOFIAN, I., JAYA, I. & WIJANARTO, A. 2018. Feature extraction of coastal surface inundation via water index algorithms using multispectral satellite on North Jakarta. *IOP Conference Series: Earth and Environmental Science,* 176**,** 012032.

ATKINSON, P. M. & TATNALL, A. R. L. 1997. Introduction Neural networks in remote sensing. *International Journal of Remote Sensing,* 18**,** 699-709.

BAGHDADI, N., GHERBOUDJ, I., ZRIBI, M., SAHEBI, M., KING, C. & BONN, F. 2004. Semi-empirical calibration of the IEM backscattering model using radar images and moisture and roughness field measurements. *International Journal of Remote Sensing,* 25**,** 3593-3623.

BAHARI, N. I. S., AHMAD, A. & ABOOBAIDER, B. M. 2014. Application of support vector machine for classification of multispectral data. *IOP Conference Series: Earth and Environmental Science,* 20**,** 012038.

BANGARE, S. L., DUBAL, A., BANGARE, P. S. & PATIL, S. 2015. Reviewing Otsu's method for image thresholding. *International Journal of Applied Engineering Research,* 10**,** 21777-21783.

BARBOSA, M. P., SINGHROY, V. & SAINT-JEAN, R. 2014. Mapping Coastal Erosion in Southern Paraíba, Brazil from RADARSAT-1. *Canadian Journal of Remote Sensing,* 25**,** 323-328.

BERNARD O. BAUER & DAVIDSON-ARNOTT, R. G. D. 2002. A general framework for modeling sediment supply to coastal dunes including wind angle, beach geometry, and fetch effects. *Geomorphology***,** 89-108.

BIRD, E. C. & COASTS, F. 1984. An introduction to coastal geomorphology. England: John Wiley & Sons, Ltd.

BOAK, E. H. & TURNER, I. L. 2005. Shoreline Definition and Detection: A Review. *Journal of Coastal Research,* 214**,** 688-703.

BRAUN, A. 2021. Retrieval of digital elevation models from Sentinel-1 radar data–open applications, techniques, and limitations. *Open Geosciences,* 13**,** 532-569.

BROCK, J. C. & PURKIS, S. J. 2009. The emerging role of lidar remote sensing in coastal research and resource management. *Journal of Coastal Research***,** 1-5.

BRUUN, P. 1962. The Bruun Rule of Erosion.

BRUUN, P. 1988. The Bruun rule of erosion by sea-level rise: a discussion on large-scale two-and three-dimensional usages. *Journal of Coastal Research***,** 627-648.

BURDIGE, D. J. 2005. Burial of terrestrial organic matter in marine sediments: A re-assessment. *Global Biogeochemical Cycles,* 19.

BURNINGHAM, H. & KNIGHT, J. 2020. Biological Zonation and Bedrock Strength on a High Energy Granite Shore Platform. *Journal of Coastal Research,* 95**,** 23-28.
CARTWRIGHT, A. 2011. Coastal Vulnerability In The Context Of Climate Change: A South African Perspective.
CARTWRIGHT, A., BRUNDRIT, G. & FAIRHURST, L. 2008. Global climate change and adaptation–A sea-level rise risk assessment. *Phase four: Adaptation and risk mitigation measures for the City of Cape Town. Prepared for the City of Cape Town by LaquaR Consultants CC*.
CCRS 2004. *Canada Centre for Remote Sensing. Remote Sensing Tutorial.Fundamentals of Remote Sensing.*
CELLIERS, L., COLENBRANDER, D. R., BREETZKE, T. & OELOFSE, G. 2015. Towards increased degrees of integrated coastal management in the City of Cape Town, South Africa. *Ocean & Coastal Management,* 105**,** 138-153.
CHANDER, G., MARKHAM, B. L. & HELDER, D. L. 2009. Summary of current radiometric calibration coefficients for Landsat MSS, TM, ETM+, and EO-1 ALI sensors. *Remote Sensing of Environment,* 113**,** 893-903.
CLAASSENS, L., DE VILLIERS, N. M. & WALTHAM, N. J. 2022. How developed is the South African coast? Baseline extent of South Africa's coastal and estuarine infrastructure. *Ocean & Coastal Management,* 222**,** 106112.
COLENBRANDER, D. & BAVINCK, M. 2017. Exploring the role of bureaucracy in the production of coastal risks, City of Cape Town, South Africa. *Ocean & Coastal Management,* 150**,** 35-50.
COLENBRANDER, D., CARTWRIGHT, A. & TAYLOR, A. 2014. Drawing a line in the sand: managing coastal risks in the City Of Cape Town. *South African Geographical Journal,* 97**,** 1-17.
COLGLAZIER, W. 2015. Sustainable development agenda: 2030. *Science,* 349**,** 1048-1050.
COMPTON, J. S. 2004. *The rocks and mountains of Cape Town*, Juta and Company Ltd.
CRACKNELL, A. P. 2010. Remote sensing techniques in estuaries and coastal zones an update. *International Journal of Remote Sensing,* 20**,** 485-496.
CSIR 1972. Effects of Proposed Harbour Developments on the Table Bay Coastline.
DAVIDSON-ARNOTT, R., OLLERHEAD, J., WALKER, I. & HESP, P. Spatial and temporal variability in intensity of aeolian transport on a beach and foredune. Proceedings Coastal Sediments, 2003. Citeseer.
DEPARTMENT OF ENVIRONMENTAL AFFAIRS 2021. A SUMMARY GUIDE TO SOUTH AFRICA'S INTEGRATED COASTAL MANAGEMENT ACT. *In:* DEPARTMENT OF ENVIRONMENTAL AFFAIRS, R. O. S. A. (ed.).
DEPARTMENT OF ENVIRONMENTAL AFFAIRS : OCEANS AND COASTS 2015. State Of The Oceans And Coasts Around South Africa.
DEPARTMENT OF ENVIRONMENTAL AFFAIRS: CLIMATE CHANGE 2018. South Africa's 3rd Climate Change Report. Pretoria.
DEPARTMENT OF RURAL DEVELOPMENT AND LAND REFORM. 2013. *Datums and Coordinate Systems* [Online]. National Geospatial Information(NGI). Available: http://www.ngi.gov.za/index.php/technical-information/geodesy-and-gps/datum-s-and-coordinate-systems [Accessed 04/01/2021].
DERONDE, B., HOUTHUYS, R., HENRIET, J. P. & LANCKER, V. V. 2008. Monitoring of the sediment dynamics along a sandy shoreline by means of airborne hyperspectral remote sensing and LIDAR: a case study in Belgium. *Earth Surface Processes and Landforms,* 33**,** 280-294.
DESPORTES, I. & COLENBRANDER, D. R. 2016. Navigating interests, navigating knowledge: Towards an inclusive set-back delineation along Cape Town's coastline. *Habitat International,* 54**,** 124-135.
DI, K., MA, R., WANG, J. & LI, R. Coastal mapping and change detection using high-resolution IKONOS satellite imagery. Proceedings of the 2003 annual national conference on Digital government research, 2003. 1-4.

DUBE, K., NHAMO, G. & CHIKODZI, D. 2021. Rising sea level and its implications on coastal tourism development in Cape Town, South Africa. *Journal of Outdoor Recreation and Tourism,* 33**,** 100346.

DUNN, S., FRIEDMAN, R. & BAISH, S. 2000. Coastal Erosion: Evaluating the Risk. *Environment: Science and Policy for Sustainable Development,* 42**,** 36-45.

EDWARDS, E. 2001. *Investigation Into The Use Of Aerial Digital Photography For Monitoring Coastal Sand Dunes.* Doctor of Philosophy, Bath Spa University College.

ELIOT, M. 2016. Coastal sediments, beaches and other soft shores. *CoastAdapt Information Manual 8, National Climate Change Adaptation Research Facility, Gold Coast.*

ENVIRONMENTAL PROTECTION AGENCY. 2017. *Climate Impacts on Coastal Areas* [Online]. United States of America. Available: https://19january2017snapshot.epa.gov/climate-impacts/climate-impacts-coastal-areas_.html [Accessed 26/11/2021 2021].

ESRI. 2016. *How IDW works* [Online]. Available: https://desktop.arcgis.com/en/arcmap/10.3/tools/spatial-analyst-toolbox/how-idw-works.htm#:~:text=Fixed%20search%20radius&text=The%20distance%20dictates%20the%20radius,input%20points%20is%20the%20same [Accessed 2022].

EUROPEAN SPACE AGENCY. 2021. *Sentinel Online* [Online]. Available: https://sentinels.copernicus.eu/web/sentinel/about-sentinel-online [Accessed 2020].

FERRETTI, A., MONTI-GUARNIERI, A., PRATI, C., ROCCA, F. & MASSONET, D. 2007. InSAR principles-guidelines for SAR interferometry processing and interpretation, TM-19.

FILIPPONI, F. 2019. Sentinel-1 GRD Preprocessing Workflow. *Proceedings,* 18.

FOODY, G. M., MUSLIM, A. M. & ATKINSON, P. M. 2007. Super-resolution mapping of the waterline from remotely sensed data. *International Journal of Remote Sensing,* 26**,** 5381-5392.

FOURIE, J.-P., ANSORGE, I., BACKEBERG, B., CAWTHRA, H. C., MACHUTCHON, M. R. & VAN ZYL, F. W. 2015. The influence of wave action on coastal erosion along Monwabisi Beach, Cape Town. *South African Journal of Geomatics,* 4**,** 96-109.

GAO, B.-C. 1996. NDWI—A normalized difference water index for remote sensing of vegetation liquid water from space. *Remote sensing of environment,* 58**,** 257-266.

GENS, R. 2010. Remote sensing of coastlines: detection, extraction and monitoring. *International Journal of Remote Sensing,* 31**,** 1819-1836.

GEOCACHING. 2014. *Low Water Springs* [Online]. geocaching. Available: https://www.geocaching.com/geocache/GC56YQP_low-water-springs?guid=03caeeea-d7af-470f-8a0f-7b612c443410 [Accessed 11/07/2021].

GESCH, D. B., BROCK, J. C., PARRISH, C. E., ROGERS, J. N. & WRIGHT, C. W. 2016. Introduction: special issue on advances in topobathymetric mapping, models, and applications. *Journal of Coastal Research***,** 1-3.

GIBSON, P. J. & POWER, C. H. 2000. Introductory remote sensing: Principles and concepts.: Psychology Press.

GIMOND, M. 2022. *Intro to GIS and Spatial Analysis* [Online]. Available: https://mgimond.github.io/Spatial/index.html [Accessed 2022].

GIS RESOURCES. 2021. *Types Of Interpolation Methods* [Online]. Available: https://gisresources.com/types-interpolation-methods_3/ [Accessed 2022].

GOMEZ, C., WULDER, M., DAWSON, A., RITCHIE, W. & GREEN, D. 2014. Shoreline Change and Coastal Vulnerability Characterization with Landsat Imagery: A Case Study in the Outer Hebrides, Scotland. *Scottish Geographical Journal,* 130.

GRANDIN, R. https://hal.archives-ouvertes.fr/hal-01621519/document

https://hal.archives-ouvertes.fr/hal-01621519/file/Grandin_Fringe2015_Final.pdf. Interferometric Processing of SLC Sentinel-1 TOPS Data. FRINGE'15: Advances in the Science and Applications of SAR Interferometry and Sentinel-1 InSAR Workshop, Frascati, Italy, 23-27 March 2015, 2015-03-23 2015 Frascati, Italy.

GRIFFITHS, C. L., ROBINSON, T. B., LANGE, L. & MEAD, A. 2010. Marine biodiversity in South Africa: an evaluation of current states of knowledge. *PLoS One,* 5**,** e12008.

GUARIGLIA, A., BUONAMASSA, A., LOSURDO, A., SALADINO, R., TRIVIGNO, M. L., ZACCAGNINO, A. & COLANGELO, A. 2006. A multisource approach for coastline mapping and identification of shoreline changes. *Annals of geophysics,* 49.

GUIMARÃES, U. S., RODRIGUES, T. W. P., GALO, M. D. L. B. T. & PAMPLONA, V. M. S. Change detection applied on shorelines in the mouth of Amazon River. 2014 IEEE Geoscience and Remote Sensing Symposium, 2014. IEEE, 2146-2149.

GUO, Q., PU, R., ZHANG, B. & GAO, L. A comparative study of coastline changes at Tampa Bay and Xiangshan Harbor during the last 30 years. 2016 IEEE International Geoscience and Remote Sensing Symposium (IGARSS), 2016. IEEE, 5185-5188.

HAMYLTON, S. M. 2017. The Application of Spatial Analysis to Coastal Environments. *In:* HAMYLTON, S. M. (ed.) *Spatial Analysis of Coastal Environments.* Cambridge: Cambridge University Press.

HARLEY, M., KINSELA, M., SÁNCHEZ-GARCÍA, E. S. & VOS, K. CoastSnap: Crowd-Sourced Shoreline Change Mapping using Smartphones. AGU Fall Meeting Abstracts, 2018. EP52D-26.

HARRIS, L., NEL, R. & SCHOEMAN, D. 2011. Mapping beach morphodynamics remotely: A novel application tested on South African sandy shores. *Estuarine, Coastal and Shelf Science,* 92**,** 78-89.

HART, J. & BLENKINSOPP, C. 2020. Using citizen science to collect coastal monitoring data. *Journal of Coastal Research,* 95**,** 824-828.

HIMMELSTOSS, E. A., HENDERSON, R. E., KRATZMANN, M. G. & FARRIS, A. S. 2018. Digital Shoreline Analysis System (DSAS) version 5.0 user guide. *Open-File Report.* Reston, VA.

HORRITT, M., MASON, D. & LUCKMAN, A. 2001. Flood boundary delineation from synthetic aperture radar imagery using a statistical active contour model. *International Journal of Remote Sensing,* 22**,** 2489-2507.

HUGHES, P. 1992. *The impacts of sea level rise on the South African Coastal Environment.* University of Cape Town.

INGLE, J. C. 2011. *The movement of beach sand: an analysis using fluorescent grains*, Elsevier.

JEONG, E., PARK, J.-Y. & HWANG, C.-S. 2018. Assessment of UAV photogrammetric mapping accuracy in the beach environment. *Journal of Coastal Research***,** 176-180.

JEZEK, K. & LIU, H. 2005. Structure of southeastern Antarctic Peninsula ice shelves and ice tongues from synthetic aperture radar imagery. *Journal of Glaciology,* 51**,** 373-376.

KAPLAN, G., FINE, L., LUKYANOV, V., MANIVASAGAM, V., TANNY, J. & ROZENSTEIN, O. 2021. Normalizing the Local Incidence Angle in Sentinel-1 Imagery to Improve Leaf Area Index, Vegetation Height, and Crop Coefficient Estimations. *Land,* 10**,** 680.

KLEMAS, V. 2011. Beach profiling and LIDAR bathymetry: An overview with case studies. *Journal of Coastal Research,* 27**,** 1019-1028.

KOVALEVA, O., CHUBARENKO, B. & PUPIENIS, D. 2016. Grain size variability as an indicator of sediment transport alongshore the Curonian Spit (south-eastern Baltic Sea). *Baltica,* 29**,** 145-155.

LAFFERTY, K., RASSWEILER, A., GOTSCHALK, C., MORTON, D., BELL, T., HENDERIKX, F., KUSHNER, D., SPRAGUE, J., JOHNSON, C. & WASHBURN, L. 2019. The response of kelp forest organisms to spatial and temporal variation in wave energy in the California Channel Islands. *US Department of the Interior, Bureau of Ocean Energy Management. OCS Study BOEM,* 64**,** 38.

LEE, H., LIM, S. & PARK, D. 2011. Application of terrestrial laser scanner and raster operations to change detection of beach. *Journal of coastal research***,** 1692-1696.

LEE, Y.-K., EOM, J., DO, J.-D., KIM, B.-J. & RYU, J.-H. 2019. Shoreline Movement Monitoring and Geomorphologic Changes of Beaches Using Lidar and UAVs Images on the Coast of the East Sea, Korea. *Journal of Coastal Research,* 90**,** 409-414.

LI, R.-R., KAUFMAN, Y. J., GAO, B.-C. & DAVIS, C. O. 2003. Remote sensing of suspended sediments and shallow coastal waters. *IEEE Transactions on Geoscience and Remote Sensing,* 41**,** 559-566.

LOUBERSAC, L. 2003. Remote Sensing and Coastal Zone Management.

MAITI, S. & BHATTACHARYA, A. K. 2009. Shoreline change analysis and its application to prediction: A remote sensing and statistics based approach. *Marine Geology,* 257**,** 11-23.

MALTHUS, T. J. & MUMBY, P. J. 2010. Remote sensing of the coastal zone: An overview and priorities for future research. *International Journal of Remote Sensing,* 24**,** 2805-2815.

MASON, D., DAVENPORT, I., ROBINSON, G., FLATHER, R. & MCCARTNEY, B. 1995. Construction of an inter-tidal digital elevation model by the 'Water-Line'Method. *Geophysical Research Letters,* 22**,** 3187-3190.

MASON, D. C., AMIN, M., DAVENPORT, I. J., FLATHER, R. A., ROBINSON, G. J. & SMITH, J. A. 1999. Measurement of recent intertidal sediment transport in Morecambe Bay using the waterline method. *Estuarine, Coastal and Shelf Science,* 49**,** pp.427-456.

MASON, D. C., GURNEY, C. & KENNETT, M. 2000. Beach topography mapping—a comparsion of techniques. *Journal of Coastal Conservation,* 6**,** pp.113-124.

MATHER, A. A. 2008. Sea level rise and it's likely financial impacts. *IMFO: Official Journal of the Institute of Municipal Finance Officers,* 8**,** 8-9.

MAULUD, K. N. A. & RAFAR, R. M. Determination the impact of sea level rise to shoreline changes using GIS. 2015 International Conference on Space Science and Communication (IconSpace), 2015. IEEE, 352-357.

MCFEETERS, S. K. 1996. The use of the Normalized Difference Water Index (NDWI) in the delineation of open water features. *International journal of remote sensing,* 17**,** 1425-1432.

MERWE, C. V. D. 2017. *A Synthesis Of Coastal Geophysical Characteristics Of Sandy Beaches Aong The South African Coastline.* Master Of Engineering, Stellenbosch University.

MIDGLEY, G., CHAPMAN, R., HEWITSON, B., JOHNSTON, P., DE WIT, M., ZIERVOGEL, G., MUKHEIBIR, P., VAN NIEKERK, L., TADROSS, M. & VAN WILGEN, B. 2005. A status quo, vulnerability and adaptation assessment of the physical and socio-economic effects of climate change in the Western Cape.

MIRANDA, N., MEADOWS, P., TYPE, D. & NOTE, T. 2015. Radiometric calibration of S-1 Level-1 products generated by the S-1 IPF. *Viewed at https://sentinel. esa. int/documents/247904/685163/S1-Radiometric-Calibration-V1. 0. pdf*.

MORTON, R. A., MILLER, T. & MOORE, L. 2005. Historical shoreline changes along the US Gulf of Mexico: a summary of recent shoreline comparisons and analyses. *Journal of Coastal Research,* 21(4 (214))**,** pp.704-709.

MUKHEIBIR, P. & ZIERVOGEL, G. 2006. Framework for adaptation to climate change in the city of Cape Town.

MUSEKIWA, C., CAWTHRA, H. C., UNTERNER, M. & VAN ZYL, F. W. 2015. An assessment of coastal vulnerability for the South African coast. *South African Journal of Geomatics,* 4**,** 123-137.

NGUYEN, C. T., CHIDTHAISONG, A., KIEU DIEM, P. & HUO, L.-Z. 2021. A Modified Bare Soil Index to Identify Bare Land Features during Agricultural Fallow-Period in Southeast Asia Using Landsat 8. *Land,* 10.

NIEDERMEIER, A., HOJA, D. & LEHNER, S. 2005. Topography and morphodynamics in the German Bight using SAR and optical remote sensing data. *Ocean Dynamics,* 55**,** 100-109.

NOVÉ-JOSSERAND, C., HEBRERO, F. C., PETIT, L., MEGILL, W., GODOY-DIANA, R. & THIRIA, B. 2018. Surface wave energy absorption by a partially submerged bio-inspired canopy. *Bioinspiration & biomimetics,* 13**,** 036006.

OCEAN RHYTHM. 2021. *South African Tidal Chart Datum* [Online]. Available: http://www.satides.co.za/chartDatum.html [Accessed 04/01/2021].

ORLIKOVA, J. & HORAK, J. L. 2019. *Land Cover Classification Using Sentinel-1 SAR Data*.

OYEDOTUN, T. D. T. 2014. Shoreline geometry: DSAS as a tool for Historical Trend Analysis. *Geomorphological Techniques (Online Edition)*.

PACHAURI, R. & MEYER, L. 2014. Climate Change 2014: Synthesis Report. Contribution of Working Groups I, II and III to the Fifth Assessment Report of the Intergovernmental Panel on Climate Change.

PARKER, B. B. 2003. The difficulties in measuring a consistently defined shoreline—the problem of vertical referencing. *Journal of Coastal Research*, 44-56.

PASCALE, S., KAPNICK, S. B., DELWORTH, T. L. & COOKE, W. F. 2020. Increasing risk of another Cape Town "Day Zero" drought in the 21st century. *Proceedings of the National Academy of Sciences,* 117, 29495.

PE'ERI, S. & LONG, B. 2011. LIDAR technology applied in coastal studies and management. *Journal of Coastal Research*, 1-5.

POLLARD, J. A., SPENCER, T., BROOKS, S. M., CHRISTIE, E. K. & MÖLLER, I. 2020. Understanding spatio-temporal barrier dynamics through the use of multiple shoreline proxies. *Geomorphology,* 354, 107058.

PRATS-IRAOLA, P., RODRIGUEZ-CASSOLA, M., DE ZAN, F., SCHEIBER, R., LÓPEZ-DEKKER, P., BARAT, I. & GEUDTNER, D. 2015. Role of the orbital tube in interferometric spaceborne SAR missions. *IEEE Geoscience and Remote Sensing Letters,* 12, 1486-1490.

QUICK, A. & ROBERTS, M. 1993. Table Bay, Cape Town, South Africa: synthesis of available information and management implications. *South African Journal of Science,* 89, 276-287.

ROBERTSON, W., WHITMAN, D., ZHANG, K. & LEATHERMAN, S. P. 2004. Mapping Shoreline Position Using Airborne Laser Altimetry. *Journal of Coastal Research,* 203, 884-892.

RONGXING LI & F, J. K. L. Y. 2001. Spatial Modeling and Analysis for Shoreline Change Detection and Coastal Erosion Monitoring. *Marine Geodesy,* 24, 1-12.

RUST, I. C. 1991. Environmental geology of the coastal zone: a South African perspective. *South African Journal of Marine Science,* 10, 397-405.

SALAMEH, E., FRAPPART, F., TURKI, I. & LAIGNEL, B. 2020. Intertidal topography mapping using the waterline method from Sentinel-1 & -2 images: The examples of Arcachon and Veys Bays in France. *ISPRS Journal of Photogrammetry and Remote Sensing,* 163, 98-120.

SALLENGER JR, A.H., K., W., B., J., , SWIFT, R., MANIZADE, S. & STOCKDON, H. 2002. Sea-cliff erosion as a function of beach changes and extreme wave runup during the 1997–1998 El Niño. *Marine Geology,* 187(3-4), pp.279-297.

SATGE, F., DENEZINE, M., PILLCO, R., TIMOUK, F., PINEL, S., MOLINA, J., GARNIER, J., SEYLER, F. & BONNET, M.-P. 2016. Absolute and relative height-pixel accuracy of SRTM-GL1 over the South American Andean Plateau. *ISPRS Journal of Photogrammetry and Remote Sensing,* 121, 157-166.

SCHMIDT, K., SCHWERDT, M., MIRANDA, N. & REIMANN, J. 2020. Radiometric Comparison within the Sentinel-1 SAR Constellation over a Wide Backscatter Range. *Remote Sensing,* 12, 854.

SEARSON, S. & BRUNDRIT, G. 1995. Extreme high sea levels around the coast of southern Africa. *South African Journal of Science,* 91, 579-588.

SHORT, A. D. 2012. *Coastal Processes and Beaches* [Online]. Nature Education Knowledge Available: https://www.nature.com/scitable/knowledge/library/coastal-processes-and-beaches-26276621/ [Accessed 7-07-2021 2021].

SONG, D.-S., KIM, I.-H. & LEE, H.-S. 2013. Preliminary 3D assessment of coastal erosion by data integration between airborne LiDAR and DGPS field observations. *Journal of Coastal Research*, 1445-1450.

SOUSA, W. R. N. D., SOUTO, M. V. S., MATOS, S. S., DUARTE, C. R., SALGUEIRO, A. R. G. N. L. & NETO, C. A. D. S. 2018. Creation of a coastal evolution prognostic model using shoreline historical data and techniques of digital image processing in a GIS environment for generating future scenarios. *International Journal of Remote Sensing,* 39, 4416-4430.

STÅHLBERG, C., BASTVIKEN, D., SVENSSON, B. H. & RAHM, L. 2006. Mineralisation of organic matter in coastal sediments at different frequency and duration of resuspension. *Estuarine, Coastal and Shelf Science,* 70**,** 317-325.

STOCKDON, H. F., SALLENGER JR, A. H., LIST, J. H. & HOLMAN, R. A. 2002. Estimation of shoreline position and change using airborne topographic lidar data. *Journal of Coastal Research***,** 502-513.

SUWANPRASIT, C. Effects of near shore land-use dynamic on coastal erosion in Phuket, Thailand. 2015 IEEE International Geoscience and Remote Sensing Symposium (IGARSS), 2015. IEEE, 4832-4835.

T.SUTTON; O. DASSAU; M. SUTTON. 2009. *A Gentle Introduction to GIS* [Online]. Available: https://docs.qgis.org/2.18/en/docs/gentle_gis_introduction/spatial_analysis_interpolation.html [Accessed 2022].

TAN, Q. & XU, X. 2014. Comparative analysis of spatial interpolation methods: an experimental study. *Sensors & Transducers,* 165**,** 155.

THERON, A. K. & ROSSOUW, M. Analysis of potential coastal zone climate change impacts and possible response options in the southern African region. 2008-11 2008.

THIEBES, B., WANG, J., BAI, S. & LI, J. 2013. Terrestrial laserscanning of tidal flats—a case study in Jiangsu Province, China. *Journal of Coastal Conservation,* 17**,** 813-823.

THOMSON, A. G., FULLER, R. M., YATES, M. G., BROWN, S. L., COX, R. & WADSWORTH, R. A. 2010. The use of airborne remote sensing for extensive mapping of intertidal sediments and saltmarshes in eastern England. *International Journal of Remote Sensing,* 24**,** 2717-2737.

TINGZON, I., DEJITO, N., FLORES, R., GUZMAN, R., CARVAJAL, L., ERAZO, K., CALA, I., VILLAVECES, J., RUBIO, D. & GHANI, R. 2020. *Mapping New Informal Settlements using Machine Learning and Time Series Satellite Images: An Application in the Venezuelan Migration Crisis*.

TOURE, S., DIOP, O., KPALMA, K. & MAIGA, A. 2019. Shoreline Detection using Optical Remote Sensing: A Review. *ISPRS International Journal of Geo-Information,* 8.

UNIVERSITY OF MINNESOTA. *Remote Sensing of Water Resources* [Online]. Available: https://water.rs.umn.edu/lwc [Accessed].

VAN ZYL, F. W. 2019. *Geological mapping of the inner shelf off Cape Town's Atlantic Seaboard, South Africa*, Council for Geoscience.

VECI, L. 2015. TOPS Interferometry Tutorial. *Sentinel-1 Toolbox*.

VIRGINIA INSTITUTE OF MARINE SCIENCE. 2022. Available: https://www.vims.edu/research/units/labgroups/tc_tutorial/tide_analysis.php [Accessed].

VOS, K., SPLINTER, K. D., HARLEY, M. D., SIMMONS, J. A. & TURNER, I. L. 2019. CoastSat: A Google Earth Engine-enabled Python toolkit to extract shorelines from publicly available satellite imagery. *Environmental Modelling & Software,* 122**,** 104528.

WANG, B., SHI, W. & LIU, E. 2015. Robust methods for assessing the accuracy of linear interpolated DEM. *International journal of applied earth observation and geoinformation,* 34**,** 198-206.

WHITE, S. A. & WANG, Y. 2003. Utilizing DEMs derived from LIDAR data to analyze morphologic change in the North Carolina coastline. *Remote sensing of environment,* 85**,** 39-47.

WIGLEY, R. 2011. Geohazards in coastal areas.

WOODBORNE, M. & FLEMMING, B. 2021. Sedimentological evidence for seiching in a swell-dominated headland-bay system: Table Bay, Western Cape, South Africa. *Geo-Marine Letters,* 41**,** 46.

WOZENCRAFT, J. M. & LILLYCROP, W. J. 2003. SHOALS airborne coastal mapping: Past, present, and future. *Journal of Coastal Research***,** 207-215.

XIONG, L., WANG, G., BAO, Y., ZHOU, X., WANG, K., LIU, H., SUN, X. & ZHAO, R. 2019. A rapid terrestrial laser scanning method for coastal erosion studies: A case study at Freeport, Texas, USA. *Sensors,* 19**,** 3252.

XU, H. 2006. Modification of normalised difference water index (NDWI) to enhance open water features in remotely sensed imagery. *International Journal of Remote Sensing,* 27**,** 3025-3033.

ZHANG, J., TEMMER, M., GOPALSWAMY, N., MALANDRAKI, O., NITTA, N. V., PATSOURAKOS, S., SHEN, F., VRŠNAK, B., WANG, Y., WEBB, D., DESAI, M. I., DISSAUER, K., DRESING, N., DUMBOVIĆ, M., FENG, X., HEINEMANN, S. G., LAURENZA, M., LUGAZ, N. & ZHUANG, B. 2021. Earth-affecting solar transients: a review of progresses in solar cycle 24. *Progress in Earth and Planetary Science,* 8**,** 56.

ZHE, Z. & C E WOODCOCK 2012. Object-based cloud and cloud shadow detection in Landsat imagery. *Remote Sensing of Environment,* 118**,** 83-94.

ZHOU, Z., LIU, Q., FAN, D., COCO, G., GONG, Z., MÖLLER, I., XU, F., TOWNEND, I. & ZHANG, C. 2021. Simulating the role of tides and sediment characteristics on tidal flat sorting and bedding dynamics. *Earth Surface Processes and Landforms,* 46**,** 2163-2176.

ZHU, Z., WANG, S. & WOODCOCK, C. E. 2015. Improvement and expansion of the Fmask algorithm: cloud, cloud shadow, and snow detection for Landsats 4–7, 8, and Sentinel 2 images. *Remote Sensing of Environment,* 159**,** 269-277.

ZOLLINI, S., ALICANDRO, M., CUEVAS-GONZÁLEZ, M., BAIOCCHI, V., DOMINICI, D. & BUSCEMA, P. M. 2020. Shoreline Extraction Based on an Active Connection Matrix (ACM) Image Enhancement Strategy. *Journal of Marine Science and Engineering,* 8.

APPENDICES

APPENDIX A PRODUCER AND USER MATRIX FOR 1991 AND 2021 LANDCOVER CLASSIFICATION

Table 18 Confusion matrix for Cape Town land cover in 1991

1991				
CLASS	PROD. ACC. (Percent)	USER ACC. (Percent)	PROD. ACC. (Pixels)	USER ACC. (Pixels)
Water Bodies	91.15	79.19	175/192	175/221
Vegetation	69.29	76.38	679/980	679/889
Shallow Coast	23.06	100.00	92/399	92/92
Ocean	99.99	98.77	23701/23703	23701/23997
Mountain Shadow	63.25	80.43	74/117	74/92
Mountains	90.83	94.09	3566/3926	3566/3790
Built Up Area	85.35	70.90	1223/1433	1223/1725
Beaches	94.98	99.57	1153/1214	1153/1158

Table 19 Confusion matrix for Cape Town land cover in 2021

2021				
CLASS	PROD. ACC. (Percent)	USER ACC. (Percent)	PROD. ACC. (Pixels)	USER ACC. (Pixels)
Water Bodies	76.59	85.58	3122/4076	3122/3648
Vegetation	51.35	65.97	1541/3001	1541/2336
Shallow Coast	2.72	42.50	17/625	17/40
Ocean	99.93	99.70	346928/347162	346928/347977
Mountain Shadow	79.37	87.27	2701/3403	2701/3095
Mountains	93.32	89.76	30048/32198	30048/33475
Built Up Area	91.47	90.31	35307/38598	35307/39094
Beaches	74.33	91.04	2438/3280	2438/2678

Table 20 Pytides Data Prediction Summary

KOMMETJIE 2021		KOMMTETJIE 2016	
4/16/2021 17:26	0.381158066871679	1/1/2016 17:26	0.383914015013843
2/20/2021 17:34	0.381180049114832	1/6/2016 17:33	0.381276161001357
1/3/2021 17:34	0.381094737054675	1/25/2016 17:26	0.384001665774743
2/3/2021 17:26	0.381065000294234	1/30/2016 17:33	0.383961937366245
3/4/2021 17:34	0.384059421605038	2/11/2016 17:33	0.381407658879351
1/15/2021 17:34	0.381461247342043	2/18/2016 17:26	0.384073524480406
2/8/2021 17:34	0.383955953462945	2/23/2016 17:33	0.381183065809152
3/16/2021 17:34	0.381354049429980	3/30/2016 17:33	0.381569110300328
1/27/2021 17:34	0.381394851069418	4/6/2016 17:26	0.381024767700185
3/28/2021 17:34	0.381225355476011	3/13/2016 17:26	0.381370117086217
4/21/2021 17:34	0.381499098003171	3/6/2016 17:33	0.384081261557639
4/28/2021 17:26	0.381651143399127	4/11/2016 17:33	0.381248398664983
		4/23/2016 17:33	0.383988350403169
MILNERTON 2021		MILNERTON 2016	
4/28/2021 17:26	0.381221006179799	1/30/2016 17:34	0.384075811372031
3/28/2021 17:34	0.381524219477416	1/25/2016 17:26	0.384001665774743
2/27/2021 17:34	0.383937680745932	2/23/2016 17:34	0.383953297563802
4/21/2021 17:34	0.384053238299457	3/18/2016 17:34	0.381325532647581
2/20/2021 17:34	0.383997052745645	2/18/2016 17:26	0.384073524480406
4/16/2021 17:26	0.381185276544059	3/13/2016 17:26	0.381370117086217
1/15/2021 17:34	0.383997760832085	11/2/2016 17:33	0.381407658879351
3/17/2021 17:26	0.383994875650915	6/4/2016 17:26	0.381024767700185

4/9/2021 17:34	0.381025517447332	1/1/2016 17:26	0.383914015013843
4/3/2021 17:34	0.381188933885097		

APPENDIX B DSAS SUMMARY REPORTS

B1. DSAS Summary for Kommetjie Beach

File name: DSAS_Summary_KomHartEN_Transect_20211004_100625.txt

Timestamp of rate calculation: 10/04/2021 10:07:54

DSAS version: 5.0.20200527.0200

ArcGIS version: 10.8

Rate types run: SCE, NSM, EPR, LRR, WLR

Baseline layer: T1991_smoothed50HartEN

Shoreline layer: MergedKom40HartEN

Shoreline dates used: 2/24/2001, 4/17/2011, 1/6/2021

Shoreline threshold: 0

Confidence Interval (CI) selected: 90

Default Uncertainty: 30

Transect spacing length: 5

Smoothing distance: 500

Coordinate system: Hartebeesthoek94_Lo19_(E-N)

Is bias applied: NO

All rates reported are in meters/year, distance values are in meters.

DISTANCE: SCE (Shoreline Change Envelope, m)

SCE OVERALL AVERAGES:

total number of transects: 578

average distance: 51.77

maximum distance: 150.88

maximum distance transect ID: 481

minimum distance: 0.2

minimum distance transect ID: 27

DISTANCE: NSM (Net Shoreline Movement, m)

NSM OVERALL AVERAGES:
total number of transects: 578
average distance: -50.84
number of transects with negative distance: 550
percent of all transects that have a negative distance: 95.16%
maximum negative distance: -150.88
maximum negative distance transect ID: 481
average of all negative distances: -53.52
number of transects with positive distance: 28
percent of all transects that have a positive distance: 4.84%
maximum positive distance: 21.4
maximum positive distance transect ID: 346
average of all positive distances: 1.71

RATE: EPR (End Point Rate, m/yr)

EPR OVERALL AVERAGES:
total number of transects: 578
average rate: -2.56
average of the confidence intervals associated with rates: 2.14
reduced n (number of independent transects): 1
uncertainty of the average rate using reduced n: 2.14
average rate with reduced n uncertainty: -2.56 +/- 2.14

number of erosional transects: 550
percent of all transects that are erosional: 95.16%
percent of all transects that have statistically significant erosion: 46.37%
maximum value erosion: -7.59
maximum value erosion transect ID: 481
average of all erosional rates: -2.7

number of accretional transects: 28

percent of all transects that are accretional: 4.84%

percent of all transects that have statistically significant accretion: 0%

maximum value accretion: 1.08

maximum value accretion transect ID: 346

average of all accretional rates: 0.09

RATE: LRR (Linear Regression Rate, m/yr)

LRR OVERALL AVERAGES:

total number of transects: 576

average rate: -2.55

average of the confidence intervals associated with rates: 6.82

reduced n (number of independent transects): 19

uncertainty of the average rate using reduced n: 1.57

average rate with reduced n uncertainty: -2.55 +/- 1.57

number of erosional transects: 549

percent of all transects that are erosional: 95.31%

percent of all transects that have statistically significant erosion: 11.98%

maximum value erosion: -7.57

maximum value erosion transect ID: 481

average of all erosional rates: -2.68

number of accretional transects: 27

percent of all transects that are accretional: 4.69%

percent of all transects that have statistically significant accretion: 0%

maximum value accretion: 1.07

maximum value accretion transect ID: 346

average of all accretional rates: 0.08

RATE: WLR (Weighted Linear Regression, m/yr)

WLR OVERALL AVERAGES:

total number of transects: 576

average rate: -2.55

average of the confidence intervals associated with rates: 6.82

reduced n (number of independent transects): 19

uncertainty of the average rate using reduced n: 1.57

average rate with reduced n uncertainty: -2.55 +/- 1.57

number of erosional transects: 549

percent of all transects that are erosional: 95.31%

percent of all transects that have statistically significant erosion: 11.98%

maximum value erosion: -7.57

maximum value erosion transect ID: 481

average of all erosional rates: -2.68

number of accretional transects: 27

percent of all transects that are accretional: 4.69%

percent of all transects that have statistically significant accretion: 0%

maximum value accretion: 1.07

maximum value accretion transect ID: 346

average of all accretional rates: 0.08

B2. DSAS Summary for Milnerton Beach

File name: DSAS_Summary_MilHartTrans_20211004_134852.txt

Timestamp of rate calculation: 10/04/2021 13:51:23

DSAS version: 5.0.20200527.0200

ArcGIS version: 10.8

Rate types run: SCE, NSM, EPR, LRR, WLR

Baseline layer: T1991_smoothed_HartEN

Shoreline layer: MergedShorelines01_11_21_HartEN

Shoreline dates used: 2/24/2001, 4/17/2011, 1/6/2021

Shoreline threshold: 0

Confidence Interval (CI) selected: 90

Default Uncertainty: 30

Transect spacing length: 5

Smoothing distance: 500

Coordinate system: Hartebeesthoek94_Lo19_(E-N)

Is bias applied: NO

All rates reported are in meters/year, distance values are in meters.

DISTANCE: SCE (Shoreline Change Envelope, m)

SCE OVERALL AVERAGES:

total number of transects: 1387

average distance: 49.35

maximum distance: 123.81

maximum distance transect ID: 212

minimum distance: 0.35

minimum distance transect ID: 873

DISTANCE: NSM (Net Shoreline Movement, m)

NSM OVERALL AVERAGES:

total number of transects: 1387

average distance: -46.61

number of transects with negative distance: 1366

percent of all transects that have a negative distance: 98.49%

maximum negative distance: -123.81

maximum negative distance transect ID: 212

average of all negative distances: -47.33

number of transects with positive distance: 21

percent of all transects that have a positive distance: 1.51%

maximum positive distance: 0.49

maximum positive distance transect ID: 892

average of all positive distances: 0.4

RATE: EPR (End Point Rate, m/yr)

EPR OVERALL AVERAGES:

total number of transects: 1387

average rate: -2.35

average of the confidence intervals associated with rates: 2.14

reduced n (number of independent transects): 1

uncertainty of the average rate using reduced n: 2.14

average rate with reduced n uncertainty: -2.35 +/- 2.14

number of erosional transects: 1366

percent of all transects that are erosional: 98.49%

percent of all transects that have statistically significant erosion: 47.37%

maximum value erosion: -6.23

maximum value erosion transect ID: 212

average of all erosional rates: -2.38

number of accretional transects: 21

percent of all transects that are accretional: 1.51%

percent of all transects that have statistically significant accretion: 0%

maximum value accretion: 0.02

maximum value accretion transect ID: 892

average of all accretional rates: 0.02

RATE: LRR (Linear Regression Rate, m/yr)

LRR OVERALL AVERAGES:

total number of transects: 1385

average rate: -2.34

average of the confidence intervals associated with rates: 7.28

reduced n (number of independent transects): 19

uncertainty of the average rate using reduced n: 1.69

average rate with reduced n uncertainty: -2.34 +/- 1.69

number of erosional transects: 1364

percent of all transects that are erosional: 98.48%

percent of all transects that have statistically significant erosion: 15.16%

maximum value erosion: -6.21

maximum value erosion transect ID: 212

average of all erosional rates: -2.37

number of accretional transects: 21

percent of all transects that are accretional: 1.52%

percent of all transects that have statistically significant accretion: 0.07%

maximum value accretion: 0.05

maximum value accretion transect ID: 892

average of all accretional rates: 0.03

RATE: WLR (Weighted Linear Regression, m/yr)

WLR OVERALL AVERAGES:

total number of transects: 1385

average rate: -2.34

average of the confidence intervals associated with rates: 7.28

reduced n (number of independent transects): 19

uncertainty of the average rate using reduced n: 1.69

average rate with reduced n uncertainty: -2.34 +/- 1.69

number of erosional transects: 1364

percent of all transects that are erosional: 98.48%

percent of all transects that have statistically significant erosion: 15.16%

maximum value erosion: -6.21

maximum value erosion transect ID: 212

average of all erosional rates: -2.37

number of accretional transects: 21

percent of all transects that are accretional: 1.52%

percent of all transects that have statistically significant accretion: 0.07%

maximum value accretion: 0.05

maximum value accretion transect ID: 892

average of all accretional rates: 0.03

APPENDIX C

1. SANHO Data Release Form

HYDROGRAPHIC OFFICE
REPUBLIC OF SOUTH AFRICA

Tel: (021) 787-2408
Teleg: 527946 HYDROSAN
Fax: (021) 787-2233
Email: hydrosan@africa.com

Hydrographic Office
Private Bag X1
Tokai
7966

Our ref: FOF/HYD/R/320/13/1

AGREEMENT FOR RELEASE OF

TIDAL INFORMATION

1. This agreement stipulates the conditions in terms of which tidal information listed below, over which the SA Navy holds copyright hereafter referred to as the information, is released.

2. Information supplied: **SANHO Predicted Hourly tide records for Cape Town 2009-2020 only.**

3. The information is released on the following conditions:

   a. The receiver of this information recognises the copyright on the information supplied by the SA Navy.

   b. The information may not be sold, released or supplied to a third party without the written approval of the National Hydrographer.

   c. The information supplied may only be used for bona vide non-profit research. The National Hydrographer reserves the right to review, upon request, any paper before being published.

   d. The information supplied may not be used for navigational purposes or as part of an ECDIS.

   e. Due recognition must be given to the National Hydrographer as the supplier and copyright holder of the information.

4. The National Hydrographer reserves the right to withdraw the release of this information at any stage.

5. Neither the National Hydrographer, the SA Navy Hydrographic Office, the SA Navy nor a member or employee is liable to any person or to any dependant of such person, for any loss or damage resulting from any bodily injury, loss of life or loss of or damage to property caused by or arising out of or in any way connected with any data displayed after being modified from the original supplied format.

6. This agreement has been reached between the National Hydrographer and

NAME: Lynn Fanikiso
COMPANY: University Of Cape Town
SIGNATURE: Signed by candidate
DATE: 20 October 2020

(T. STOKES)
SOUTH AFRICAN NATIONAL HYDROGRAPHER: CAPTAIN (SA NAVY)

DATE: 20 October 2020

Your Chart, Our Art.
Actively Contributing to South Africa's Development

2. Harmonic Constituents For Granger Gay Tide Gauge In 2014

```
name,amplitude,phase
mean,1.074089611692746,0.0
M2,0.517849442008462,261.0773158019804
S2,0.23028292102353098,176.99118432766286
N2,0.11321945454096209,105.71088762223062
K1,0.055162046487388074,158.5324363851685
K2,0.042406014319661935,150.4487304370416
SSA,0.03654784815591951,95.07924298652513
MU2,0.022521292299545848,348.6102903284482
NU2,0.022080122771668098,146.89834684697237
MSF,0.019213981009569673,330.65130305927465
2N2,0.016042019124340 53,305.2564475008116
L2,0.013916514988699932,48.236307197749575
O1,0.012872331680613 84,67.15324764313804
P1,0.012538920286096 51,170.45092563475586
MF,0.012485809750369128,134.56422286205702
MSM,0.011170850700987374,202.85095649993124
MKS2,0.011051504377649733,28.241397658656517
Q1,0.010294635812314 05,268.0267249252156
NO1,0.008397673479212314,15.350823605112783
MM,0.006792177073259 4046,203.9070473026763
ETA2,0.006151093530497993,259.7391970477308
M3,0.005723238244148 3945,281.0131391246828
EPS2,0.005520138931990277,171.07859708162863
J1,0.005312677334790 2684,337.3835133453943
M4,0.004261906240776492,143.36715545439284
OQ2,0.004071751304711155,162.71090172522142
LDA2,0.003607215618274 8363,356.7948112088133
ALP1,0.003245679605939152,263.0296439834263
2Q1,0.002713178062559 71,69.63757632713693
SK3,0.002685638881075 3565,254.32196313869326
RHO1,0.002442690679244648,317.20279642265734
MS4,0.002428672252353081,87.16405991314973
SIG1,0.002298743493388 3348,124.00075314714996
MSN2,0.002287627664614 6268,140.17916473668433
MO3,0.002193864502923676,125.30059934512812
MN4,0.002016193448002169,290.3089462201048
PHI1,0.001862392308914 2642,69.23052907121331
OO1,0.001850641355497756,22.140709642661072
SO3,0.001731500967357 4376,92.62901224491935
THE1,0.001724724480789 9584,327.6094164950816
CHI1,0.001712194408875 2978,32.85332087055643
SK4,0.001601520219641 6596,358.27375328521975
SO1,0.001426213690293 5217,168.22089592375838
2MS6,0.001408832269959 2174,164.59028754098873
2MK6,0.001244074759130 1606,160.46270054415626
UPS1,0.001211957287059 3015,240.72479865460582
S4,0.001137870226386 4285,48.39327023556655
M6,0.001092391155662 0103,191.78794160389475
```

2SK5,0.0010402485479229498,128.1570932305896
SN4,0.0010135038565828043,342.19515489797055
BET1,0.00075436354630491,6.305744873153586
MK4,0.0006812379465285478,86.24790464576495
3MK7,0.0006760278660428947,251.7476178467823
MK3,0.0006425298543494344,136.1099891286499
TAU1,0.0005855018113547906,152.78424931203296
2SM6,0.0005528904375123981,319.05086243216726
2MN6,0.0004681485592580242,63.63627514803087
2MK5,0.0003242598320118871,106.51575184584773
MSK6,0.00029206791927601194,229.6345451815595
M8,0.0001310035467331056,211.22743242430312

APPENDIX D PYTIDES PREDICTION PYTHON CODE

```
"""
Created on Wed Mar 23 19:03:09 2022

@author: FNKLYN001
"""


import pandas as pd
import numpy as np
from pandas import DataFrame
from pytides.tide import Tide
from datetime import datetime

#Read data from csv made up of date time, sea level and flag
columns.
#DT refers to date time column whilst SeaLevel is the actual
measured tide from SANHO's tide gauge in Granger Bay
#Flag column represents missing or NULL values
data_columns = ['DT', 'SeaLevel','Flag']
date_cols = ['DT']


#Specify csv file to read from. Parsing of date time column
very important for data reading and import.
TideData =
pd.read_csv('Actual_2014_January_WT.csv',parse_dates=
date_cols, decimal='.')

#distinguish between usable and missing data
bad = TideData['Flag'] == 0
corrected = TideData['Flag'] == 1

#Calculate data anomaly and use it to interpolate missing
values
TideData.loc[bad, 'SeaLevel'] = np.nan
TideData['anomaly']= TideData['SeaLevel'] -
TideData['SeaLevel'].mean()
TideData['anomaly'] =TideData['anomaly'].interpolate()
print('{} points were flagged "bad" and
interpolated'.format(bad.sum()))
print('{} points were flagged "corrected" and left
unchanged'.format(corrected.sum()))

#Convert column data to python readable and usable formats.
Dating = pd.to_datetime(TideData["DT"])
Heights=pd.to_numeric(TideData["SeaLevel"])
```

```
#Predict specific tide level at specified time. Whilst data is
collected hourly,this code is predicting at 6minute intervals
prediction_t0 = datetime(2020,1,1,00,00,00) #Date and time to
predict tide at
hours = 0.1*np.arange(7 * 24 * 10) #Prediction at 6 minute
intervals
times = Tide._times(prediction_t0, hours)


tide = Tide.decompose(Heights,times) #Tide is modelled based
on tide constituents and amplitude
constituent = [c.name for c in tide.model['constituent']]

df = DataFrame(tide.model,
index=constituent).drop('constituent', axis=1)

df.sort_values('amplitude', ascending=False).head(10)

#Form number helps to inform the type of tide e.g diurnal,
mixed e.t.c.
print('Form number %s, the tide is %s.' %
      (tide.form_number()[0], tide.classify()))

#The prediction must be readjusted from the LAT hydrographic
datum to Hartebeesthoek 94 land datum using the -0.98m offset
my_prediction = tide.at(times)
my_predictionStacked= np.column_stack((times,my_prediction))
DatumOffset=my_prediction+(-0.98)
PredictedTide=np.column_stack((times,DatumOffset))
print (PredictedTide) #Final Predicted tide used in Waterline
interpolation
```

APPENDIX E LIDAR VERTICAL ADJUSTMENT CALCULATIONS

Table 21 Lidar Adjustment of Milnerton Waterline Interpolated Elevation Models

OBJECTID	Milnerton_lidar2020 elevation	Milnerton2016_waterline elevation	Milnerton2021_waterline elevation	2016_elevation difference	2021_elevation difference
1	2.089999914	0.383122504	0.382396877	1.70687741	1.707603037
2	3.349999905	0.383216888	0.383074105	2.966783017	2.9669258
3	2.85520649	0.383241117	0.38272211	2.471965373	2.47248438
4	2.596565008	0.383073449	0.382539123	2.213491559	2.214025885
5	4.909999847	0.383223325	0.382562697	4.526776522	4.52743715
6	3.680000067	0.383121729	0.382508397	3.296878338	3.29749167
7	3.506125689	0.383145809	0.382548392	3.122979879	3.123577297
8	2.543017626	0.382928878	0.382481873	2.160088748	2.160535753
9	4.117491722	0.383122563	0.382645071	3.734369159	3.734846652
10	3.329999924	0.383013904	0.382507622	2.94698602	2.947492301
11	2.279999971	0.383097321	0.382513851	1.896902651	1.89748612
12	2.700000048	0.38328594	0.382515252	2.316714108	2.317484796
13	1.99543941	0.382991612	0.382504761	1.612447798	1.612934649
14	2.541407824	0.382923841	0.382501185	2.158483982	2.158906639
15	2.758913279	0.3830311	0.382465124	2.375882179	2.376448154
16	4.253242016	0.382991731	0.382484913	3.870250285	3.870757103
17	3.539999962	0.383167058	0.382499665	3.156832904	3.157500297
Average				**2.737335878**	**2.737878687**

APPENDIX F ELEVATION MODELLING ACCURACY

Table 22 Elevation Modelling Accuracy Calculation

OBJECTID	Kommetjie2021 RTK elevation (R)	Kommetjie2021 DInSAR elevation (D)	Adjusted DEM elevation (W)	ΔRD	ΔRW
1	1.22973001	-0.164539337	7.255190849	1.394269347	-6.025460839
2	2.095507622	0.666469574	7.255192757	1.429038048	-5.159685135
3	3.045413494	1.745182037	7.255187035	1.300231457	-4.20977354
4	1.420195341	2.494235992	7.255177498	-1.074040651	-5.834982157
5	2.406088829	3.033817291	7.255185604	-0.627728462	-4.849096775
6	3.597523689	3.033824921	7.255187988	0.563698769	-3.657664299
7	1.109041452	1.597301483	7.255170822	-0.488260031	-6.14612937
8	1.869042516	2.620628357	7.255167961	-0.751585841	-5.386125445
9	2.884921789	2.114940643	7.255172729	0.769981146	-4.37025094
10	1.444765687	0.854763031	7.255134583	0.590002656	-5.810368896
11	2.229128122	1.405490875	7.255141258	0.823637247	-5.026013136
12	3.348627567	1.835063934	7.255134106	1.513563633	-3.906506538
13	1.407234311	1.347484589	7.255075455	0.059749722	-5.847841144
14	2.240434647	1.726680756	7.255068779	0.513753891	-5.014634132

OBJECTID	Kommetjie2021 RTK elevation (R)	Kommetjie2021 DInSAR elevation (D)	Adjusted DEM elevation (W)	ΔRD	ΔRW
15	3.066060305	2.166858673	7.255080223	0.899201632	-4.189019918
16	1.497279167	1.647079468	7.255025387	-0.149800301	-5.75774622
17	2.322575331	2.201301575	7.25502634	0.121273756	-4.93245101
18	2.922353745	2.505264282	7.255023956	0.417089462	-4.332670212
19	1.302408814	-2.081323624	7.255034447	3.383732438	-5.952625632
20	2.109583139	-2.09167099	7.255009651	4.201254129	-5.145426512
21	2.720377922	-2.376054764	7.254992485	5.096432686	-4.534614563
22	1.185450792	-2.080974579	7.255147934	3.266425371	-6.069697142
23	1.776270747	-2.081212997	7.255068302	3.857483745	-5.478797555
24	2.88370204	-2.081331253	7.255007267	4.965033293	-4.371305227
25	1.063968062	-2.081148148	7.255084515	3.14511621	-6.191116452
26	1.465392232	-2.08093071	7.255039215	3.546322942	-5.789646983
27	2.511478424	-2.080732346	7.255012989	4.59221077	-4.743534565
28	2.106730938	-2.081451416	7.255039692	4.188182354	-5.148308754
29	2.527629614	-2.285768509	7.255028725	4.813398123	-4.727399111
30	2.539871216	-2.422311783	7.255019665	4.962182999	-4.715148449
31	1.068357468	-2.081516266	7.255158901	3.149873734	-6.186801434

OBJECTID	Kommetjie2021 RTK elevation (R)	Kommetjie2021 DInSAR elevation (D)	Adjusted DEM elevation (W)	ΔRD	ΔRW
32	2.87456584	-2.35577774	7.255146027	5.23034358	-4.380580187
33	4.130164146	-2.500324249	7.255111694	6.630488396	-3.124947548
34	1.142472148	-2.556507111	7.255332947	3.698979259	-6.112860799
35	2.399052382	-0.702171326	7.25529623	3.101223707	-4.856243849
36	3.540192127	3.557182312	7.255277157	-0.016990185	-3.71508503
			RMSE	3.037951013	5.111967965
			MEAN	2.197660251	-5.047237764

Application for Approval of Ethics in Research (EiR) Projects
Faculty of Engineering and the Built Environment, University of Cape Town

ETHICS APPLICATION FORM

Please Note:
Any person planning to undertake research in the Faculty of Engineering and the Built Environment (EBE) at the University of Cape Town is required to complete this form before collecting or analysing data. The objective of submitting this application *prior* to embarking on research is to ensure that the highest ethical standards in research, conducted under the auspices of the EBE Faculty, are met. Please ensure that you have read, and understood the EBE Ethics in Research Handbook (available from the UCT EBE, Research Ethics website) prior to completing this application form: http://www.ebe.uct.ac.za/ebe/research/ethics1

APPLICANT'S DETAILS		
Name of principal researcher, student or external applicant		LYNN
Department		GEOMATICS
Preferred email address of applicant:		FNIKLYN001@myuct.ac.za
If Student	Your Degree: e.g., MSc, PhD, etc.	MSC (DISSERTATION) GEOMATICS
	Credit Value of Research: e.g., 60/120/180/360 etc.	180
	Name of Supervisor (if supervised):	JULIAN SMIT
If this is a research contract, indicate the source of funding/sponsorship		INTERNATIONAL and REFUGEE STUDENTS SCHOLARSHIP - FORM 10C (UCT)
Project Title		THE APPLICATION OF OPTICAL LIDAR AND SAR REMOTE SENSING IN MONITORING SOFT SHORE EROSION OF THE SOUTHAFRICAN COASTLINE

I hereby undertake to carry out my research in such a way that:

- there is no apparent legal objection to the nature or the method of research; and
- the research will not compromise staff or students or the other responsibilities of the University;
- the stated objective will be achieved, and the findings will have a high degree of validity;
- limitations and alternative interpretations will be considered;
- the findings could be subject to peer review and publicly available; and
- I will comply with the conventions of copyright and avoid any practice that would constitute plagiarism.

APPLICATION BY	Full name	Signature	Date
Principal Researcher/ Student/External applicant	LYNN FANIKISO	Signed by candidate	20/07/2020
SUPPORTED BY	**Full name**	**Signature**	**Date**
Supervisor (where applicable)	J. SMIT		20 Jul 2020

APPROVED BY	Full name	Signature	Date
HOD (or delegated nominee) Final authority for all applicants who have answered NO to all questions in Section 1; and for all Undergraduate research (including Honours).	Dr Patroba Odera		14 Sept. 2020
Chair: Faculty EIR Committee For applicants other than undergraduate students who have answered YES to any of the questions in Section 1.			

Page 1 of 1